

# Supplementary Information

## Data mining, dashboards and statistics: a powerful framework for the chemical design of molecular nanomagnets

Yan Duan<sup>†,1,2</sup>, Joana T. Coutinho<sup>†,\*,1,3</sup>, Lorena E. Rosaleny<sup>†,\*,1</sup>, Salvador Cardona-Serra<sup>1</sup>, José J. Baldoví<sup>1</sup>, Alejandro Gaita-Ariño<sup>\*,1</sup>

<sup>2</sup> Department of Chemistry and the Ilse Katz Institute for Nanoscale Science & Technology, Ben-Gurion University of the Negev, Beer Sheva 84105, Israel

<sup>3</sup> Centre for Rapid and Sustainable Product Development, Polytechnic of Leiria, 2430-028 Marinha Grande, Portugal

<b>Supplementary Section 1. Construction of the dataset</b>	<b>2</b>
<b>Supplementary Section 2. Classification in chemical families</b>	<b>6</b>
2.1. LnPc <sub>2</sub> family	7
2.2. POM family	9
2.3. Schiff base family	10
2.4. Metallocene family	11
2.5. Diketonate family	12
2.6. Radical family	13
2.7. TM near Ln family	14
2.8. Mixed ligands family	15
2.9. Other families	16
<b>Supplementary Section 3. A graphical, interactive, browsable App</b>	<b>17</b>
3.1. Gallery of SIMDAVIS graphs: chemical variables to optimize the physical properties	19
3.2. Extended gallery of SIMDAVIS graphs: Arrhenius equation parameters	26
<b>Supplementary Section 4. Statistical analysis of the chemical variables</b>	<b>28</b>
4.1. Initial multiple correspondence analysis	28
4.2. Clustering studies for the chemical variables	32
4.3. Lognormal modelling	37
<b>Supplementary Section 5. Statistical analysis of the physical variables</b>	<b>37</b>
5.1. Overview of the main statistical relationships	37
5.2. Simple frequency distributions	40
5.3. Correlations between physical variables	40
<b>Supplementary Section 6. FAMD and magnetostructural clustering</b>	<b>49</b>
6.1. Magnetostructural clusters	51
<b>Supplementary Section 7. Annex: articles included in the study</b>	<b>56</b>
<b>Supplementary References</b>	<b>76</b>

## Supplementary Section 1. Construction of the dataset

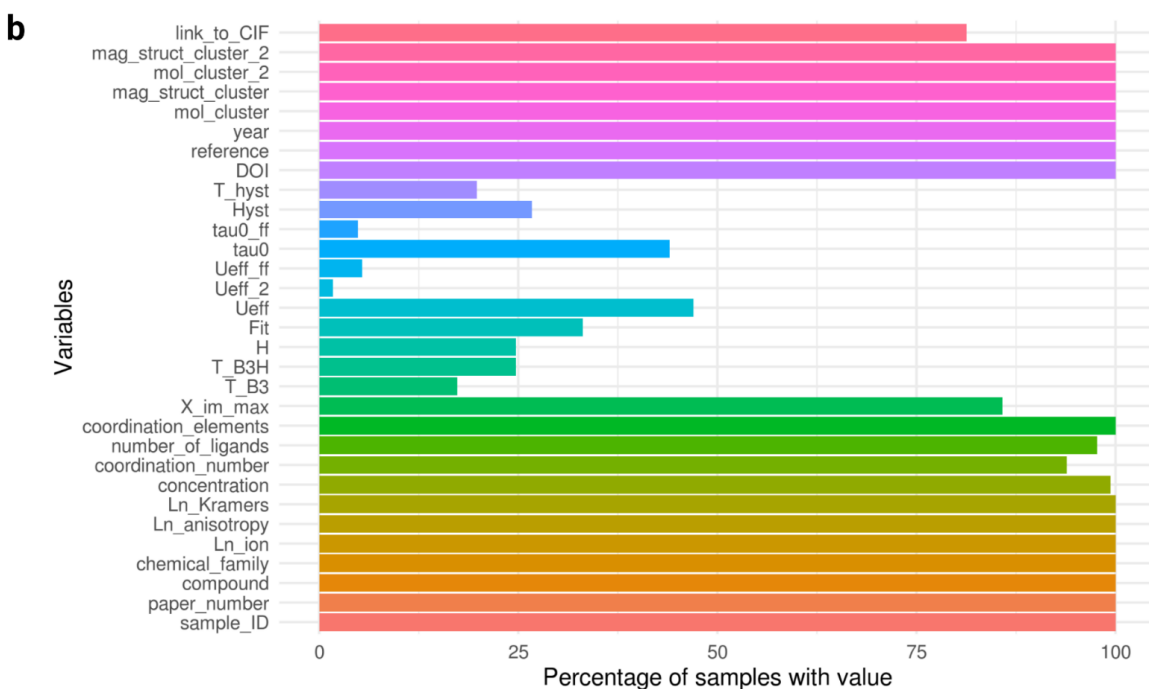
Data extraction was restricted to variables that can be systematically extracted from articles included in the present study. Our objectives for the data analysis were twofold: the correlation between different variables of the same (physical or chemical) category and the correlation between two variables from different (chemical and physical) categories. In the first case, the goal is to determine whether the variables are closely correlated with each other, and thus to simplify our analysis and to avoid false correlations. In the second case, the goal is to determine which chemical variables are proven to be the most influential on the physical performance.

For physical variables, we focus on the magnetic hysteresis and the behaviour of the out-of-phase component of the ac susceptibility. These two kinds of experimental observations are the most basic experimental tell-tale signs for SIM behaviour. For both, we extract from the articles qualitative and quantitative information. For ac susceptibility, we extract as qualitative information whether the out-of-phase component of the ac susceptibility  $\chi''$  vs the temperature has a maximum when there is no external dc magnetic field, or whether this maximum is absent but there is a frequency-dependent behaviour of  $\chi''$  with the temperature. As quantitative information, we extract the temperature of said  $\chi''$  vs T maximum. If the maximum of the out-of-phase component of the ac susceptibility appears in the presence of an external dc magnetic field, we extract the temperature at which the said maximum value appears and the applied external field. From reported magnetisation vs the magnetic field experiments, we extract as qualitative information the presence of full hysteresis (with remnant magnetisation and/or a coercive field), or at least a pinched hysteresis, and as quantitative information the maximum hysteresis temperature reported. In addition, a series of variables from the more extended theoretical analysis of the experimental data, namely the effective energy barrier  $U_{\text{eff}}$  and the relaxation time  $\tau_0$ , as well as relevant information on what kind of fit gave rise to these parameters are also included.

In the case of the chemical variables, the information we collected and analysed is as follows: (a) the chemical family of the complex; (b) the lanthanide (Ln) ion; (c) whether the Ln ion is oblate, prolate or isotropic; (d) whether the Ln ion is Kramers or not; (e) the concentration of the sample (if the diamagnetic dilution is studied); (f) the coordination number of the Ln ion; (g) the number of coordinated ligands; (h) the coordination elements.

A full list of the variables, including the number of data points and the percentage of samples with valid values for each variable in the dataset, can be found in Supplementary Fig. 1.

<b>a</b>	<b>Chemical Variables</b>	<b>N</b>	<b>Physical Variables</b>	<b>N</b>
Chemical Family	1405		$\chi_{\max}''$ : Presence of maximum in $\chi''(T)$	1206
Ln ion	1405		$T_{B3}$ : Temperature of $\chi_{\max}''$ at zero-field	244
Ln anisotropy	1405		$T_{B3H}$ : Temperature of $\chi_{\max}''$ at field H	347
Ln Kramers	1405		$H$ : External Applied Magnetic Field	347
Concentration	1396		$Fit$ : $U_{\text{eff}}$ fitted by $T_{B3}$ or Argand	465
Coordination Number	1319		$U_{\text{eff}}$ : Effective barrier with Orbach process	660
Number of Ligands	1373		$U_{\text{eff}2}$ : $U_{\text{eff}}$ for a second relaxation process	24
Coordination Elements	1405		$U_{\text{eff,ff}}$ : $U_{\text{eff}}$ for all processes (full fit)	76
			$\tau_0$ : Attempt time with Orbach process	618
			$\tau_{0,ff}$ : Attempt time with all relaxation processes	68
			$Hyst$ : Presence of pinched or full hysteresis	375
			$T_{Hyst}$ : Maximum hysteresis temperature	278



**Supplementary Figure 1.1 | Chemical and physical variables included in the dataset. a,** Correspondence between variables and symbols and number (N) of samples in the dataset containing that information. **b,** Percentage of samples containing valid values for each variable.

Let us start by defining the chemical variables and explaining the different values they can take. When appropriate a numerical labelling equivalence for each value is given in square brackets, this is used in some of the statistical plots in later sections.

-The parameter “Chemical family” is categorical and takes one of the following 9 values for each sample: {LnPc<sub>2</sub> [1]; polyoxometalate [2]; Schiff base [3]; metallocene [4]; diketonate [5]; radical [6]; TM near Ln [7]; mixed ligands [8]; other families [9]}. Details on this classification are given in Supplementary Section 2.

-The parameter “Ln ion” is categorical and takes one of the following 10 values for each sample: {Pr<sup>3+</sup> [1]; Nd<sup>3+</sup> [2]; Sm<sup>3+</sup> [3]; Gd<sup>3+</sup> [4]; Tb<sup>3+</sup> [5]; Dy<sup>3+</sup> [6]; Ho<sup>3+</sup> [7]; Er<sup>3+</sup> [8]; Tm<sup>3+</sup> [9]; Yb<sup>3+</sup> [10]}.

-The parameter “Ln anisotropy” is categorical and takes one of the following 3 values for each sample: {prolate [0]; oblate [1]; isotropic [2]}. This is determined directly by the Ln ion.

-The parameter “Ln Kramers” is categorical and takes one of the following 2 values for each sample: {non Kramers [0]; Kramers [1]}. Like the anisotropy, this is determined directly by the Ln ion.

-The parameter “concentration” takes the percentage value, e.g. concentration=1 is read as 1% concentration of the magnetic lanthanide ion in a diamagnetic matrix where 99% of the molecules are e.g. the Y<sup>3+</sup> analog.

-The parameter “Coordination Number” (or CN) is an integer number between 2 and 9. Note that, for LnPc<sub>2</sub> we assigned CN = 8, as corresponding to the 8 N donor atoms; and for metallocenes we assigned CN = 2, assuming that the electron density is delocalized within each aromatic ring.

-The parameter “Number of ligands” is an integer number between 2 and 9, corresponding to the total number of ligands contributing donor atoms. The absolute number of ligands is registered, not the number of chemically different ligands: N identical ligands count as N.

-The parameter “Coordination Elements” is categorical and takes one of the following 5 values for each sample: {Oxygen [1]; Nitrogen [2]; Oxygen+Nitrogen [3]; Carbon [4]; Others [5]}. Any combination of oxygens and nitrogens is counted as “Oxygen+Nitrogen”, and complexes with coordination elements different from O, N or C in the coordination sphere of lanthanide ions are in the category of “Others”.

Let us continue by defining the physical variables.

-The parameter labelled as  $\chi''_{\max}$  (in plots), or  $\chi_{\text{im},\max}$  (in data table), takes one of these possible values:

·[0]: Freq-independent  $\chi''$  (neither  $T_{B3} > 2$  K reported, nor frequency-dependence in  $\chi''$  vs T),

- [1]: Freq-dependent  $\chi''$  (no  $T_{B3} > 2$  K, but frequency-dependence in  $\chi''$  vs T measured),
- [2]:  $T_{B3} > 2$  K, and
- [3]: Not Measured (no available data to assign the sample into one of the previous three categories).

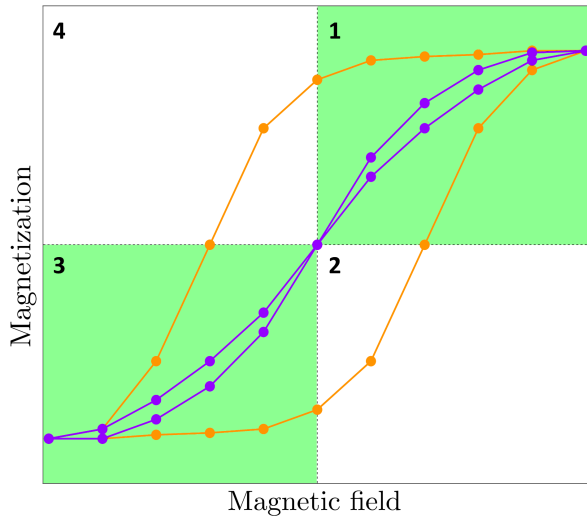
- $T_{B3}$  ( $T_{B3H}$ ) is the temperature at which one finds the maximum value of  $\chi''$  vs T at  $10^3$  Hz, in absence (in presence) of an external magnetic field; H is the magnetic field, if present. It can be understood as the maximum temperature for which the system maintains short-term (millisecond) magnetic memory. For articles that provide  $\chi''$  vs T with a curve for each different frequency, we simply chose the curve corresponding to the frequency  $10^3$  Hz (or the closest one) and registered the temperature for the maximum  $\chi''$ , or the absence of a maximum. However, if the articles represent  $\chi''$  vs frequency as isothermal curves for each different temperature, the same information is accessible indirectly by reading the points in the graph vertically at the abscissa value corresponding to the frequency  $10^3$  Hz and checking in consecutive temperature curves whether  $\chi''$  values present a non-monotonic evolution with respect to temperature, and therefore a maximum.

-“Fit” registers whether the parameters to determine  $U_{\text{eff}}$  and  $\tau_0$  were obtained from  $\chi''(T)$  maxima at different frequencies or from an Argand plot.

- $U_{\text{eff}}$ ,  $U_{\text{eff},2}$ ,  $U_{\text{eff,ff}}$  are the effective energy barriers and  $\tau_0$ ,  $\tau_{0,\text{ff}}$  are the attempt times, which means the pre-exponential factors. The values of the effective energy barrier  $U_{\text{eff}}$  and of the attempt time  $\tau_0$  are recorded if they are determined from a fit considering a single Orbach process. In the cases where a second Orbach process is considered, we register (besides  $U_{\text{eff}}$ ,  $\tau_0$  for the first process) its effective energy barrier  $U_{\text{eff},2}$ . If a more complete model for relaxation is employed including an Orbach process as well as the Raman process, Quantum Tunneling of the Magnetization and/or a direct process, we consider this a “full fit”(in short: ff), and record the value of the effective energy barrier  $U_{\text{eff,ff}}$  and the attempt time or pre-exponential factor  $\tau_{0,\text{ff}}$ .

-The parameter labelled as “*Hyst*” takes one of the four values as follows:

- [0]: No hysteresis above 2 K reported,
- [1]: Pinched Hysteresis (magnetic hysteresis above 2 K reported, but no magnetic coercivity field or remnant magnetisation can be determined; see Supplementary Fig. 1.2),
- [2]: Full Hysteresis (magnetic hysteresis above 2 K reported, and additionally either magnetic coercive field or remnant magnetisation can be determined; see Supplementary Fig. 1.2),
- [3]: Not Measured (no available data to assign the sample into one of the previous three categories).



**Supplementary Figure 1.2 | Full vs pinched hysteresis.** Full hysteresis curves (orange) present at least one point either in quadrants 2,4 (*i.e.* different signs for Magnetic field and Magnetization) or in the x and/or y axes. Pinched hysteresis curves (violet) present points only in quadrants 1,3 (*i.e.* same signs for  $H$  and  $M$ ) and, sometimes, also at the origin of coordinates.

-The related parameter “ $T_{\text{hyst}}$ ” takes the highest temperature value at which hysteresis is reported. In contrast with  $T_{\text{B3}}$ , this quantifies the temperature up to which the system maintains long-term magnetic memory.

One of the main problems for the data extraction during the construction of the dataset was that different criteria are chosen by different groups to characterize the hysteresis. For example, the hysteresis is measured only at 2 K in many studies, resulting in an overrepresentation of  $T_{\text{hyst}} = 2$  in the dataset; while in many other cases the hysteresis is measured up to the highest possible temperature. Therefore, the very same compound could then present different  $T_{\text{hyst}}$  depending on an arbitrary choice by the researchers, decreasing the quality of the dataset. Another difficulty is that the information of the applied magnetic field sweep rate which directly affects  $T_{\text{hyst}}$  is missing in some articles. In addition, in some articles, not only a full hysteresis, presenting coercive field and magnetic remanence, is measured up to a certain temperature but also a pinched hysteresis is measured up to a higher temperature. This introduces some noise in the dataset, but is less problematic since both cases are going to be registered as a SIM with good properties.

## Supplementary Section 2. Classification in chemical families

Lanthanides are a group of *f*-block elements with atomic number ranging from 57 (lanthanum) to 71 (lutetium). Most of the Ln elements exhibit the oxidation state of +3. Our dataset only includes the trivalent  $\text{Ln}^{3+}$  (Pr, Nd, Sm, Gd, Tb, Dy, Ho, Er, Tm and Yb) ions containing

complexes. Ln ions possess large coordination numbers (CNs) due to their large ionic radii. The geometrical arrangement around these trivalent ions basically depends on the steric properties of the coordinated ligands; thus a suitable design of the ligand molecules leads to an easy tuning of the CNs. In particular, CNs between 2 and 12 are documented for Ln ions. Note that in this work we consider one rigid aromatic ring as equivalent to a contribution to CN/ring = 1 when it is of the cyclopentadienyl/cyclooctatetraenyl kind, whereas we consider a contribution of CN/ring = 4 when it is of the phthalocyaninato kind. In the low CN cases, the coordination ligands are usually bulky ligands, e.g. bis(trimethylsilyl) amine gives CN = 3; whereas cyclopentadienyl ligands need to be smartly substituted to achieve the same steric impediment. In contrast, in the case of complexes with high CN, the ligands are usually small bidentate ligands, such as nitrate and/or macrocyclic ligands. In the present work, we found that the most frequent are CN = 8 and CN = 9. This coincides with what is known for Ln ions, namely, Ln ions tend to spontaneously favour these CNs, typically with distorted square antiprismatic coordination (CN = 8) or distorted tricapped trigonal prism coordination (CN = 9).

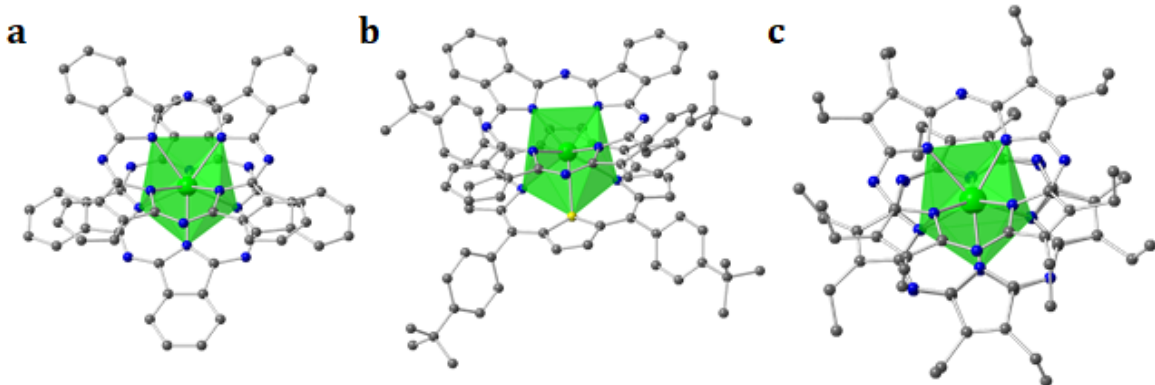
Ln-based SIMs are interesting because the  $4f$  electrons are less exposed to ligand field effects and exhibit larger spin-orbital coupling if compared with the  $d$ -shell. The first Ln-based mononuclear single molecule magnets (SMMs) were generated by Ishikawa and co-workers in 2003 using two macrocyclic ligands to sandwich the  $\text{Ln}^{3+}$  ion in a double-decker fashion.<sup>1</sup> They can also be prepared by using a range of acyclic ligands, such as polyoxometalates (POMs),<sup>2-4</sup> Schiff bases,<sup>5,6</sup> radicals,<sup>7-15</sup> and ketones.<sup>16-18</sup> Between 2003 and 2019, several hundreds of articles referring to Ln-based SIMs have been published. Among them, the vast majority focused on the chemical approaches in designing lanthanide-based SIMs with superior properties. A fundamental key parameter of the magnetic properties of SIMs is the molecular symmetry which can be controlled by: (a) the ligand design and modification, (b) the substitution of the coordination elements as a means to alter electrostatic potential and/or Ln to coordination atom bond lengths, and (c) the peripheral ligand functionalization/substitution. Here, we classify the collected complexes into 9 categories according to the type of coordination ligands or the chemical strategy used for the design of the magnetic complex. These 9 categories (Chemical Family) are listed below and will be briefly described in this section.

- 1) LnPc<sub>2</sub> family
- 2) POM family
- 3) Schiff Base family
- 4) Metallocene family
- 5) Diketonate family
- 6) Radical family
- 7) TM near Ln family
- 8) Mixed ligands family
- 9) Other families

## 2.1. LnPc<sub>2</sub> family

The first category is constituted by “double-decker complexes” related to the classical LnPc<sub>2</sub> family, namely, the Ln ion in the complex is octa-coordinated by nitrogen atoms from two Pc (or their related functionalized complexes, or porphyrin-like, or even tetraaza[14]annulenes) ligands. As we will see below, this criterion has priority over the presence of a spin S = 1/2 (radical ligand, in this case corresponding to oxidized or reduced Pc ligands) and also over the presence of diamagnetic transition metal ions in the vicinity (in this case often corresponding to multiple deckers which coordinate Cd<sup>3+</sup>). In both cases, these complexes are classified as LnPc<sub>2</sub> family. Complexes composed of phthalocyanine ligands or porphyrins with nitrogen-based donating atoms have shown very important roles in Ln-based SIMs. There are several reasons for choosing phthalocyanines and porphyrins for SIM design: a) these tetrapyrrole macrocyclic ligands containing four isoindole or pyrrole nitrogen atoms have the ability to strongly coordinate to Ln ions; b) special features such as intramolecular  $\pi$ - $\pi$  stacking interaction and the intrinsic nature of their macrocyclic rotation;<sup>19</sup> and c) their structural characteristics of those sandwich-type complexes since the ligand field constructed by this type of ligands with a C<sub>4</sub>-symmetric axis (pseudo-D<sub>4d</sub> symmetry) is very important for the zero-field splitting of the ground state into the magnetic sublevels. The combination of the large magnetic anisotropy with strong spin-orbital interactions leads to the SIMs behaviours.

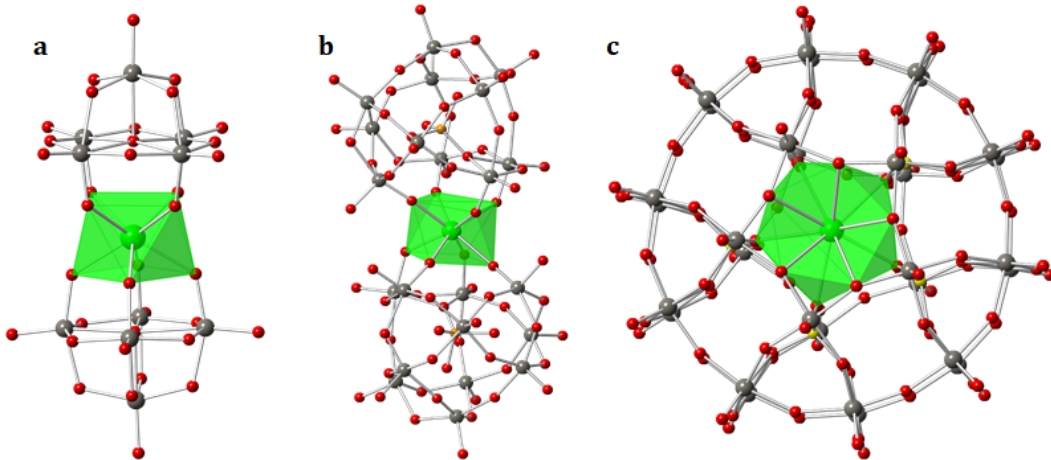
The first examples of Ln-based SIMs reported are from the LnPc<sub>2</sub> family, which was proposed in 2003 by Ishikawa and co-workers.<sup>1</sup> They successfully demonstrated that slow magnetic relaxation could occur in mononuclear lanthanide complexes, such as those in which a Ln ion is sandwiched between two Pc ligands, formulated as (Bu<sub>4</sub>N)[LnPc<sub>2</sub>] (Ln<sup>3+</sup> = Tb<sup>3+</sup> or Dy<sup>3+</sup>, Bu<sub>4</sub>N = tetrabutylammonium) (Supplementary Fig. 2a). Later on, a massive synthetic effort has led to an ever-increasing number of compounds from the LnPc<sub>2</sub> family, which includes the introduction of a wide range of substituents at the periphery of the Pc macrocycles without significantly interfering with the metal binding properties of the ligands.<sup>20-24</sup> Some structure representations of examples from this family studied in this work are shown below (Supplementary Fig. 2), as the sandwich complex [Bu<sub>4</sub>N][DyPc(OTBPP)], (Supplementary Fig. 2b) in which one of the nitrogen atoms of one porphyrin pyrrole is replaced by an oxygen atom. Compared with the typical LnPc<sub>2</sub> complex, the atom replacement significantly enhances the effective energy barrier of the SIMs.<sup>24</sup> Another example is the use of tetraazaporphyrins (or porphyrazines) in place of the bulkier Pc ligands, giving rise to a series of neutral double-decker complexes that show analogous magnetic features as their Pc counterparts (Supplementary Fig. 2c).<sup>25</sup>



**Supplementary Figure 2 | Combined polyhedral and ball-and-stick models of the coordination spheres around Ln ions of some cases from the  $\text{LnPc}_2$  family. a,  $[\text{Pc}_2\text{Ln}]^-$  from reference [1]. b, The sandwich-type mixed phthalocyaninato with core-modified porphyrinato double-decker complexes  $[\text{DyPc}(\text{OTBPP})]^+$  or  $[\text{Dy}(\text{Pc})(\text{STBPP})]^+$  from reference [24]. c,  $[\text{Ln}(\text{OETAP})_2]^+$ , where OETAP is octa(ethyl)tetraazaporphyrin.<sup>25</sup> (Color code: grey sphere, C; green sphere and polyhedron, Ln; blue sphere, N.)**

## 2.2. POM family

The second representative family consists of polyoxometalates (POMs). This family contains all compounds where  $\text{Ln}^{3+}$  ions coordinate with POM ligands, including the cases where the coordination sphere is completed with other ligands. POMs are molecular metal-oxo clusters with early transition metals (W, Mo, Nb, Ta or V) in their highest oxidation states. The ability of these inorganic species to incorporate almost any kind of metal or non-metal addenda heteroatoms, together with their enormous molecular and electronic structural diversity, makes them of relevance in the molecular magnetism field. One relevant feature of POM ligands is that their diamagnetic structures can encapsulate Ln ions with coordination geometries similar to those of bis(phthalocyaninato)lanthanide complexes from  $\text{LnPc}_2$  family.<sup>1</sup> More recently, POMs were used as extremely versatile inorganic building blocks for the construction of SMMs based either on  $3d$  or  $4f$  metal ions.<sup>26</sup> Some representative cases of complexes included in this study are shown below in Supplementary Fig. 3. The first example from the POM family exhibiting SIM behaviour is  $[\text{ErW}_{10}\text{O}_{36}]^{9-}$  (Supplementary Fig. 3a).<sup>2</sup> Later on, two families of POM-based SIMs with formula  $[\text{Ln}(\text{W}_5\text{O}_{18})_2]^{9-}$  and  $[\text{Ln}(\beta_2\text{-SiW}_{11}\text{O}_{39})_2]^{13-}$  (Supplementary Fig. 3b) are reported in 2009, both of which show slow relaxation of the magnetisation, typical of the SIM-like behaviour.<sup>3</sup> Another well-known series of complexes is  $[\text{LnP}_5\text{W}_{30}\text{O}_{110}]^{12-}$  (Supplementary Fig. 3c), in which its unusual  $C_5$  axial symmetry allows the study of new SIMs having 5-fold symmetry. The  $\text{Dy}^{3+}$  and  $\text{Ho}^{3+}$  derivatives exhibit SIM behaviour.<sup>4</sup>



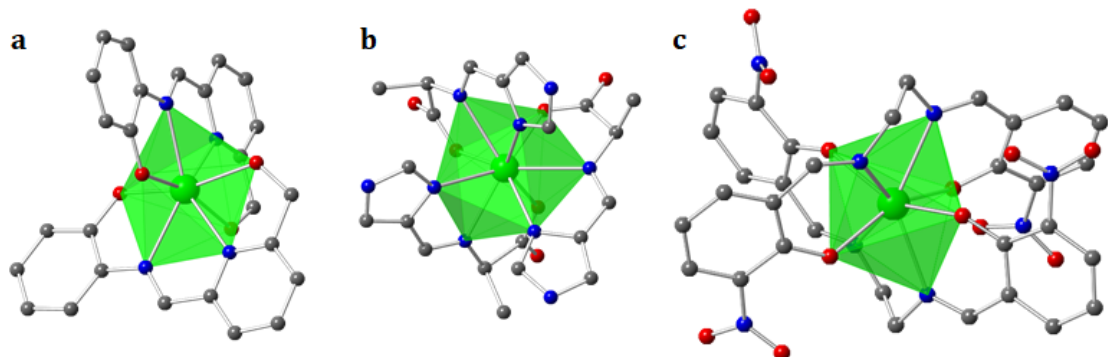
**Supplementary Figure 3 | Combined polyhedral and ball-and-stick models of the coordination spheres around Ln ions of three representative cases from the POM family. a,  $[\text{ErW}_{10}\text{O}_{36}]^{9-}$  from reference [2]. b,  $[\text{Ln}(\beta_2\text{-SiW}_{11}\text{O}_{39})_2]^{13-}$  from reference [3]. c,  $[\text{LnP}_5\text{W}_{30}\text{O}_{110}]^{12-}$  from reference [4].** (Color code: grey sphere, W; green sphere and polyhedron, Ln; red sphere, O; yellow sphere, P; orange sphere, Si.)

### 2.3. Schiff base family

The third family is based on Schiff base ligands. This includes all samples where the  $\text{Ln}^{3+}$  ion coordinates to only Schiff base ligands; in addition, we included the cases where the strategy pursued by the authors (as stated in the title) relies on Schiff base ligand, even if other small ligands are used to complete the coordination sphere. Schiff base ligands are polydentate macrocyclic or macro-acyclic ligands, which typically contain both nitrogen and oxygen donors. However, the donor atom can be varied between sulfur, phosphorus, nitrogen, and oxygen. Due to their facile synthesis, Schiff base ligands are considered to be “privileged ligands”, which can easily make a coordination bond with many different metal ions and stabilize them in various oxidation states. In addition, when two equivalents of salicylaldehyde are combined with a diamine, a particular chelating Schiff base is produced, which is called salen ligands. Salen ligands present four coordinating sites (tetradentate) and two axial sites that are open to ancillary ligands, thus similar to porphyrins but with an easier preparation process.

Schiff bases derived from condensation reactions of aromatic aldehydes with primary amines have been the subject of extensive research because of their enormous versatility with respect to the formation of metal complexes with sophisticated discrete or expanded architectures and functional properties. The choice of initial reagents for the condensation determines the ligand coordination fashion and allows one to utilize both chelate and bridging functions of the obtained Schiff base. Schiff base complexes continue to intrigue chemists regarding their structure and reactivity. Their geometries are strongly influenced by the ligands and tend to be five- or six-coordinate. The first case listed here comprises two mono-deprotonated Schiff base  $[\text{LH}]^-$  ligands, showing SIM behaviour and with a  $U_{\text{eff}}$  of 44.4 K in presence of a dc field

(Supplementary Fig. 4a).<sup>27</sup> Another case from this family is the  $Dy^{3+}$  complex with tridentate NNO ligands of  $N$ -[(imidazol-4-yl)methylidene]-DL-alanine (Supplementary Fig. 4b), which shows an out-of-phase signal with frequency-dependence in ac susceptibility under a dc bias field of  $10^3$  Oe, indicative of field induced SIM.<sup>28</sup> One other representative case from this family is the Salen-type mononuclear  $Ln^{3+}$  complex  $[Ln(3-NO_2-salen)_2]^-$  (Supplementary Fig. 4c), which shows slow magnetisation relaxation processes associated with SIM behaviour.<sup>29</sup>

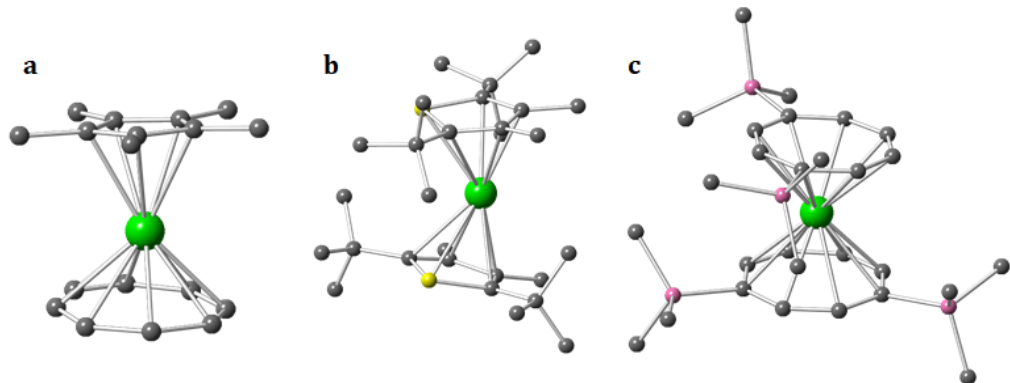


**Supplementary Figure 4 | Combined polyhedral and ball-and-stick models of the coordination spheres around Ln ions of some cases from the Schiff base family.** **a**,  $[Ln(LH)_2]^-$  where  $H_2L = 2-((6-(hydroxymethyl)pyridin-2-yl)-methyleneamino)phenol$ .<sup>27</sup> **b**, ‘fac’- $[Dy^{III}(HL^{DL-ala})_3]$ , where  $H_2L^{DL-ala}$  is  $N$ -[(imidazol-4-yl)methylidene]-DL-alanine.<sup>28</sup> **c**,  $[Ln(3-NO_2-salen)_2]^-$ , where  $Ln$  can be  $Dy$ ,  $Er$  or  $Yb$ , and  $3-NO_2-salen^{2-} = N,N'$ -bis(3-nitro-salicylaldehyde)ethylenediamine dianion.<sup>29</sup> (Color code: grey sphere, C; green sphere and polyhedron, Ln; red sphere, O; blue sphere, N.)

#### 2.4. Metallocene family

The fourth family is based on the small aromatic ligands derived from conjugated hydrocarbon ligands, typically cyclopentadienyl or cyclooctatetraene anions. We only include in this classification the complexes where the coordination sphere is completed by this kind of ligands, in contrast with cases with an extra “equatorial” coordination site. Compared with heteroatomic donor atoms such as oxygen and nitrogen, which have limited orbital overlap with the shielded  $4f$  orbitals, the aromatic ligands allow the perturbation of the crystal field of the lanthanide ions through the use of an electron  $\pi$ -cloud. Thus, it can further control over the anisotropic axis and induction of  $f-f$  interactions, making donor atoms as conjugated hydrocarbons.<sup>30</sup> Here we list some examples by employing delocalized ligands to design SIMs with prominent uniaxial anisotropy. An  $Er^{3+}$  ion sandwiched by two aromatic ligands, pentamethylcyclopentadienide anion ( $C_5Me_5^-$ ,  $Cp^*$ ) and cyclooctatetraenide dianion ( $C_8H_8^{2-}$ , COT) (Supplementary Fig. 5a), displays a butterfly-shaped hysteresis loop at 1.8 K up to even 5 K.<sup>31</sup> Another example is a bis-monophospholyl  $Dy^{3+}$  SIM,  $[Dy(Dtp)_2][Al\{OC(CF_3)_3\}_4]$  (Supplementary Fig. 5b), which shows an effective energy barrier to magnetisation reversal of 1760 K ( $1223\text{ cm}^{-1}$ ) and magnetic

hysteresis up to 48 K.<sup>32</sup> The use of planar cyclooctatetraenide (COT<sup>2-</sup>) ligands allows the access to the sandwich type complex [Dy(COT)<sub>2</sub>]Li(DME)<sub>3</sub> (Supplementary Fig. 5c), which exhibits slow relaxation of the magnetisation indicating its SMM behaviour.<sup>33</sup>

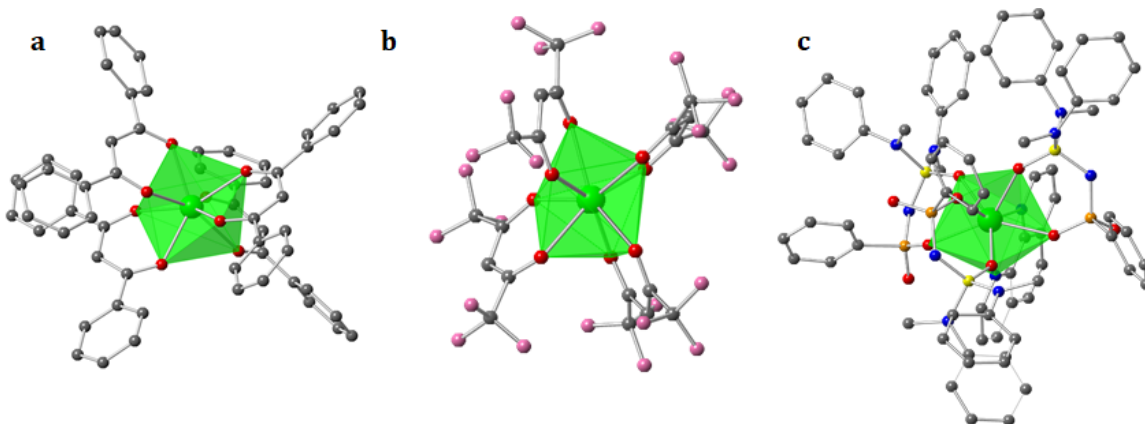


**Supplementary Figure 5 | Ball-and-stick models of the coordination spheres around  $\text{Ln}^{3+}$  ions of some cases from the metallocene family. a,  $(\text{Cp}^*)\text{Er}(\text{COT})$ , where  $\text{Cp}^* = \text{C}_5\text{Me}_5^-$  and  $\text{COT} = \text{C}_8\text{H}_8^{2-}$ , from reference [31]. b,  $[\text{Dy}(\text{Dtp})_2][\text{Al}\{\text{OC}(\text{CF}_3)_3\}_4]$ , where  $\text{Dtp} = \{\text{P}(\text{C}^*\text{BuCMe})_2\}$ .<sup>32</sup> c,  $[\text{DyCOT}^{2-}]$ , where  $\text{COT}^{2-}$  = cyclooctatetraenide rings.<sup>33</sup> (Color code: grey sphere, C; green sphere, Ln; pink sphere, Si; yellow sphere, P.)**

## 2.5. Diketonate family

The fifth family is the diketonate family of complexes, it includes those samples with  $\text{Ln}^{3+}$  ions coordinated with diketonate ligands and diketonate ligands mixed with other molecules which are not defined in the classification. The diketonate ligands are bidentate and bond through delocalized chelate rings formed through two oxygen atoms.  $\beta$ -diketone SMMs have received much attention in recent years, since  $\beta$ -diketone can provide a stable bidentate chelating mode to afford eight-coordinated mononuclear lanthanide complexes. There are two different polyhedron coordination geometries for the  $\beta$ -diketone complexes, square antiprism with  $D_{4d}$  symmetry and triangular dodecahedron with  $D_{2d}$  symmetry. After the SMM behaviour of a simple acetylacetone complex has been reported on several  $\beta$ -diketone complexes, much effort is devoted to the synthesis and investigation of  $\beta$ -diketone SMMs. In addition to the coordination geometry, the stability of the SMMs upon heating is also an important topic. Lanthanide  $\beta$ -diketonate complexes with fluorides as substituent groups, such as hexafluoroacetylacetone (hfac), can make the complexes stable upon heating. By using the  $\beta$ -diketonate ligand dibenzoylmethane (DBM) anion, mononuclear Dy complex  $[\text{Hex}_4\text{N}][\text{Dy}(\text{DBM})_4]$  (Supplementary Fig. 6a) was obtained, in which slow magnetic relaxation is observed.<sup>16</sup> A typical compound of  $\beta$ -diketone is formulated as (cation) $[\text{Ln}(\beta\text{-diketone})_4]$ , in which the  $\text{Ln}^{3+}$  ion is surrounded by four  $\beta$ -diketone forming a  $\text{LnO}_8$  environment. The complex shown in Supplementary Fig. 6b, using hfac ligand, exhibits field-induced slow magnetization relaxation.<sup>17</sup> Another case is the use of a sulfonyl amidophosphate (SAPH), acting as a  $\beta$ -diketone homologue

for the complexation of  $\text{Ln}$  ion, which gives rise to complex  $\text{LnL}_3\text{Phen}$  ( $\text{L} = \text{C}_6\text{H}_5\text{SO}_2\text{NP}(\text{O})[\text{N}(\text{CH}_3)(\text{C}_6\text{H}_5)]_2$ ) with in-field SIM behaviours (Supplementary Fig. 6c).<sup>34</sup>

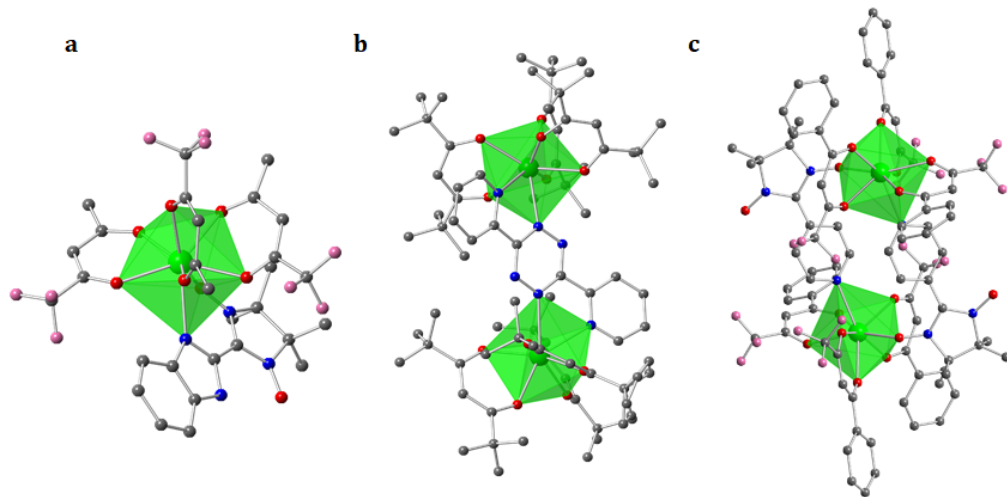


**Supplementary Figure 6 | Combined polyhedral and ball-and-stick models of the coordination spheres around  $\text{Ln}$  ions of some cases from the diketonate family.** a,  $[\text{Dy}(\text{DBM})_4]^-$ , where DBM = dibenzoylmethane anion ligand.<sup>16</sup> b,  $\{\text{Dy}(\text{hfac})_4\}$ , where hfac = hexafluoroacetylacetone.<sup>17</sup> c,  $[\text{LnL}_3(\text{phen})]$ , where  $\text{Ln}$  can be Dy or Er, and  $\text{L}$  is deprotonated bis(methyl(phenyl)amino)phosphoryl)-benzenesulfonamide,  $\text{C}_6\text{H}_5\text{SO}_2\text{NP}(\text{O})[\text{N}(\text{CH}_3)(\text{C}_6\text{H}_5)]_2$ , and Phen = phenanthroline.<sup>34</sup> (Color code: grey sphere, C; green sphere and polyhedron, Ln; red sphere, O; yellow sphere, P; pink sphere, F; blue sphere, N; orange sphere, S.)

## 2.6. Radical family

The sixth family is composed of complexes in which  $\text{Ln}^{3+}$  ion is coordinated with radical-based ligand(s), such as nitronyl nitroxide and semiquinones. Radical ligands are one of the most efficient bridging ligands for the design of molecular magnetic materials.<sup>35</sup> The radical systems are relatively abundant in our dataset, being more numerous than any other family presented so far. The reason of choosing radical ligands is that they possess  $2p$  diffuse spin orbitals that can potentially penetrate the core electron density of the lanthanide ions to reach deeply buried  $4f$  orbitals, whose shielded magnetic orbitals are usually a drawback for their use in extended magnetically coupled structures.<sup>36</sup> The strong  $2p$ - $4f$  heterospin exchange coupling effectively shifts degenerated  $m_J$  sublevels to different energies and, furthermore, significantly reduces the probability of resonant quantum tunnelling and lengthens the relaxation time. We will show some examples from this family (Supplementary Fig. 7). The first case is the nitronyl nitroxide radical complex  $[\text{Ln}(\text{tfa})_3(\text{NIT-BzImH})]$ , (Supplementary Fig. 7a) in which  $\text{Ln}^{3+}$  ion is 8-coordinated to one NIT-BzImH and three trifluoroacetylacetone (tfa) ligands. It shows slow magnetic relaxation suggesting that they behave as SIMs.<sup>10</sup> The second case is a dinuclear  $\text{Ln}^{3+}$  compound with its formula as  $\{\text{Cp}_2\text{Co}\}\{\text{[Dy(tmhd)}_3]_2(\text{bptz})\}$  in radical anion form (Supplementary Fig. 7b), in which the rare earth ions are isolated by an organic ligand bridged species. It exhibits out-of-phase ac susceptibility signals below 4 K.<sup>15</sup> Another relevant case is a

cyclic dimer structure, in which each pyridine substituted radical links two different metal ions through the oxygen of a nitroxide group and the pyridine nitrogen (Supplementary Fig. 7c). It shows frequency-dependent ac magnetic susceptibility, indicating SIM behaviour.<sup>9</sup>

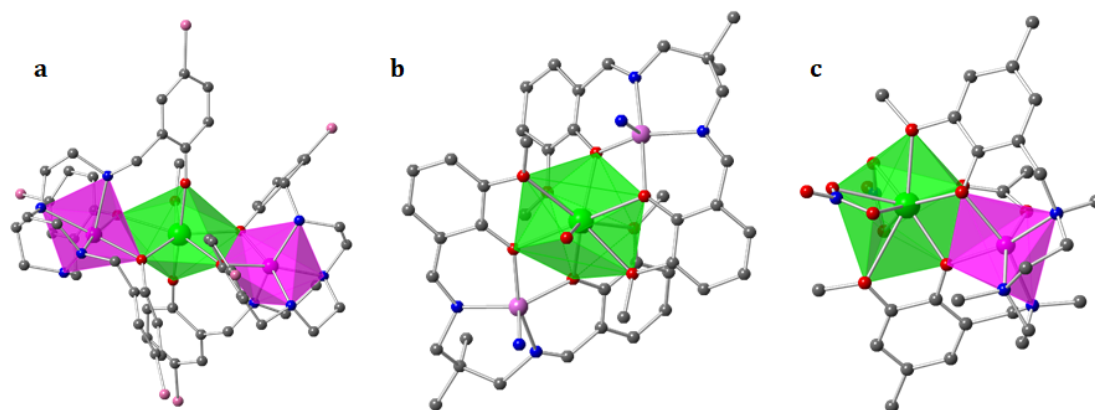


**Supplementary Figure 7 | Combined polyhedral and ball-and-stick models of the coordination spheres around Ln ions of some cases from the radical family.** a,  $[\text{Ln}(\text{tfa})_3(\text{NIT-BzImH})]$ , where tfa = trifluoroacetylacetone; NIT-BzImH = 2-(2'-benzimidazolyl)-4,4,5,5-tetramethylimidazolyl-1-oxyl-3-oxide.<sup>10</sup> b,  $\{\text{Cp}_2\text{Co}\}\{\text{[Dy}(\text{tmhd})_3\]_2(\text{bptz})\}$ , where tmhd = 2,2,6,6-tetramethyl-3,5-heptane dionate and bptz = 3,6-bis(2-pyridyl)-1,2,4,5-tetrazine.<sup>15</sup> c,  $[\text{Ln}(\text{Phtfac})_3(\text{NITpPy})]_2$ , where HPhtfac = 4,4,4-trifluoro-1-phenylbutane-1,3-dione and NITpPy = 2-(4-pyridyl)-4,4,5,5-tetramethyl-4,5-dihydro-1H-imidazolyl-1-oxyl-3-oxide.<sup>9</sup> (Color code: grey sphere, C; green sphere and polyhedron, Ln; red sphere, O; pink sphere, F; blue sphere, N.)

## 2.7. TM near Ln family

This family of complexes is defined when a diamagnetic transition metal (TM) ion exists in the coordination sphere of  $\text{Ln}^{3+}$  ion. There are several Ln-based SIMs containing one or more  $3d$  metal ions.<sup>37-40</sup> Most of this type of complexes contain Schiff base ligand or a diketone ligand.<sup>37</sup> For example, Yamashita *et al.* reported an Er-based SIM,<sup>41</sup> where the  $\text{Er}^{3+}$  ion is coordinated with a Schiff base ligand, which in turn is connected to the diamagnetic transition metal  $\text{Zn}^{2+}$  through oxygen. Macroyclic ligands provide discrete metal binding pockets and, therefore, offer a more predictable cluster nuclearity and structure than acyclic analogues can.<sup>37</sup> For example, the [3+3] macrocycle provides three  $\text{N}_2\text{O}_2$  pockets for  $3d$  metal ions and one central  $\text{O}_6$  pocket for a Ln ion, making mixed-metal  $\text{M}_3\text{Ln}$  tetrametallic macrocyclic complexes predictable.<sup>41,42</sup> Macrocycles usually provide enhanced stability, solubility and fine-tunability (vary the choice of M and Ln, whilst retaining the  $\text{M}_3\text{Ln}$  core) over acyclic analogues. It's documented that the  $U_{\text{eff}}$  of Ln-based SIMs can be enhanced by introducing diamagnetic metal ions in the coordination sphere. The

diamagnetic ion may induce large electrostatic interaction between the  $\text{Ln}^{3+}$  ion and coordination atoms, giving rise to the destabilization of excited states and increasing the gap between the ground state and the first excited state.<sup>43-45</sup> There are many compounds that fall into the “diamagnetic TM near the Ln center” category. For instance, the pentagonal-bipyramidal (quasi- $D_{5h}$ )  $[\text{Zn}-\text{Dy}-\text{Zn}]$  complex (Supplementary Fig. 8a) exhibits a large thermally activated barrier with long relaxation times.<sup>45</sup> Other cases are  $\{[\text{Zn}(\text{Me}_2\text{valpn})_2\text{Dy}(\text{H}_2\text{O})\text{Cr}(\text{CN})_6\}_2$  (Supplementary Fig. 8b)<sup>40</sup> and  $[\text{Zn}(\mu-\text{L})(\mu-\text{OAc})\text{Er}(\text{NO}_3)_2]$  (Supplementary Fig. 8c)<sup>46</sup>, both exhibit SIM behaviour.

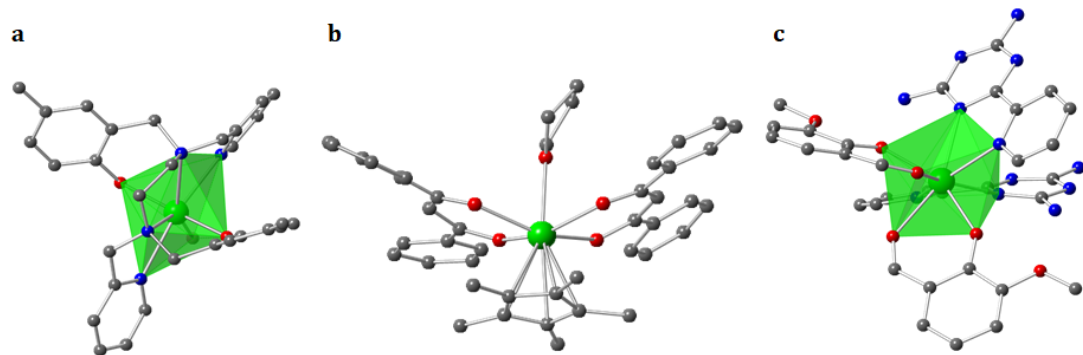


**Supplementary Figure 8 | Combined polyhedral and ball-and-stick representations of the coordination spheres around Ln ions of examples from the TM near Ln family. a,  $[\text{Zn}_2\text{DyL}_2(\text{MeOH})]^-$ , where  $\text{L}$  is  $2,2',2''-(((\text{nitrilotris}(\text{ethane-2,1-diyl}))\text{tris}(\text{azanediyl}))\text{tris}(\text{methylene}))\text{tris}-(4\text{-bromophenol})$ .<sup>45</sup> b,  $\{[\text{Zn}(\text{Me}_2\text{valpn})_2\text{Dy}(\text{H}_2\text{O})\text{Cr}(\text{CN})_6\}_2$ , where  $\text{Me}_2\text{valpn}^{2-}$  is dianion of  $\text{N},\text{N}'\text{-2,2-dimethylpropylenebis(3-methoxysalicylideneimine)}$ .<sup>40</sup> c,  $[\text{Zn}(\mu-\text{L})(\mu-\text{OAc})\text{Er}(\text{NO}_3)_2]$ , where  $\text{H}_2\text{L}$  is  $\text{N},\text{N}',\text{N}''\text{-trimethyl-N},\text{N}''\text{-bis(2-hydroxy-3-methoxy-5-methylbenzyl)diethylenetriamine}$ .<sup>46</sup> (Color code: grey sphere, C; green sphere and polyhedron, Ln; magenta sphere and polyhedron, Zn; red sphere: O; pink sphere, Br; blue sphere: N.)**

## 2.8. Mixed ligands family

The eighth category is defined as mixed ligands. It contains all cases where the  $\text{Ln}^{3+}$  ion is coordinated with one kind of ligands defined above together with another ligand not defined, thus, mixed ligands. The design strategy of using mixed ligands for high performance SIMs is promising. There are many complexes from this category which possess SIM behaviour. One example is using  $\text{N},\text{N}'\text{-bis(2-hydroxybenzyl)-N},\text{N}'\text{-bis(2-methylpyridyl)ethylenediamine}$  and  $\text{Cl}$  (or  $\text{Br}$ ) as ligands for synthesis of the seven-coordinate complex  $[\text{Dy}(\text{bbpen-CH}_3)\text{X}]$ , which produces high performance SIMs (Supplementary Fig. 9a).<sup>47</sup> Another representative case is the half-sandwich organometallic complex  $[\text{Cp}^*\text{Dy}(\text{DBM})_2(\text{THF})]$  (Supplementary Fig. 9b) with a

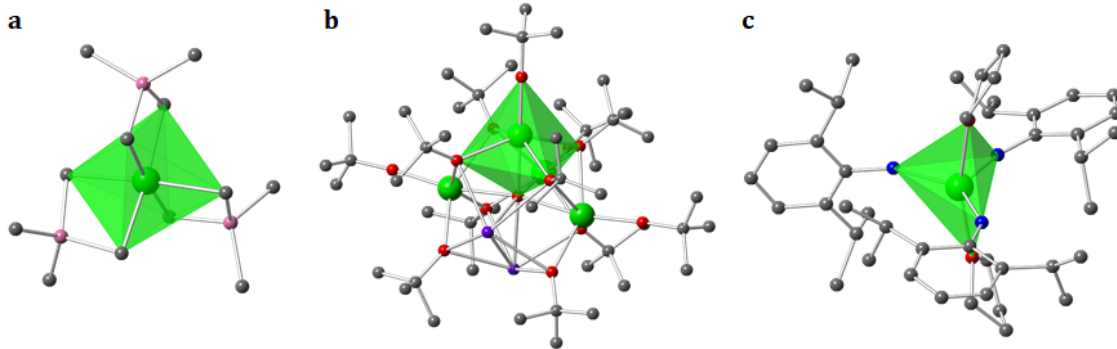
Janus structural motif, where the ligands are composed of THF, DBM<sup>-</sup> and [Cp<sup>\*</sup>]<sup>-</sup>. It displays slow magnetic relaxation in the absence of an applied magnetic field, indicating SIMs properties.<sup>48</sup> By combination of  $\beta$ -diketonate with 6-pyridin-2-yl-[1,3,5]triazine-2,4-diamine ligands, a series of SIMs were obtained and investigated (Supplementary Fig. 9c).<sup>49</sup>



**Supplementary Figure 9 | Combined polyhedral and ball-and-stick models of the coordination spheres around Ln ions of some cases from the mixed ligands family.** **a**, [Dy(bbpen-CH<sub>3</sub>)X], where X = Cl or Br and H<sub>2</sub>bbpen = N,N'-bis(2-hydroxybenzyl)-N,N'-bis(2-methylpyridyl)ethylenediamine.<sup>47</sup> **b**, [Cp\*<sup>+</sup>Dy(DBM)<sub>2</sub>(THF)], where Cp\* = C<sub>5</sub>Me<sub>5</sub><sup>-</sup> and DBM = dibenzoylmethanoate anion.<sup>48</sup> **c**, [DyLz<sub>2</sub>(o-vanilin)<sub>2</sub>]<sup>+</sup>, where Lz = 6-pyridin-2-yl-[1,3,5]triazine-2,4-diamine and X = Br<sup>-</sup>, NO<sub>3</sub><sup>-</sup>, CF<sub>3</sub>SO<sub>3</sub><sup>-</sup>, from reference [49]. (Color code: grey sphere, C; green sphere and polyhedron, Ln; red sphere, O; blue sphere, N.)

## 2.9. Other families

The last category is named as “other families”. It includes all complexes which fall into the criterion of complex selection but the coordination ligands of Ln ions are not in the ligand families previously defined. Large numbers of complexes included in this work are from this category. For instance, the octahedral dysprosium aluminate complex [Dy(AlMe<sub>4</sub>)<sub>3</sub>] shows fast relaxation of the magnetisation via quantum tunnelling (Supplementary Fig. 10a).<sup>50</sup> Also, the alkoxide cage complexes [DyY<sub>3</sub>K<sub>2</sub>O(O'Bu)<sub>12</sub>] and [DyY<sub>4</sub>O(O'Pr)<sub>13</sub>] (Supplementary Fig. 10b) incorporate a small amount of DyCl<sub>3</sub> in the synthesis of [Dy<sub>4</sub>K<sub>2</sub>O(O'Bu)<sub>12</sub>] and [Dy<sub>5</sub>O(O'Pr)<sub>13</sub>] to produce {DyY<sub>3</sub>K<sub>2</sub>} in a {Y<sub>4</sub>K<sub>2</sub>} matrix, or {DyY<sub>4</sub>} in {Y<sub>5</sub>}. These complexes show a single dominant relaxation process with very high  $U_{\text{eff}}$  values.<sup>51</sup> Another relevant cases are the five-coordinate complexes Ln(NHPh'Pr<sub>2</sub>)<sub>3</sub>(THF)<sub>2</sub>, (Ln = Dy and Er), with trigonal bipyramidal geometry, both of which exhibit slow magnetic relaxation under a zero/non-zero dc applied magnetic field (Supplementary Fig. 10c).<sup>52</sup>



**Supplementary Figure 10 | Combined polyhedral and ball-and-stick models of the coordination spheres around Ln ions of three examples from the other families. a, [Dy(AlMe<sub>4</sub>)<sub>3</sub>] from reference [50]. b, [DyY<sub>3</sub>K<sub>2</sub>O(O'Bu)<sub>12</sub>] from reference [51]. c, Ln(NHPh'Pr<sub>2</sub>)<sub>3</sub>(THF)<sub>2</sub>, in which Ln<sup>3+</sup> can be Dy<sup>3+</sup> or Er<sup>3+</sup>, from reference [52]. (Color code: grey sphere, C; green sphere and polyhedron, Ln or Y<sup>3+</sup>; red sphere, O; blue sphere, N; pink sphere, Al.)**

### Supplementary Section 3. A graphical, interactive, browsable App

To facilitate a broader use by the chemical community of the data collected in the present study, we developed the tool SIMDAVIS (Single Ion Magnet DAta VISualization): a graphical, interactive, browsable online database of over 1400 samples. Employing SIMDAVIS, any user can study the data in different and complementary ways. The four modes of operation, accessible in different tabs within the program, are “ScatterPlots”, “BoxPlots”, “BarCharts” and “Data” table. There is also an information subtab denoted as “Variables” within the “About SIMDAVIS” tab in which the definition of each variable can be found.

The basic use of the “ScatterPlots” tab is the representation of quantitative data against each other, *e.g.* the maximum hysteresis temperature ( $T_{\text{hyst}}$ ) *vs* the effective energy barrier ( $U_{\text{eff}}$ ). This allows a visual estimate on the relation between different experimental and theoretical descriptors of the magnetic behaviour. Other relevant numerical variables in the dataset include  $T_{\text{B3}}$ ,  $T_{\text{B3H}}$ , the alternate estimate for the effective energy barrier ( $U_{\text{eff,fr}}$ ), or the pre-exponential factors  $\tau_0$ ,  $\tau_{0,\text{ff}}$ , for either the simplistic equation or the full fit (see details about the variables in Supplementary Section 1). Furthermore, the “ScatterPlots” tab allows to distinguish the data points plotted according to a number of qualitative (categorical) variables, which can be of chemical nature, such as the chemical family, or which lanthanide ion was employed. Also, you may distinguish the points by some categorical variables of physical nature, such as presence or absence of magnetic memory above 2 K, in form of hysteresis or maximum in the  $\chi''$  (categorical variable  $\chi''_{\text{max}}$  in our dataset). It also allows the user to select or deselect the represented data depending on these qualitative variables, to help distinguish quantitative correlations that might be different for different classes of compounds. Finally, there is also an option to fit linear

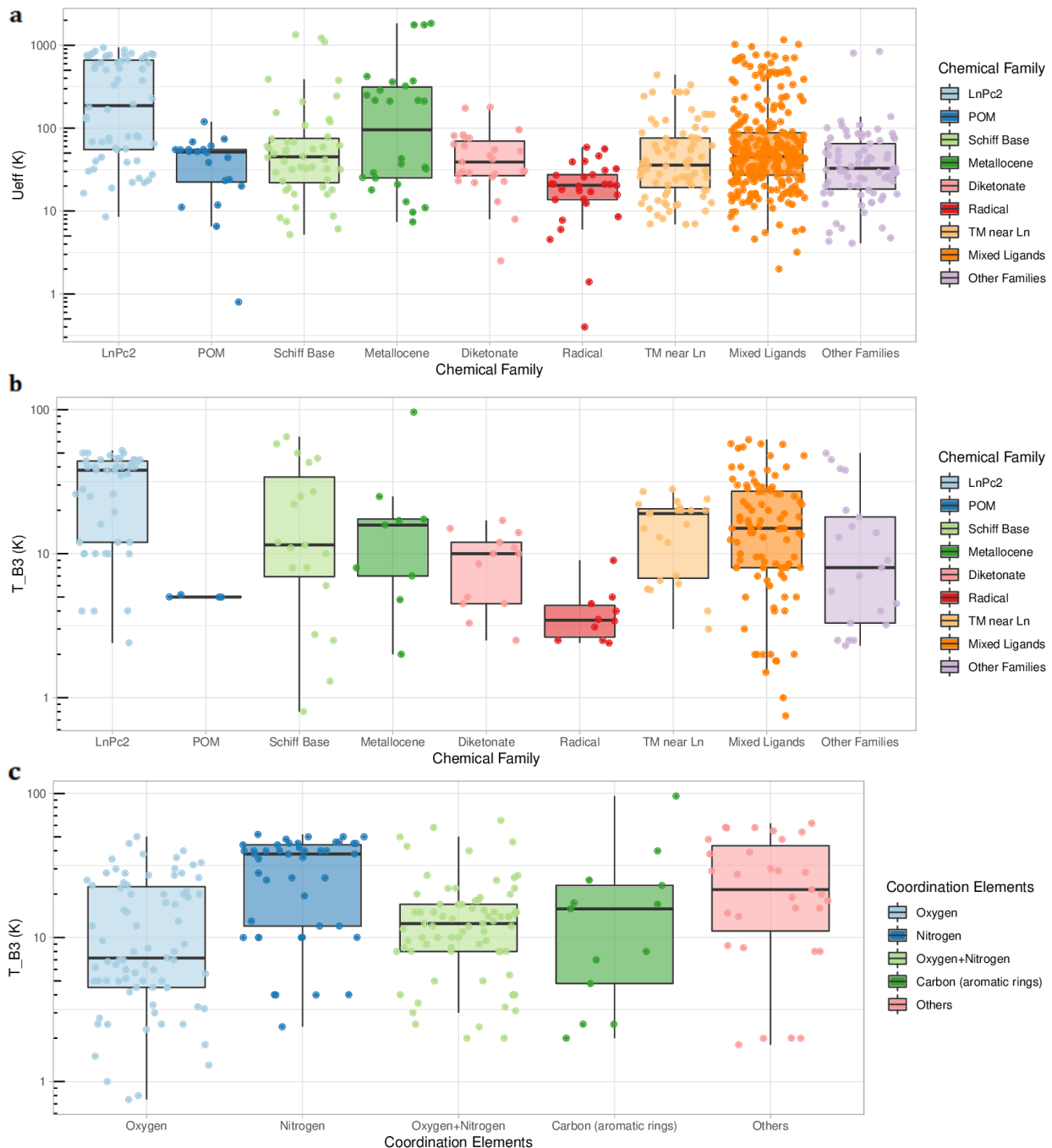
regressions between the two represented quantitative variables for each of the categorical classes. These variations can combine to hundreds of thousands of distinct meaningful plots.

The “BoxPlot” tab allows a different type of representation. One can plot the values of any of the quantitative variables *vs* any of the qualitative variables, for a total of 108 possible variable pairs producing distinct representations. The distribution of a single quantitative variable (*e.g.*  $U_{\text{eff}}$ ) is represented, showing the data points, the median, the low (first or Q1) quartile, upper (third or Q3) quartile, and whiskers. The upper whisker extends from the hinge to the largest value no further than 1.5xIQR from the hinge (where IQR is the interquartile range, or distance between the first and third quartiles). The lower whisker extends from the hinge to the smallest value at most 1.5xIQR of the hinge. This representation is done in parallel for different values of a qualitative variable, *e.g.* “Coordination Elements”. An advantage of these boxplots *vs* the more sophisticated scatterplots is a larger amount of data to be represented at any given time. Note that there is virtually no paper that contains simultaneously all the kinds of information recorded in the dataset. For example, only a minority of the papers have historically performed a full fit considering Orbach, Raman, quantum tunneling and/or direct mechanism of relaxation. This means that the scatter plots, by being restricted to samples where two particular quantitative data kinds are well defined, effectively work with less data, so while they enable us to extract more nuanced dependencies, inevitably some information is lost.

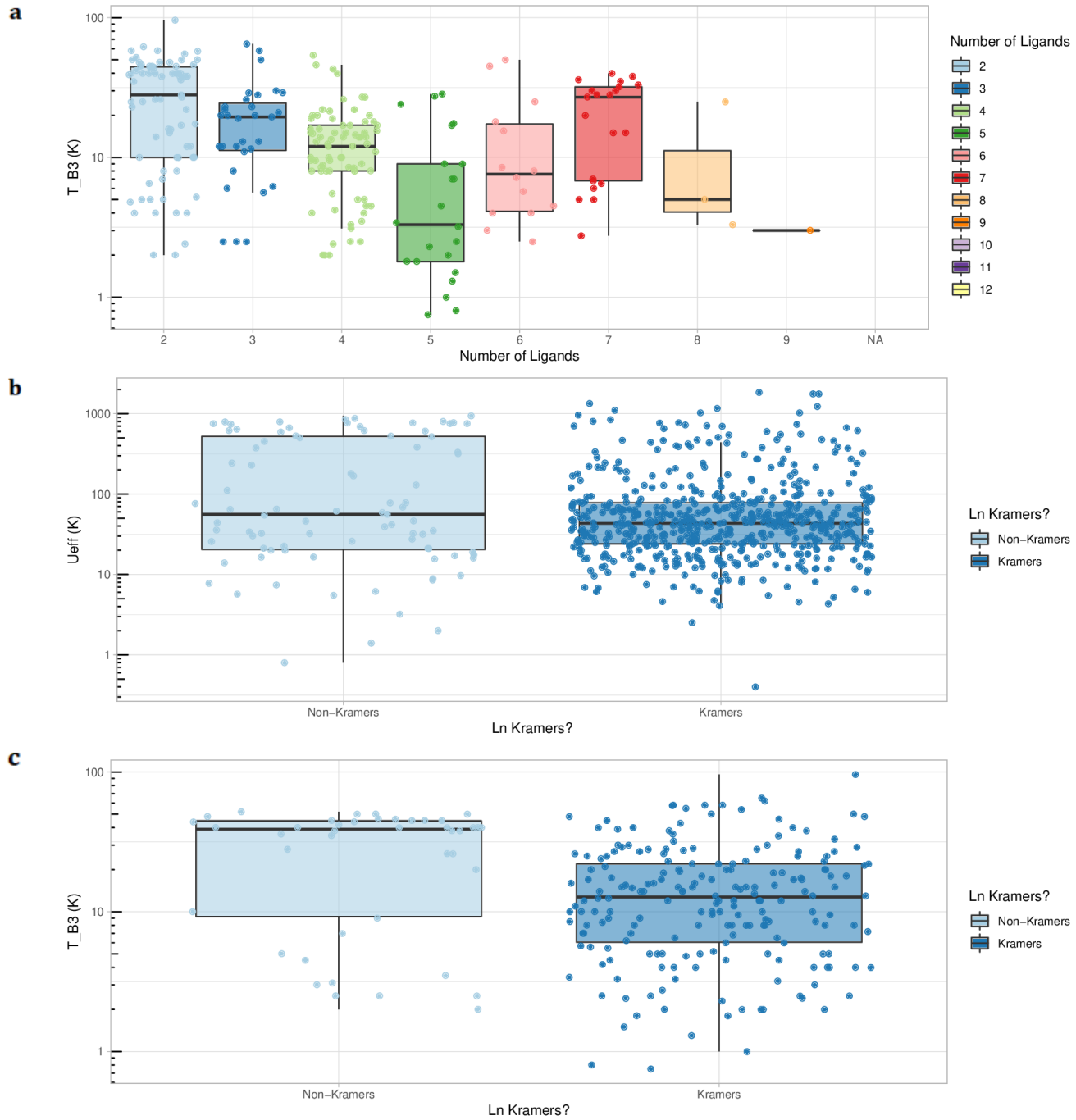
In the “BarCharts” tab, the different qualitative data types can be represented *vs* each other, for a total of 144 variable pairs producing distinct representations. Since qualitative information is available for almost all samples, bar charts contain almost all data points and allow for a quick frequency check of frequencies of different values in the dataset. Again, they provide a complementary mode of analysis of correlations. In our case, rather than the standard bar chart, SIMDAVIS employs stacked bar graphs meaning we can analyze the covariation of two variables, *e.g.*  $\text{Tb}^{3+}$  is more common in the SIM literature than  $\text{Er}^{3+}$ , but whereas this is especially true for the chemical families of “ $\text{LnPc}_2$ ” and “radicals”, the reverse trend is found for the metallocene family.

The “Data” tab contains a mini-menu with two options: it allows the user to download the raw dataset, and it allows the user to browse the data set. The browsing is interactive in different, complementary ways. First, it allows the user to select the columns to show, *e.g.* by default each entry just shows 7 columns of data, namely the sample ID, formula of the compound, its chemical family, the Ln ion, the coordination elements,  $U_{\text{eff}}$ , and the DOI of the article where the information was obtained, while the other 24 columns are hidden. Second, it allows the user to arrange the information by ascending or descending order of the chosen variable. Finally, it includes a search tool that filters for text strings in real time.

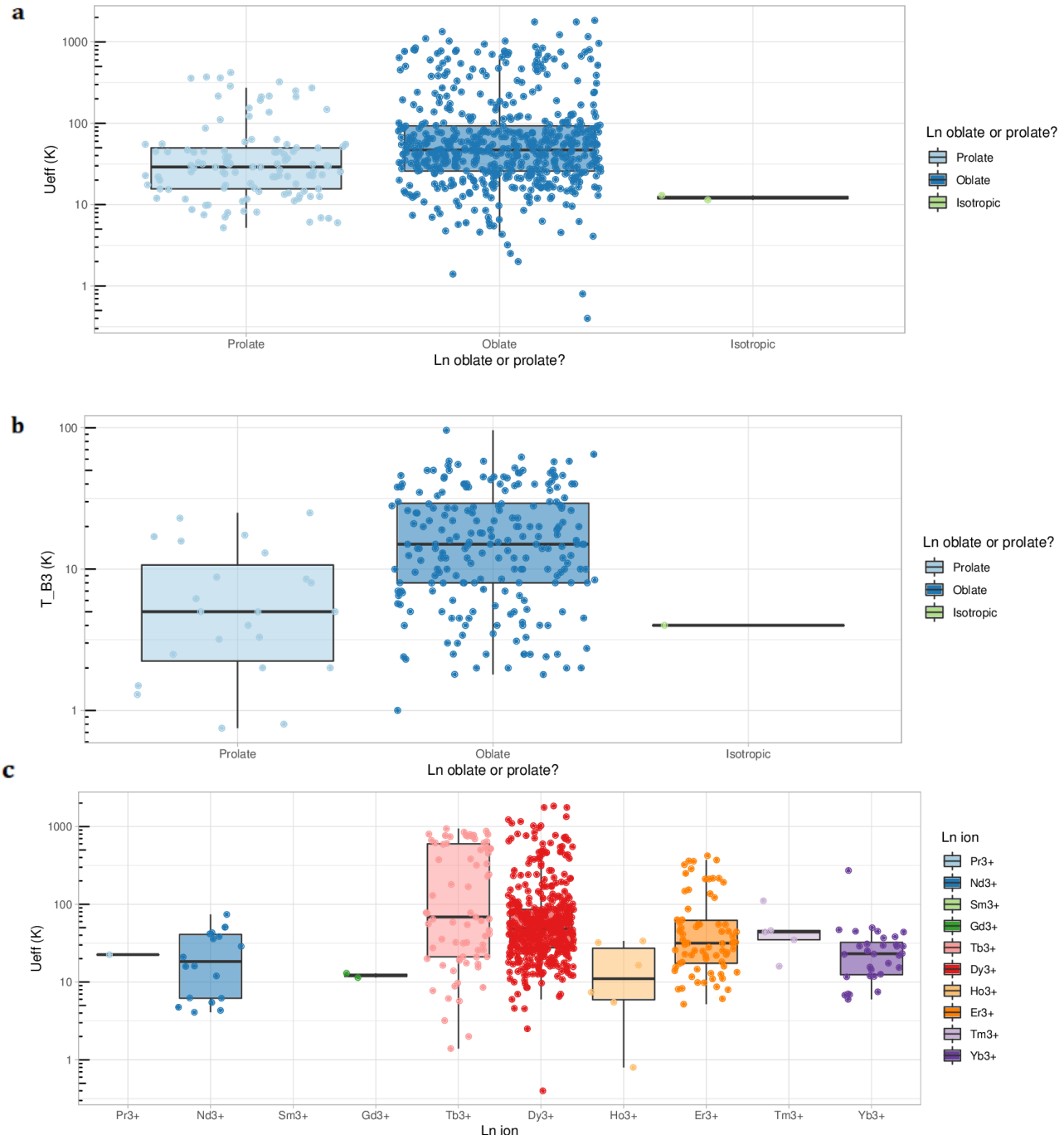
### 3.1. Gallery of SIMDAVIS graphs: chemical variables to optimize the physical properties



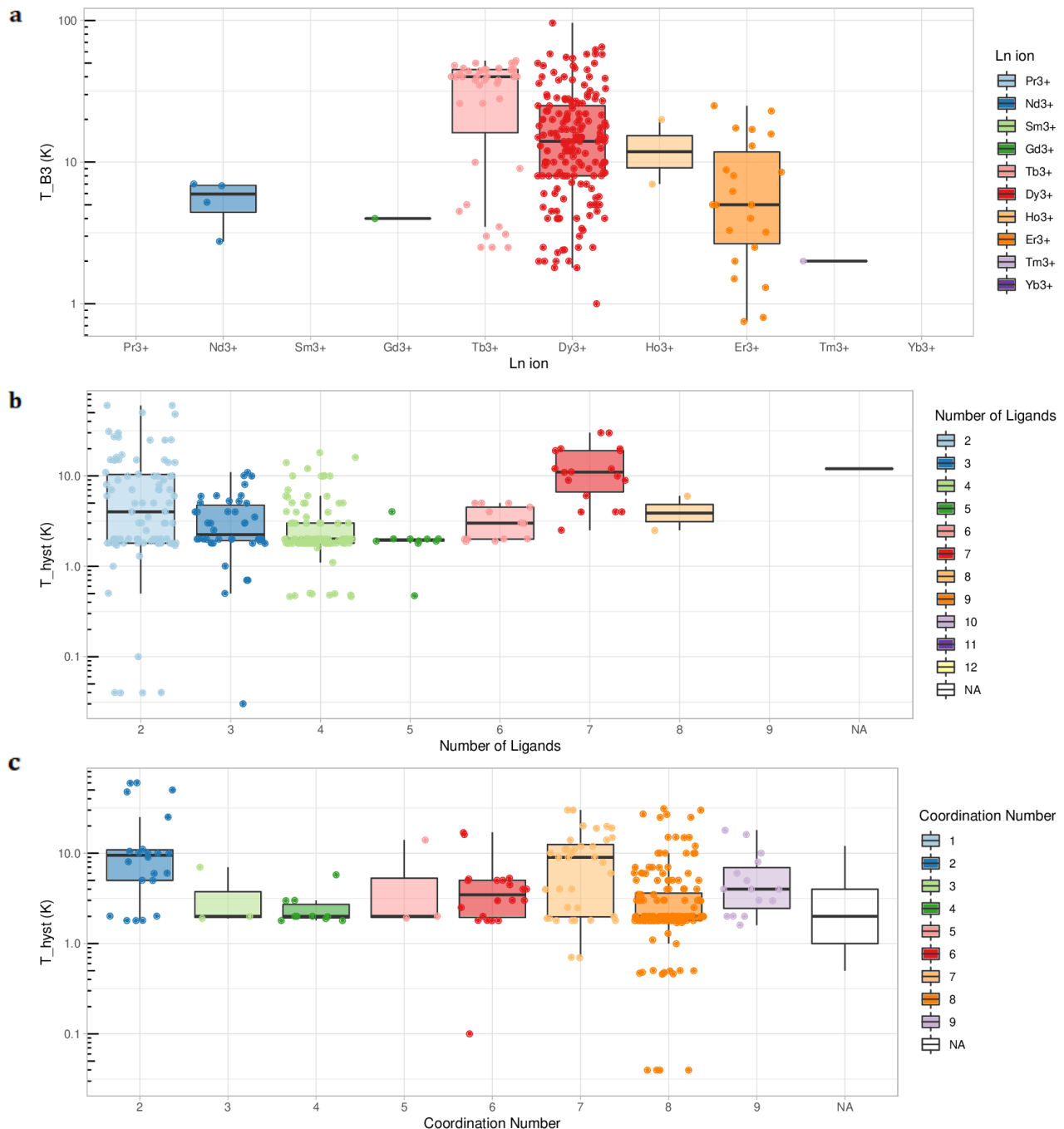
**Supplementary Figure 11.1 | Boxplots of physical variables vs chemical variables. a,  $U_{\text{eff}}$  vs chemical family. b,  $T_{\text{B}3}$  vs chemical family. c,  $T_{\text{B}3}$  vs coordination elements.**



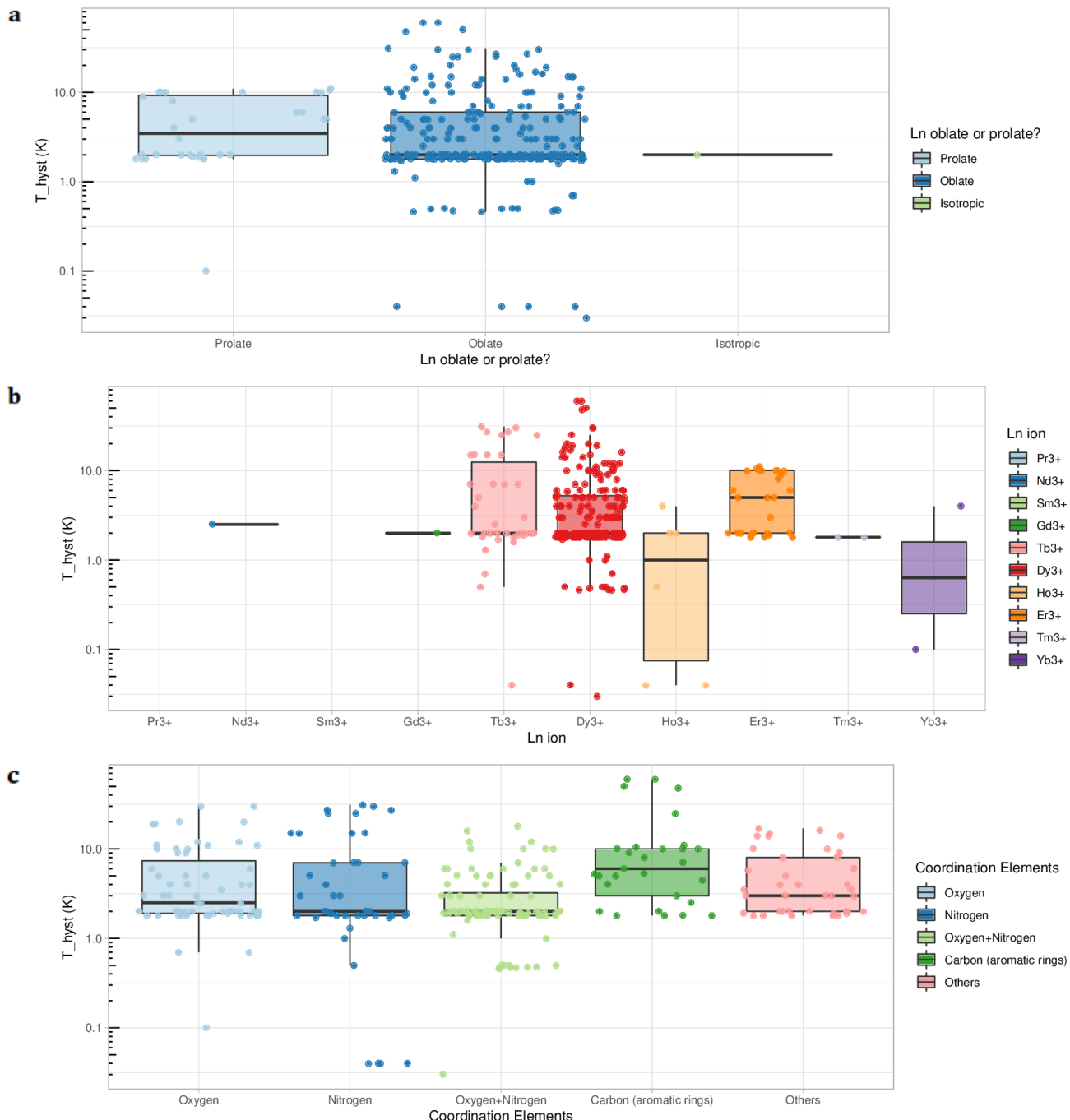
**Supplementary Figure 11.2 | Boxplots of physical vs chemical variables. a**,  $T_{B3}$  vs number of ligands. **b**,  $U_{eff}$  vs spin parity of the metal ion. **c**,  $T_{B3}$  vs spin parity of the lanthanide ion.



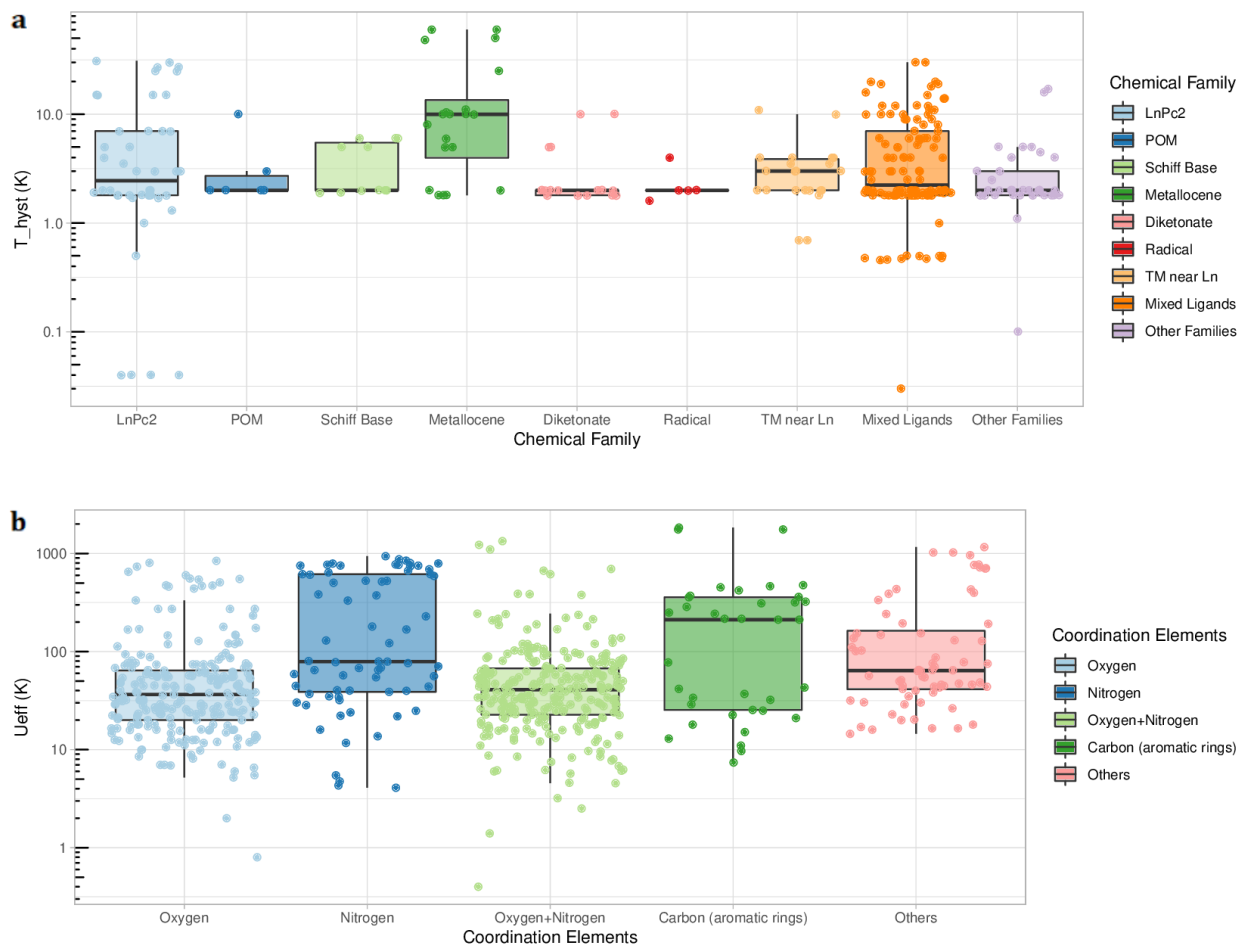
**Supplementary Figure 11.3 | Boxplots of physical vs chemical variables. a**,  $U_{\text{eff}}$  vs anisotropy of the lanthanide ion. **b**,  $T_{\text{B}3}$  vs anisotropy of the lanthanide ion. **c**,  $U_{\text{eff}}$  vs lanthanide ion.



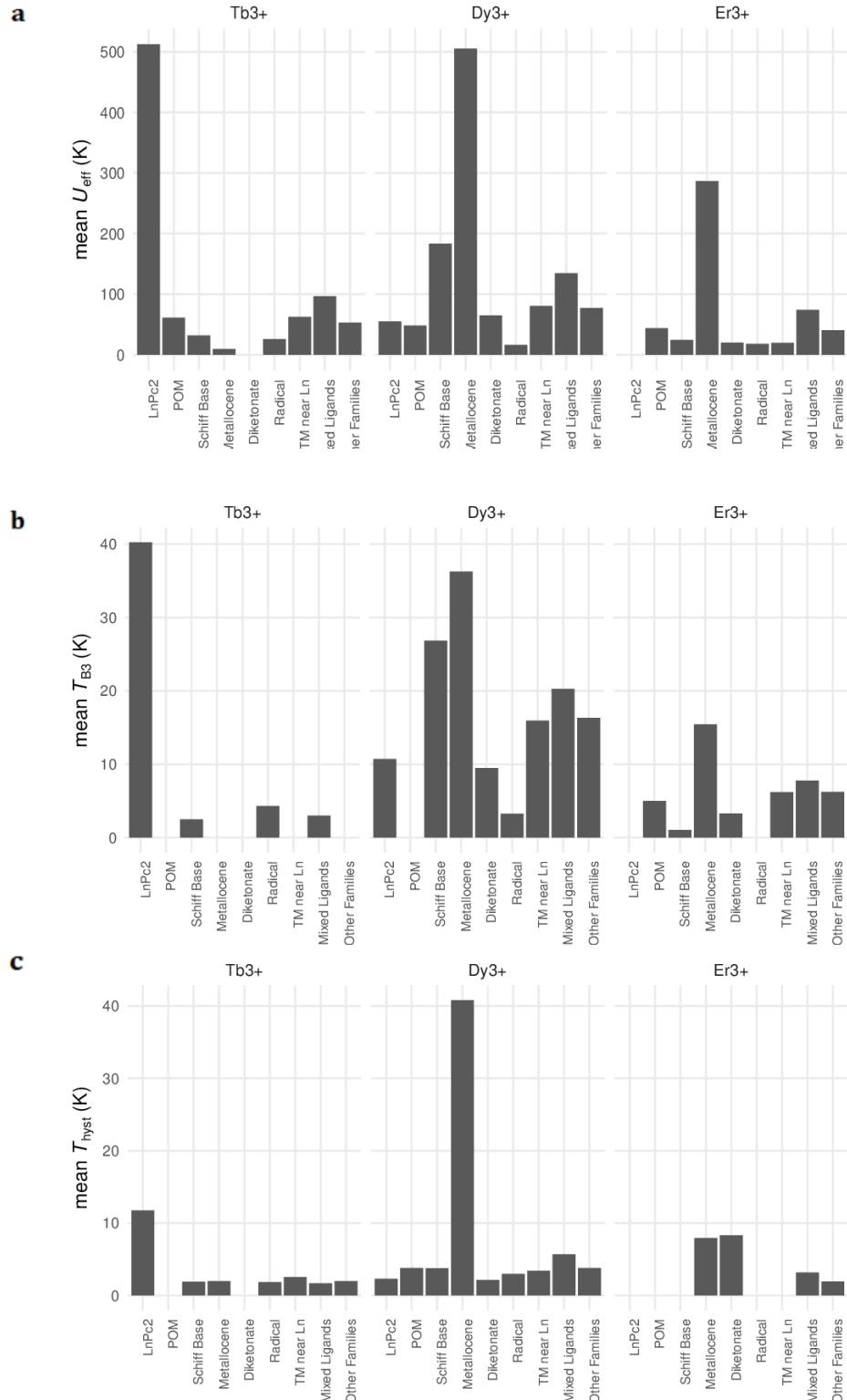
**Supplementary Figure 11.4 | Boxplots of physical vs chemical variables. a**,  $T_{B3}$  vs lanthanide ion. **b**,  $T_{hyst}$  vs number of ligands. **c**,  $T_{hyst}$  vs coordination number.



**Supplementary Figure 11.5 | Boxplots of physical vs chemical variables. a,**  $T_{\text{hyst}}$  vs anisotropy of the lanthanide ion. **b,**  $T_{\text{hyst}}$  vs lanthanide ion. **c,**  $T_{\text{hyst}}$  vs coordination elements.

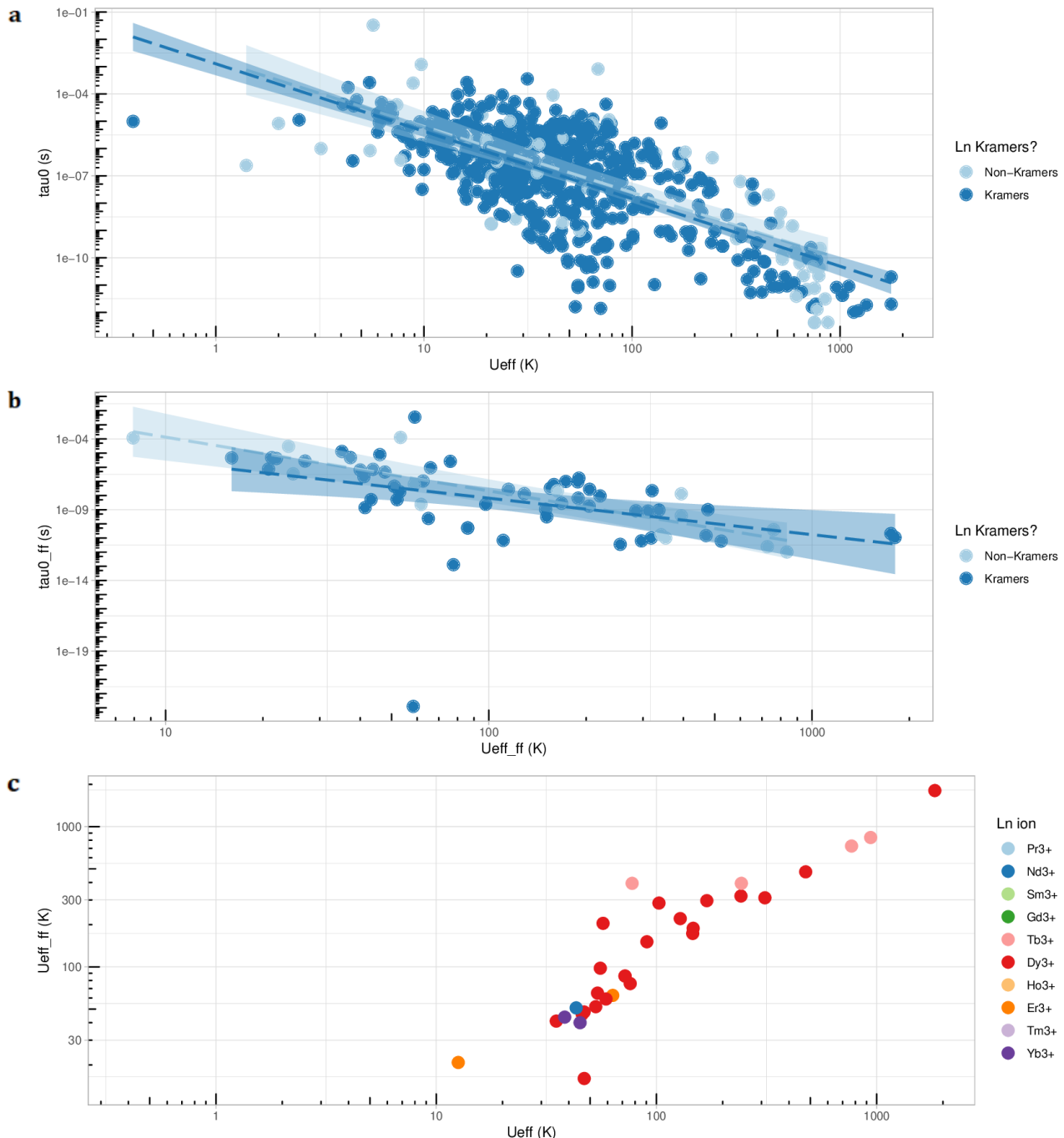


**Supplementary Figure 11.6 | Boxplots of physical vs chemical variables. a,  $T_{\text{hyst}}$  vs chemical family. b,  $U_{\text{eff}}$  vs coordination elements.**

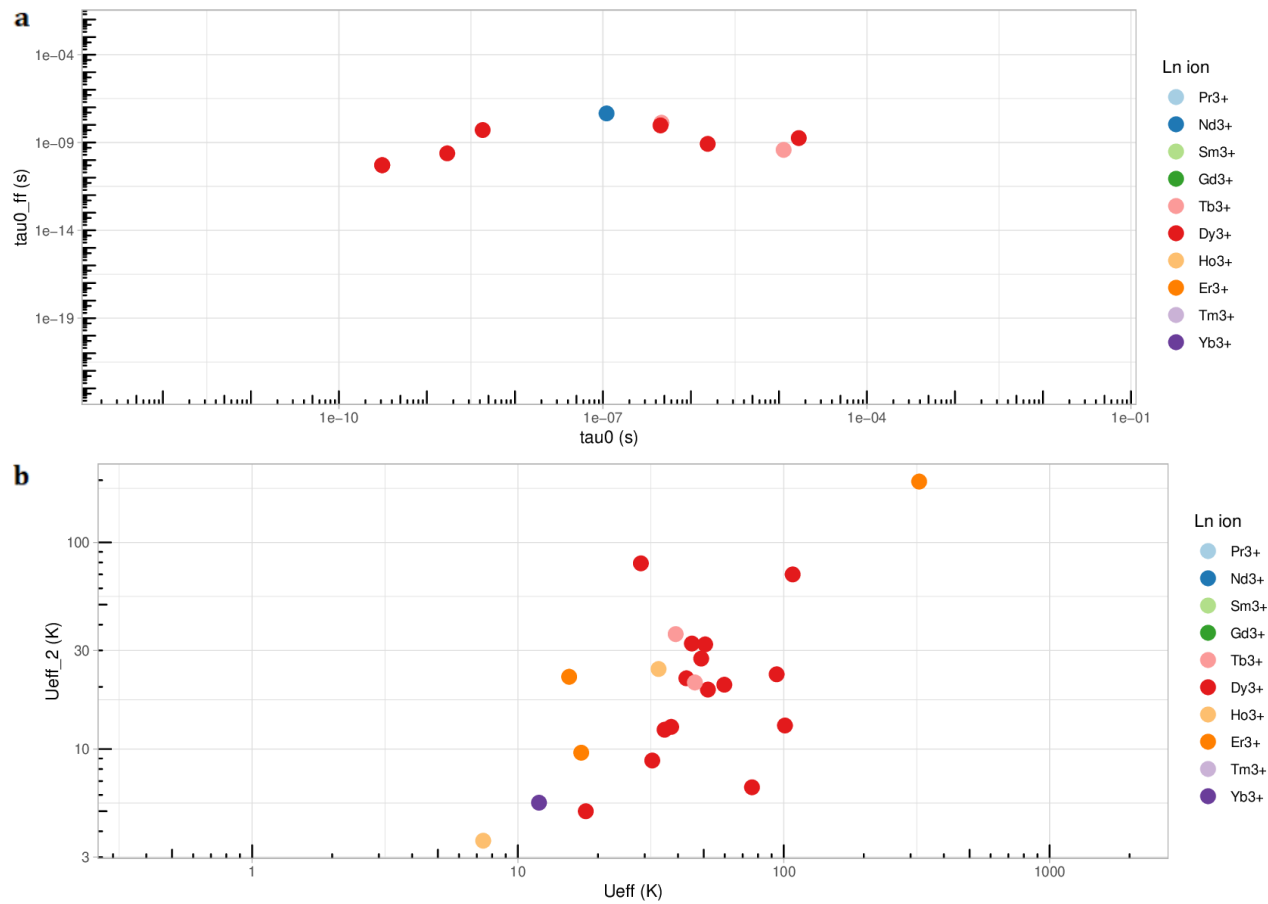


**Supplementary Figure 12 | Bar chart representations of the relation between Ln ion, chemical family and arithmetic mean of  $U_{\text{eff}}$ ,  $T_{\text{B}3}$  and  $T_{\text{hyst}}$ .** Bar charts showing the mean values for every combination of categories between the main metal ions  $\{\text{Tb}^{3+}, \text{Dy}^{3+}, \text{Er}^{3+}\}$  and all chemical categories. **a**,  $U_{\text{eff}}$ , **b**,  $T_{\text{B}3}$ , **c**,  $T_{\text{hyst}}$ .

### 3.2. Extended gallery of SIMDAVIS graphs: Arrhenius equation parameters



**Supplementary Figure 13.1** Scatterplot representations of the relation between  $U_{\text{eff}}$ ,  $U_{\text{eff,ff}}$ ,  $\tau_0$ ,  $\tau_{0,\text{ff}}$ . **a**,  $\tau_0$  vs  $U_{\text{eff}}$ , or Kramers and non-Kramers ions, with linear regressions; **b**,  $\tau_{0,\text{ff}}$  vs  $U_{\text{eff,ff}}$ , for Kramers and non-Kramers ions, with linear regressions; **c**,  $U_{\text{eff,ff}}$  vs  $U_{\text{eff}}$  for different lanthanide ions, with a visible linear behaviour.



**Supplementary Figure 13.2 | Scatterplot representations of  $\tau_{0,ff}$ ,  $U_{eff,2}$  vs  $\tau_0$ ,  $U_{eff,ff}$ .** **a**,:  $\tau_{0,ff}$  vs  $\tau_0$  for different lanthanide ions, with no discernible relation between the parameters; **b**,  $U_{eff,2}$  vs  $U_{eff}$  for different lanthanide ions, with no discernible relation between the parameters.

#### Supplementary Section 4. Statistical analysis of the chemical variables

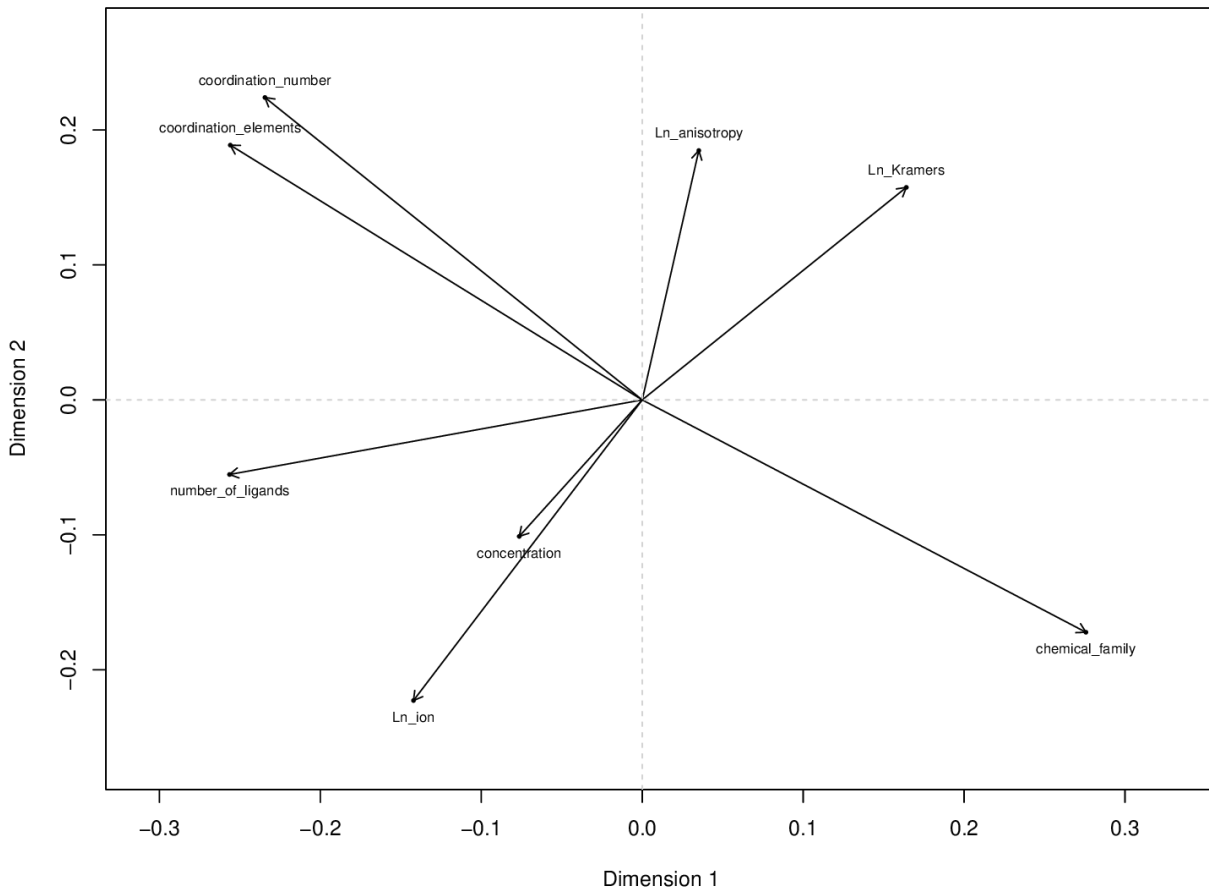
All qualitative results presented in this section considered the whole dataset containing data from literature from 2003 to 2019 for the analyses of chemical variables that follow. Additionally, we repeated the study with the data subset in the timeframe 2003-2017 (~1000 samples instead of ~1400), and the conclusions were robust, with no difference resulting from whether one considers the whole data set from 2003-2019 or only 2003-2017 subset. All quantitative numbers given herein are also consistent between the two studies, within a 5% difference. We can therefore conclude that the relations among the chemical variables are stable, *i.e.* no new trend has been revealed since 2017.

##### 4.1. Initial multiple correspondence analysis

Here we are striving to determine the existing statistical correlations among the chemical variables in the studied sample. This is necessary in order to avoid being misled later on by meaningless correlations between chemical design variables and physical behaviour. For example, we find that the variables “number of ligands” and “coordination elements” happen to be strongly correlated with each other, then it is likely that they will both display the same correlations with a given physical behaviour. In particular, one can expect that an “all-nitrogen coordination environment” will be strongly correlated with “number of ligands = 2”, and with “chemical family =  $\text{LnPc}_2$ ”, and relatively few other complexes in the dataset present only nitrogens as donor atoms. Therefore, if one obtains a correlation between a desirable physical behavior and “chemical family =  $\text{LnPc}_2$ ”, it would be unwarranted to deduce that this behavior can be obtained solely by employing an all-nitrogen coordination environment, or solely by preparing complexes with 2 ligands.

Correspondence Analysis (CA) or reciprocal averaging is a multivariate statistical technique that is employed for the graphical analysis of the dependence or independence of a set of categorical variables from data in a contingency table. It consists in summing up the information in the rows and columns so that it can be projected on a reduced subspace, and represent simultaneously the row and the column data, allowing to obtain conclusions about each pair of variables.

CA only requires data to be organized in categories. Since in our case there are more than two variables, we employed Multiple Correspondence Analysis (MCA). Different approaches for MCA have been proposed; we employed the widely used Gifi system.<sup>53</sup> This system consists of a set of multivariate methods developed around the Alternating Least Squares (ALS) algorithm. Among these methods, Homogeneity Analysis provides a model that is equivalent to MCA. ALS’s solution for Homogeneity Analysis is known as HOMALS. We employed the R homals package to obtain the following graphical representations.<sup>54</sup> Results are plotted in Supplementary Figs. 14, 15 and 16.



**Supplementary Figure 14 | Multiple Correspondence Analysis: minimal representation of each of the variable loadings on the two main dimensions.**

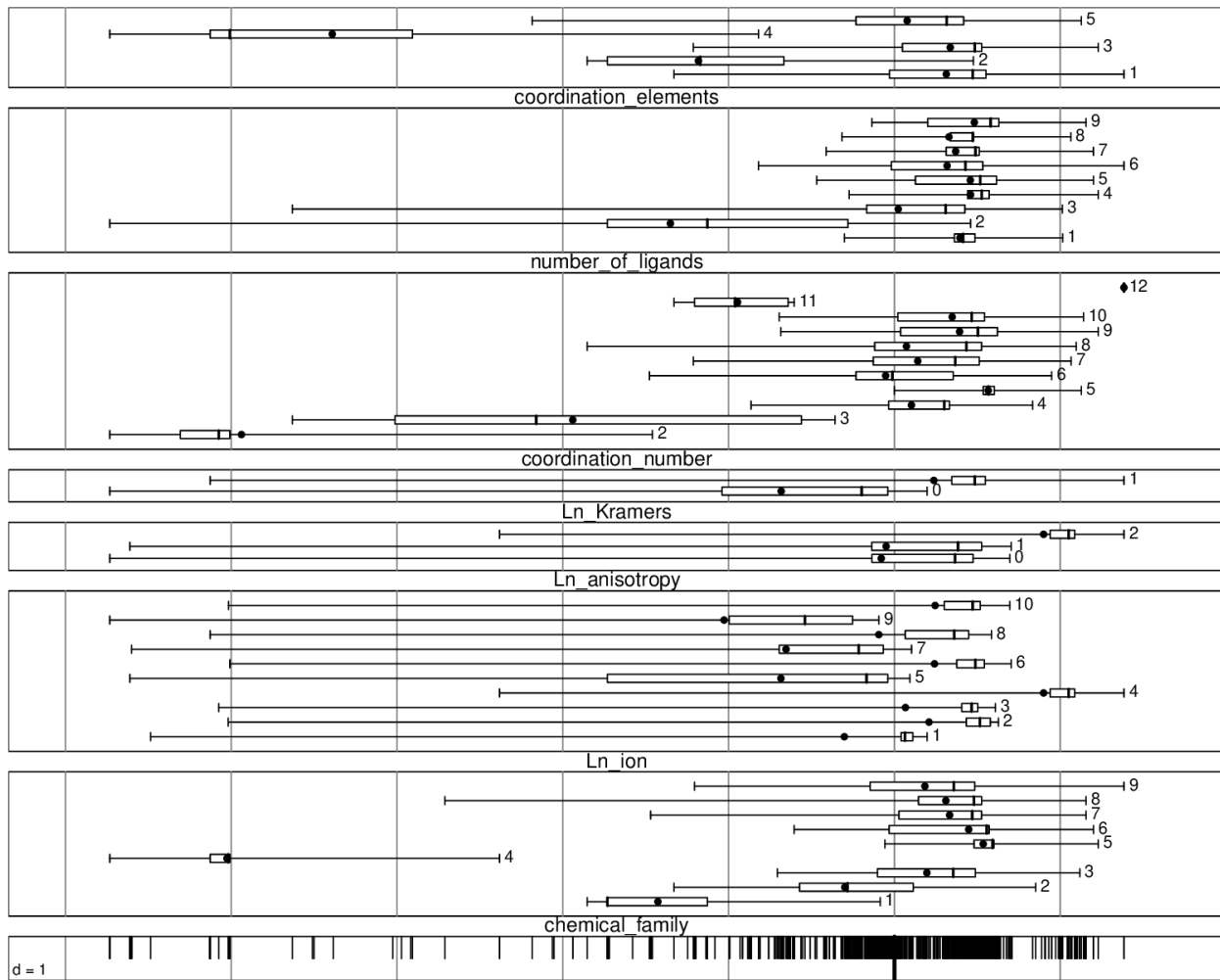
The graph in Supplementary Fig. 14 is read as follows: (i) the length of the vector approximates the variation within each variable, (ii) the cosine between two vectors approximates the correlation between two variables, *i.e.* parallel vectors correspond to perfectly correlated variables, (iii) the distance between the endpoints of two vectors approximates the dissimilarity between the two variables, (iv) the projection of each vector allows to order the data points for that variable. These two MCA dimensions will be employed to understand further analysis, in particular clustering studies. Supplementary Figures 15 and 16 are complementary to Supplementary Fig. 14, and allow for a more complete understanding.

We employed the R ade4 package<sup>55</sup> for MCA, which only allows the analysis of categorical variables, and obtained the results collected in Supplementary Table 1 for the correlation ratio of each variable.

**Supplementary Table 1 | Correlation ratio of each chemical variable with the two MCA dimensions.**

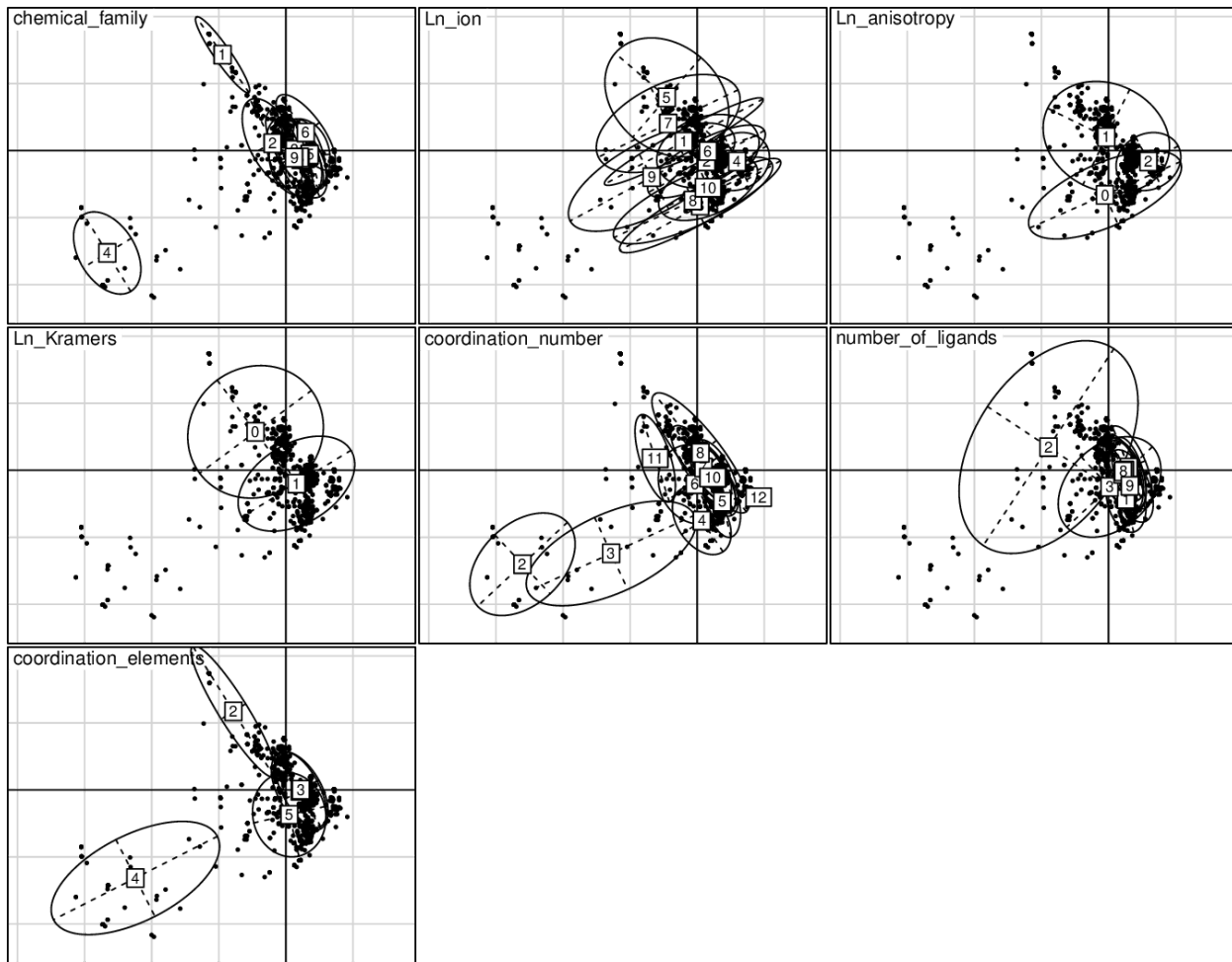
	RS1	RS2
chemical_family	0.81096423	0.6147058
Ln_ion	0.20607706	0.5364464
Ln_anisotropy	0.05097696	0.3121107
Ln_Kramers	0.16243450	0.2918366
coordination_number	0.62057925	0.3528815
number_of_ligands	0.47815893	0.1020615
coordination_elements	0.73301849	0.5353323

To achieve some clarity in the following data-rich representations, we assigned numerical labels to all categorical values as indicated in Supplementary Section 1. Employing these labels and within the same package we obtained the following complementary boxplot representation (Supplementary Fig. 15) that allows us to see the distribution of values, for each variable, along the axis defined by the MCA dimension 1. It is easy to see that the most extreme negative values of MCA dimension 1 are displayed by samples that have carbon or nitrogen as coordination elements, 2 ligands, CN = 2 or 3, as well as those of the metallocene chemical family. As significant positive values in MCA dimension 1, one needs to highlight  $\text{Gd}^{3+}$ , as well as isotropic complexes which are obviously the same ones.



**Supplementary Figure 15 | Boxplots for the distribution along the first MCA dimension of the different categorical values for the chemical variables.** See the numbering convention for the categories of the variables in Supplementary Section 1.

A further alternative representation, depicting the distribution of values for the different variables in the dataset as subsets of points was also done (Supplementary Fig. 16). This allows to locate the different values for each chemical variable in terms of positive and negative value ranges for the MC dimensions 1 and 2 simultaneously. At the same time, it allows us to observe overlap between chemical variables, *e.g.* CN = 2 or 3 are in overlap with the metallocene family and with coordination by carbon. Similarly, there is a significant overlap between the LnPc<sub>2</sub> family, complexes with 2 ligands, Ln = Tb and a coordination sphere formed by nitrogen atoms. As we will see in Supplementary Section 4.2, while this kind information points into a clear direction, specialised representations and statistical studies will allow us to study parameter association by clustering.



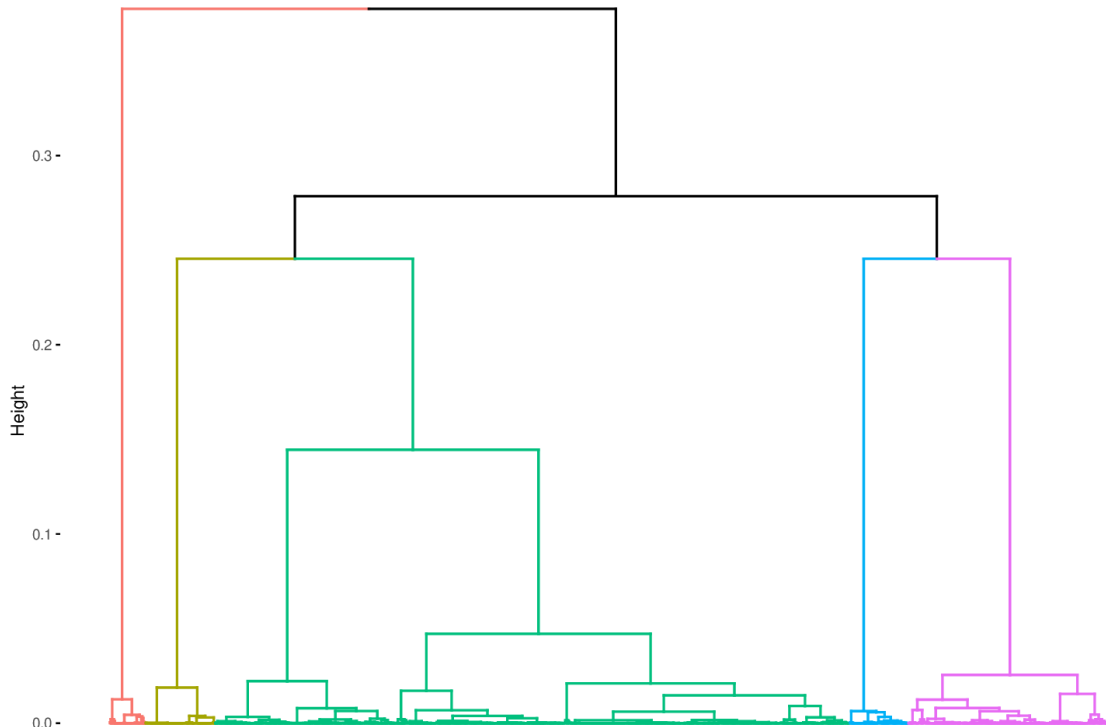
**Supplementary Figure 16 | Subsets for the different values of each of the seven categorical chemical variables in the plane of the two MCA dimensions.**

#### 4.2. Clustering studies for the chemical variables

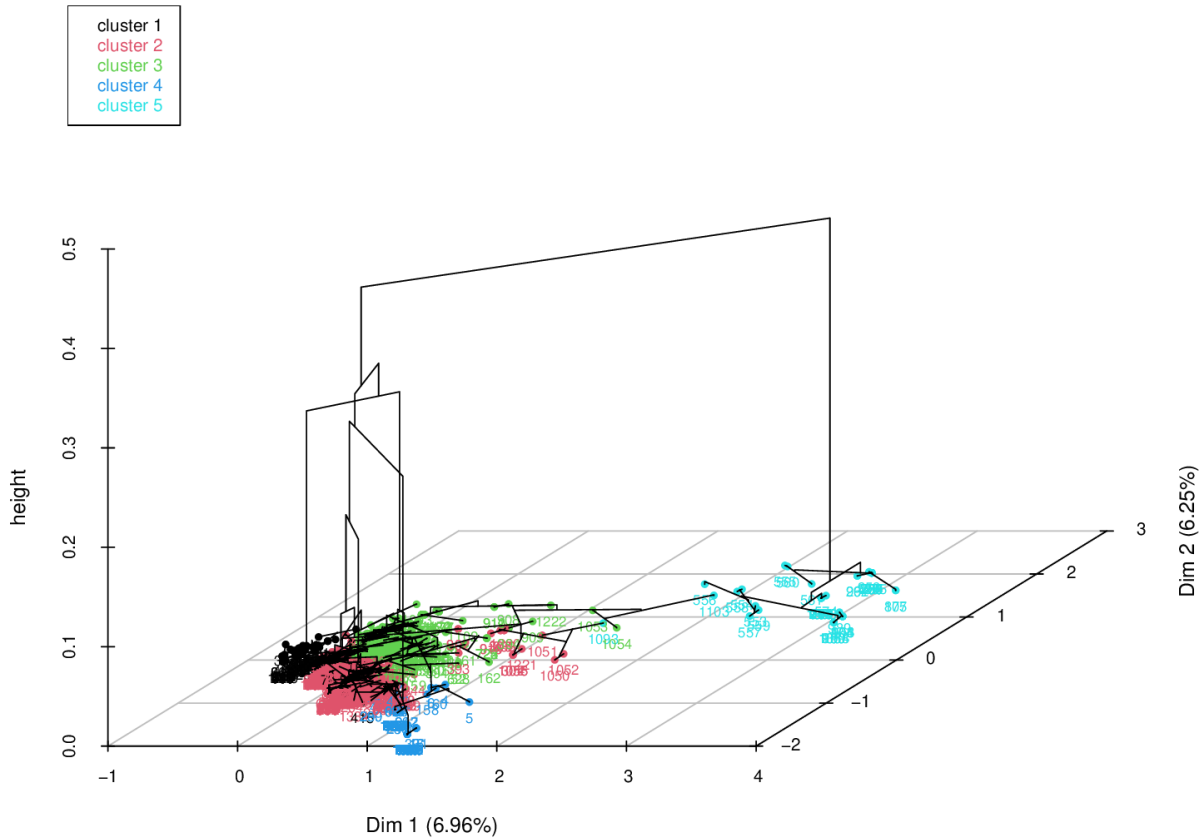
Clustering studies were performed as an independent test. In particular, we employ the package FactoMineR in R to perform the MCA.<sup>56</sup> This allows a graphical representation of the distances between individual samples and the relations between variables and their values. The goal in this case is to detect within the data types or profiles of data with similar characteristics. In other words, this procedure groups the values for the chemical parameter sets corresponding to individual measurements in families that present an overall similarity.

Due to the nature of our study, this is a crucial step since in practice chemical parameters are not homogeneously distributed as in a purely combinatorial approach. On the contrary, different research groups have chemical expertise in the preparation of different classes of compounds, and often, also evolving ideas on which design strategies would be more relevant for the desired physical property. This means that different research groups at different times focus on different chemical families and strategies for the molecular design of SIMs. As a result, the overall

number of samples (~1400) can be judiciously divided in a small set of hierarchical clusters which share certain common features, as a kind of molecular taxonomy. Again, this will help us put in context our findings: it is to be expected that, when finding a pattern or a magneto-structural trend, we will actually be seeing the behaviour of a cluster rather than the influence of an isolated parameter. Supplementary Figs. 17 and 18 show two different perspectives on the dendrogram resulting from the clustering.



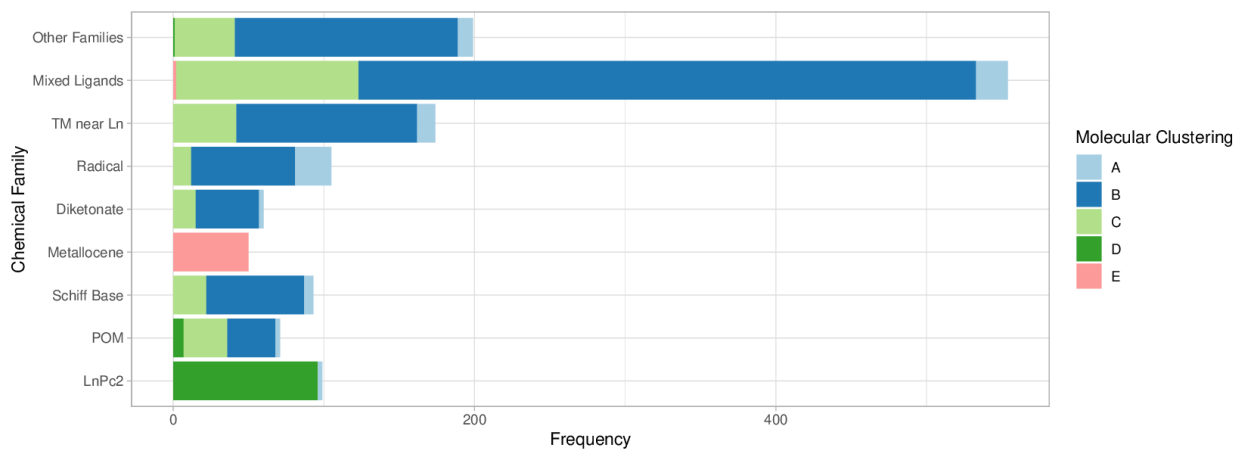
**Supplementary Figure 17 | Dendrogram visualization of the calculated hierarchical clustering on the factor map.**



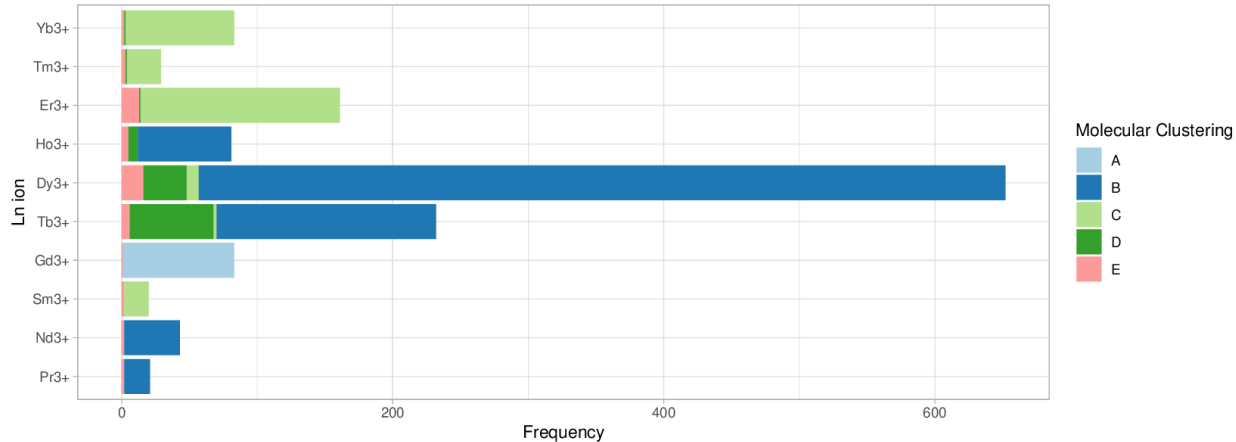
outside this Cluster (Supplementary Fig. 19.2). 60% of the samples in Cluster D are based on  $Tb^{3+}$ , 30% are based on  $Dy^{3+}$ .

-Cluster E, which is the smallest (3.7% of the samples), corresponds almost perfectly to the metallocene family and, like in Cluster D, the match with all-Carbon coordination, coordination number = 2, and number of ligands = 2 is weaker since some samples with these features are outside this cluster. The samples in Cluster E are more often based on prolate than oblate ions (~40% prolate), but significantly less so than in the total set (~20% prolate). This can be related with the fact that, while ~30% of samples in Cluster D are based on  $Dy^{3+}$ , this is much less than for the total dataset (~50% Dy).

**a**

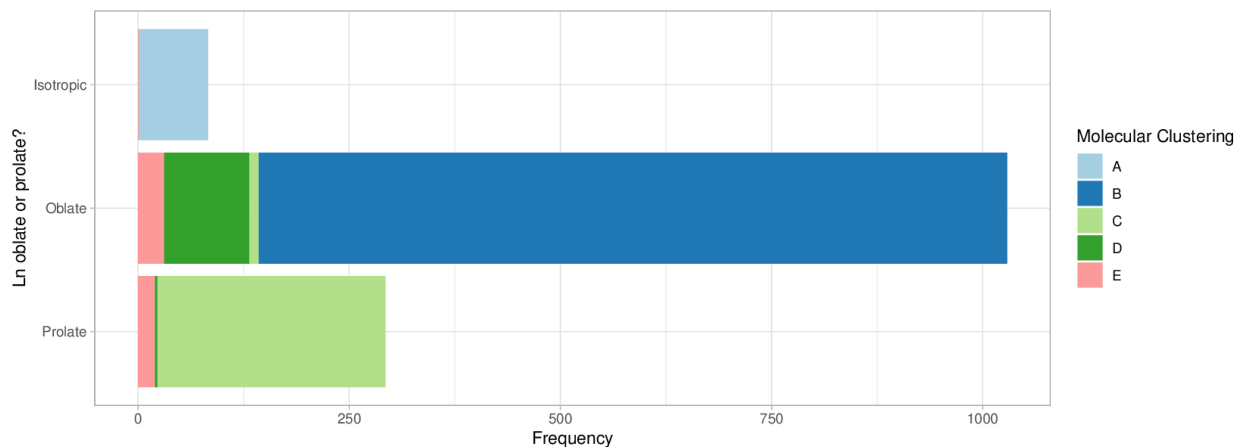
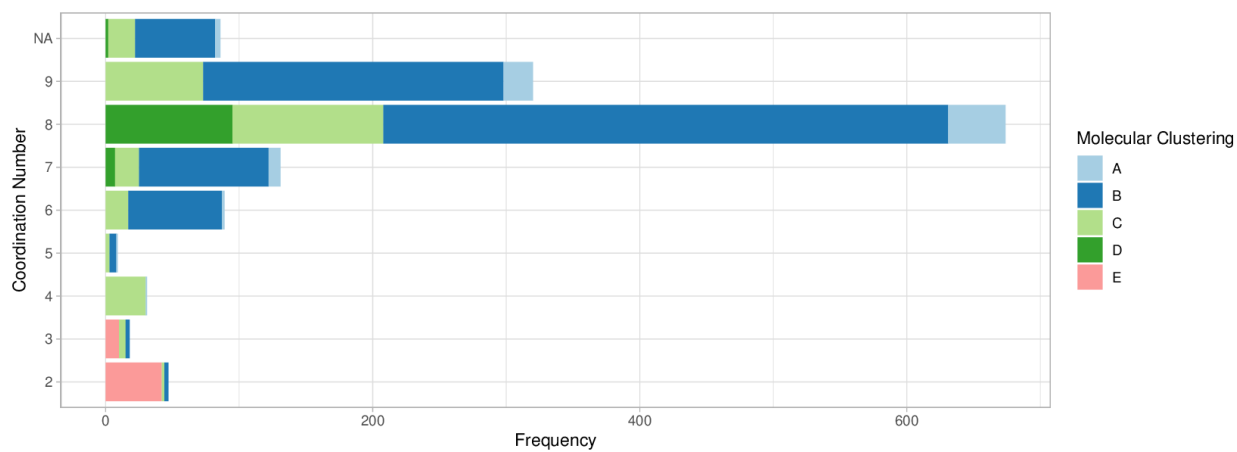
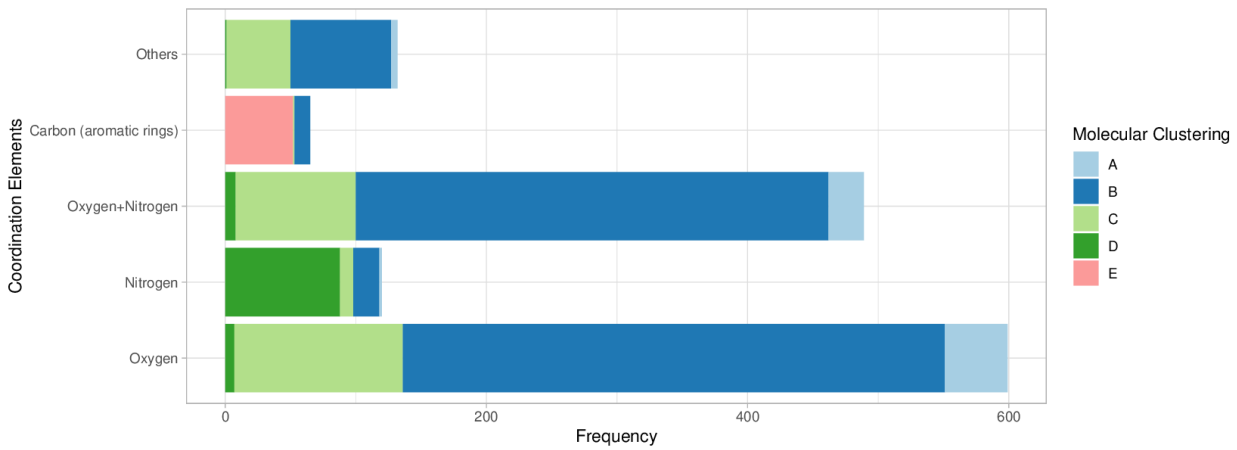


**b**



**Supplementary Figure 19.1 | Bar charts representing the frequencies of chemical variables, filled according to the molecular clustering described in this section. a, chemical families, b, Ln ions.**

Note that the dataset downloadable from the SIMDAVIS dashboard includes an alternate lower cut to the same hierarchical clustering mol\_cluster\_2, finding up to 7 distinct molecular clusters.

**a****b****c**

**Supplementary Figure 19.2 | Bar charts representing the frequencies of chemical variables, filled according to the molecular clustering described in this section. a, oblate vs prolate nature of the ion, b, coordination numbers, c, coordination elements.**

### 4.3. Lognormal modelling

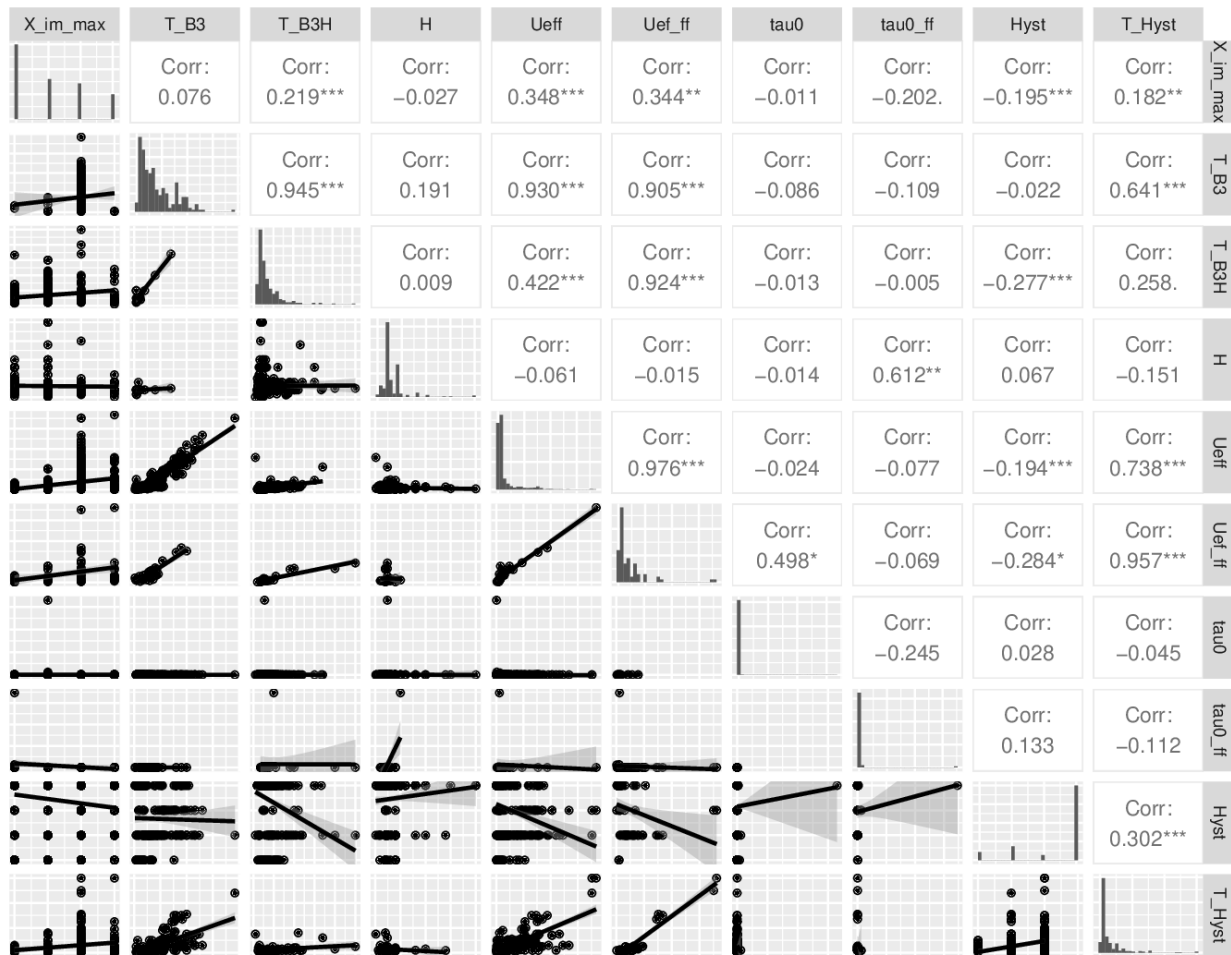
Finally, we applied a lognormal model to detect possible association between variables. The different factors within the model indicate the different associations between the studied variables and parameters. This model works with the frequencies of each variable in the crosstabulation. These frequencies result from each combination of variables, so Poisson's distribution was employed. For any modelization one needs to declare the link function: a function of the expected value of the dependent variable, taking the form of a linear combination of the independent variables. For lognormal modelling, we do not distinguish between dependent and independent variables, since one is rather interested in associations between variables, but one does have a link function which unites the average frequency with the linear predictor, which in this case is the logarithmic function. Within the chemical variables we have many categorical ones, with many levels each. To avoid a useless complication of the analysis, we start by studying the relation between the lanthanide ion, its anisotropy and spin parity (Kramers or not). This serves solely as a test for the modelling and the integrity of our data, since we know that these are associated beforehand: for every lanthanide ion, its anisotropy type and Kramers nature is well defined, with no exceptions. As expected, our model found that it is sufficient to work with the lanthanide ion, and we discarded the other two variables for the subsequent clustering studies. We proceeded to use lognormal models, introducing the rest of the chemical variables, one by one, together with the lanthanide ion. We found that the chemical family, lanthanide ion and coordination elements are the main variables and sufficient to reasonably explain the frequencies of the rest of the variables.

### Supplementary Section 5. Statistical analysis of the physical variables

For all the statistical analyses of the physical variables that follow in Supplementary Sections 5.1 and 5.3, additionally to the analyses performed for the complete dataset (data from years 2003-2019), we repeated the study with the data subset in the timeframe 2003-2017 (~1000 samples instead of ~1400). All qualitative results presented here are robust whether one considers the whole dataset 2003-2019 or the 2003-2017 subset. Each of the weak numerical correlations indicated in Supplementary Fig. 20 are stable within a 0.2 window, and in particular all correlations higher than 0.9 are stable with deviations within 0.05 window between both subsets. All values for the Akaike Information Criterion (AIC) in Supplementary Tables 2, 3, 4 are higher on average by about a factor of 1.5-2, as expected, since they are roughly proportional to the number of samples.<sup>57</sup> We can therefore conclude that the quantitative and qualitative relations among the physical variables are stable, *i.e.* no new significant trends have been revealed recently.

## 5.1. Overview of the main statistical relationships

Here, our goal is to identify statistical relationships among the physical variables. At first, we want to confirm whether the simple model parameters  $U_{\text{eff}}$ ,  $U_{\text{eff},2}$ ,  $\tau_0$  are good statistical predictors (*i.e.* present a high correlation with) of the experimental behavior. In particular, whether they are good predictors of  $T_{\text{B3}}$ ,  $T_{\text{B3H}}$ ,  $T_{\text{hyst}}$ ,  $H$ ,  $\chi_{\text{im,max}}$  and “Hyst”. Next, we want to determine whether the predictive power is different between  $U_{\text{eff}}$  vs  $U_{\text{eff,ff}}$ , and  $\tau_0$  vs  $\tau_{0,ff}$ . Supplementary Fig. 20 represents graphically all physical variables, with their relationships in pairs;  $U_{\text{eff},2}$  was eliminated from the graph since the scarcity of data produced errors in the correlation test.



**Supplementary Figure 20 | Statistical relationships among the physical variables.** The diagonal shows the frequency of each value (range) for each of the physical variables. Below the diagonal we see graphical representations to visually show the relation between every pair of variables, and above the diagonal we find the quantification of each correlation, in the case of numerical variables, or an alternate boxplot, in the case of categorical variables.

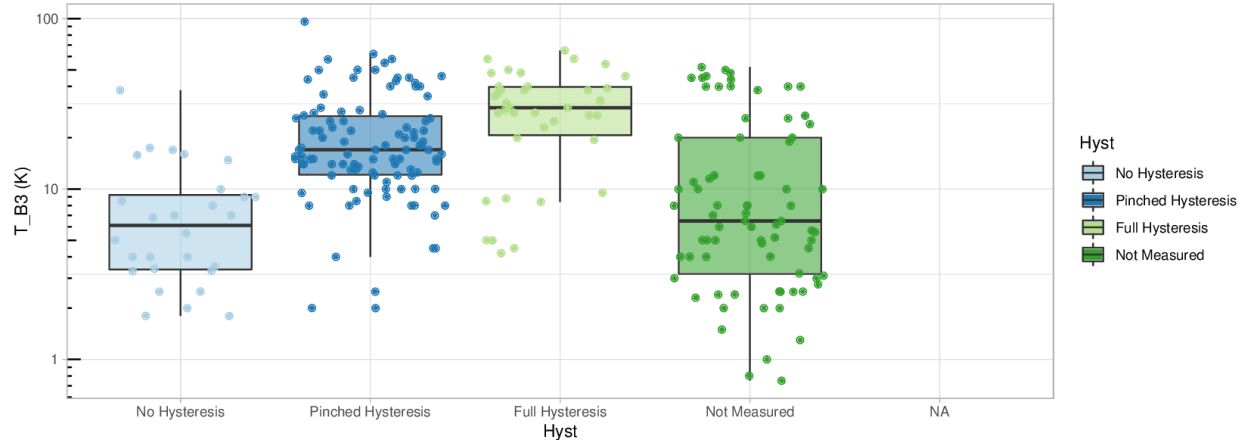
Let us first go over this bidimensional array of statistical representations and analyses, and later on we will focus on the most significant pieces of information.

Keeping in mind the definition of  $\chi_{\text{im},\text{max}}$  (Supplementary Section 1), the properties as SIM are better when  $\chi_{\text{im},\text{max}}$  takes higher numbers ( $0 < 1 < 2$ ), *e.g.* only the samples with  $\chi_{\text{im},\text{max}} = 2$  present values for  $T_{\text{B}3}$ , while  $\chi_{\text{im},\text{max}} = 3$  means having no information. The most frequent value is  $\chi_{\text{im},\text{max}} = 0$  (Freq-independent  $\chi''$ ), with the rest being similarly abundant. For  $T_{\text{B}3}$  and  $T_{\text{B}3\text{H}}$ , higher temperature values are associated with higher values of  $\chi_{\text{im},\text{max}}$ . Higher effective energy barriers  $U_{\text{eff}}$ ,  $U_{\text{eff},2}$ ,  $U_{\text{eff,ff}}$  were estimated for  $\chi_{\text{im},\text{max}} = 3$  (corresponding to cases where the SIM properties are not necessarily bad, but just were not characterised via  $\chi''$  vs T plots) and especially for  $\chi_{\text{im},\text{max}} = 2$  (as expected), compared with systems with worse properties, where almost no difference is found between  $\chi_{\text{im},\text{max}} = 0$  and  $\chi_{\text{im},\text{max}} = 1$ . As in the case of the effective energy barriers, higher hysteresis temperatures  $T_{\text{hyst}}$  were reported for  $\chi_{\text{im},\text{max}} = 3$ , and especially for  $\chi_{\text{im},\text{max}} = 2$ , as expected, compared with systems with worse properties.

The temperatures of the maximum in  $\chi''$  at  $10^3$  Hz are labelled as  $T_{\text{B}3}$  (when no magnetic field is applied) and  $T_{\text{B}3\text{H}}$  (when a magnetic field  $H$  is applied). There are more cases reported in presence of a magnetic field. In both cases, there is a distribution similar to an inverse exponential, meaning higher temperatures are less frequent, but this is more marked for  $T_{\text{B}3\text{H}}$ : when a magnetic field is applied to detect a maximum in  $\chi''$ , high temperature values for this maximum are rare. Higher values of the magnetic field  $H$  do not correlate with higher values of  $T_{\text{B}3\text{H}}$ . There is a marked difference in the correlations of the temperatures  $T_{\text{B}3}$ ,  $T_{\text{B}3\text{H}}$  with the effective energy barriers  $U_{\text{eff}}$ ,  $U_{\text{eff,ff}}$ . While there is a very strong correlation between  $T_{\text{B}3}$  and  $U_{\text{eff}}$ , for  $T_{\text{B}3\text{H}}$  the correlation only exists for  $U_{\text{eff,ff}}$ . This is consistent with the presence of other relaxation mechanisms in these cases, such as the QTM, which are quenched in presence of a strong field. In contrast with the effective energy barriers, there are no significant correlations between  $T_{\text{B}3}$ ,  $T_{\text{B}3\text{H}}$  and  $\tau_0$ ,  $\tau_{0,\text{ff}}$ . This is initially puzzling, since each pair of effective energy barrier and preexponential time are extracted from a single fit (Supplementary Section 5.3). Finally, there is a systematic qualitative improvement of the hysteretic behaviour with higher values of  $T_{\text{B}3}$ ,  $T_{\text{B}3\text{H}}$ . In other words, high values of  $T_{\text{B}3}$ , meaning short-term (millisecond) magnetic memory up to a high temperature, are frequently associated with the presence of hysteresis. Moreover, within cases with hysteresis, short-term magnetic memory up to a high temperature is associated with the presence of full hysteresis rather than pinched hysteresis. While this cannot be clearly seen in Fig. 20, it is evident in Fig. 21. In contrast, the quantitative correlation of the hysteretic temperature  $T_{\text{hyst}}$  with higher values of  $T_{\text{B}3}$ ,  $T_{\text{B}3\text{H}}$  is relatively weak in the case of  $T_{\text{B}3}$ , and nonexistent for  $T_{\text{B}3\text{H}}$ .

$H$  is the external magnetic field applied to measure  $T_{\text{B}3\text{H}}$ . It presents very weak (and negative) correlations with the effective energy barriers (both  $U_{\text{eff}}$  and  $U_{\text{eff,ff}}$ ). High values of  $U_{\text{eff}}$  are visibly correlated with the sample presenting hysteresis ( $\text{Hyst} = 1$ ), and within it, with samples

presenting coercivity (Hyst = 2). These correlations are stronger in the case of  $U_{\text{eff,ff}}$ . The attempt times  $\tau_0$  and  $\tau_{0,\text{ff}}$  are however very poorly correlated, both with their corresponding barriers and with the other properties. As we will see in Supplementary Section 5.3, this is probably due to the high dispersion in values: at least a qualitative correlation is visible when one works on a logarithmic scale.



**Supplementary Figure 21 | Boxplots of  $T_{\text{B}3}$  grouped by categories of hysteretic behaviour.**

## 5.2. Simple frequency distributions

Let us start by examining the individual frequency distributions of  $T_{\text{B}3}$ ,  $T_{\text{B}3\text{H}}$ ,  $U_{\text{eff}}$ ,  $U_{\text{eff,ff}}$  and  $T_{\text{hyst}}$ , *i.e.* the five single-variable bar chart representations of their distribution of values throughout the population (diagonal graphics in Supplementary Fig. 20). In all cases, an initial visual inspection evidences a roughly inverse exponential decay, or perhaps a gaussian distribution centered around very small values. This can be interpreted as a mostly random distribution of values, a signal that the studied population is large and mostly unbiased. An interesting exception can be found in  $T_{\text{B}3}$ , which takes a bimodal distribution. This has different possible interpretations, but likely just means that a fraction of the research in the field was focused on types of compounds where the median of  $T_{\text{B}3}$  is at or above the maximum values of the other chemical families, *i.e.* the  $\text{LnPc}_2$  family, see Supplementary Fig. 11.1, where it can be compared with the much less marked difference in the case of  $U_{\text{eff}}$ , where the distribution of the  $\text{LnPc}_2$  family is less skewed to very high values.

## 5.3. Correlations between physical variables

As can be seen in Supplementary Fig. 20, the highest correlations involve  $U_{\text{eff}}$  and  $U_{\text{eff,ff}}$ .  $U_{\text{eff}}$  is highly correlated with  $T_{\text{B}3}$  and with  $T_{\text{hyst}}$ .  $U_{\text{eff,ff}}$  is highly correlated with  $U_{\text{eff}}$ ,  $T_{\text{B}3}$  and  $T_{\text{B}3\text{H}}$ . Furthermore, we apply Pearson's test to verify the correlation between  $U_{\text{eff}}$  and  $U_{\text{eff,ff}}$ . We obtained a very robust correlation between the two variables, with a p-value  $< 2.2 \cdot 10^{-16}$ , a 95% confidence interval for the correlation of 0.951-0.989 and an estimated correlation of 0.976. The

same procedure is applied to  $U_{\text{eff}}$  and  $U_{\text{eff},2}$ , obtaining results that are robust but substantially less so: p-value  $< 1.113 \cdot 10^{-7}$ , with a 95% confidence interval for the correlation of 0.701-0.941 and an estimated correlation of 0.864.

We apply the Akaike Information Criterion (AIC), a well-established method that evaluates how well a statistical model fits the data it was generated from. This method allows to compare the quality of a series of candidate models using the same data, so that the AIC estimates the quality of each of the models relative to the others. As the models are used to represent the process that generated the data, this representation will be losing some information because of the flaws of the model, and the AIC estimates the relative amount of information lost by each candidate model. This means, the preferred model will have the lowest AIC value in a given set of candidate models. To implement AIC, we employ the R functions `lm`, `glm` with `family = binomial` (stats package from R base)<sup>58</sup>, and `multinom` (nnet package).<sup>59</sup> The results can be found in Supplementary Tables 2, 3 and 4.

**Supplementary Table 2 | AIC modelling experimental physical (response) variables as a function of modelling variables  $U_{\text{eff}}$ ,  $U_{\text{eff},2}$ ,  $\tau_0$ .**

Response variable	Data points	Variables included in the model	Significant variable	AIC
$\chi''_{\text{max}}$	23	$U_{\text{eff}}$ , $U_{\text{eff},2}$ , $\tau_0$	-	55.04
		$U_{\text{eff}}$ , $U_{\text{eff},2}$	-	49.04
		$U_{\text{eff}}$ , $\tau_0$	-	65.52
		$U_{\text{eff},2}$ , $\tau_0$	-	55.62
$T_{\text{B3}}$	4	-	-	-
$T_{\text{B3H}}$	14	$U_{\text{eff}}$ , $U_{\text{eff},2}$ , $\tau_0$	$\tau_0$	2.64
		$U_{\text{eff}}$ , $U_{\text{eff},2}$	-	35.35
		$U_{\text{eff}}$ , $\tau_0$	$\tau_0$	0.98
		$U_{\text{eff},2}$ , $\tau_0$	$\tau_0$	4.25
		$\tau_0$	$\tau_0$	2.27
Hyst	23	$U_{\text{eff}}$ , $U_{\text{eff},2}$ , $\tau_0$	-	44.49
		$U_{\text{eff}}$ , $U_{\text{eff},2}$	-	40.49
		$U_{\text{eff}}$ , $\tau_0$	-	40.56
		$U_{\text{eff}}$	-	36.56
		$U_{\text{eff},2}$ , $\tau_0$	-	43.13
$T_{\text{hyst}}$	4	-	-	-

Supplementary Table 2 contains the analysis based on the modelling variables  $U_{\text{eff}}$ ,  $U_{\text{eff},2}$  and  $\tau_0$ . The analysis quantifies the models employing these three variables to explain the different response variables:  $\{\chi''_{\text{max}}, T_{\text{B3}}, T_{\text{B3H}}, \text{Hyst}, T_{\text{hyst}}\}$ . The results are heterogeneous. Depending on

the response variable chosen, the best modelling variables can be either  $\{U_{\text{eff}}, U_{\text{eff},2}\}$ , or  $\tau_0$ , or  $U_{\text{eff}}$ . Since very few samples are modelled considering two independent barriers ( $U_{\text{eff}}, U_{\text{eff},2}$ ), the data are scarce and the results are not statistically significant.

**Supplementary Table 3 | AIC modelling experimental physical (response) variables as a function of modelling variables  $U_{\text{eff}}$ ,  $\tau_0$ .**

Response variable	Data points	Variables included in the model	Significant variable	AIC
$\chi''_{\text{max}}$	608	$U_{\text{eff}}$ , $\tau_0$	-	1381.05
		$U_{\text{eff}}$	-	1378.16
		$\tau_0$	-	1542.43
$T_{\text{B3}}$	186	$U_{\text{eff}}$ , $\tau_0$	$U_{\text{eff}}$	693.98
		$U_{\text{eff}}$	$U_{\text{eff}}$	692.98
		$\tau_0$	-	1051.61
$T_{\text{B3H}}$	261	$U_{\text{eff}}$ , $\tau_0$	$U_{\text{eff}}$	770.73
		$U_{\text{eff}}$	$U_{\text{eff}}$	768.74
		$\tau_0$	-	818.99
Hyst	601	$U_{\text{eff}}$ , $\tau_0$	-	40.56
		$U_{\text{eff}}$	$U_{\text{eff}}$	36.56
		$\tau_0$	-	42.04
$T_{\text{hyst}}$	134	$U_{\text{eff}}$ , $\tau_0$	$U_{\text{eff}}$	650.3
		$U_{\text{eff}}$	$U_{\text{eff}}$	648.32
		$\tau_0$	-	780.94

Supplementary Table 3 contains the analysis including  $U_{\text{eff}}$  and  $\tau_0$ , *i.e.* when an Orbach-only model with a single energy barrier is considered, and quantifies the models employing these variables to explain different response variables:  $\{\chi''_{\text{max}}, T_{\text{B3}}, T_{\text{B3H}}, \text{Hyst}, T_{\text{hyst}}\}$ . The results are very robust in this case.  $U_{\text{eff}}$  is consistently found to be the significant variable and the one producing the lowest AIC value.

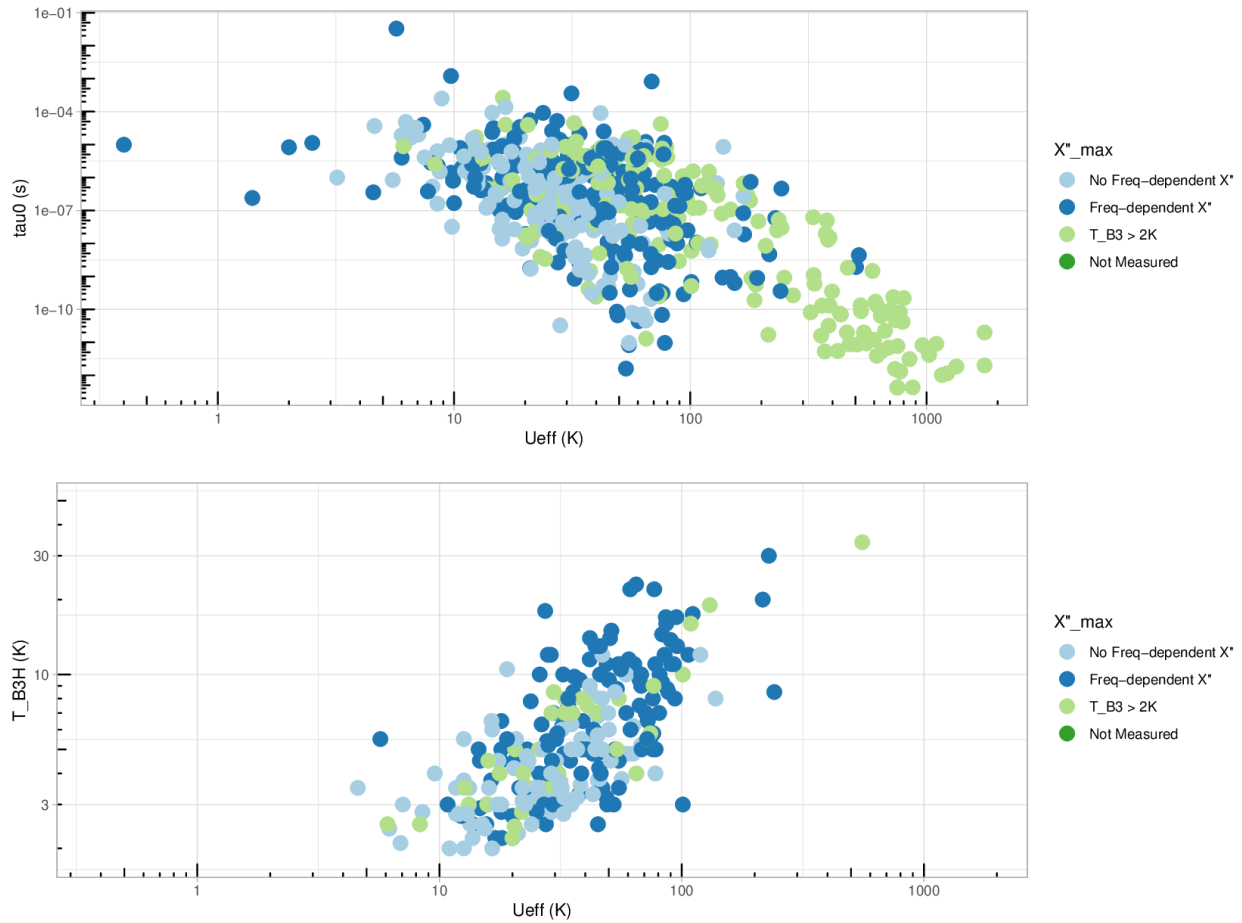
**Supplementary Table 4 | AIC modelling experimental physical (response) variables as a function of modelling variables  $U_{\text{eff,ff}}$ ,  $\tau_{0,\text{ff}}$ .**

Response variable	Data points	Variables included in the model	Significant variable	AIC
$\chi''_{\text{max}}$	68	$U_{\text{eff,ff}}$ , $\tau_{0,\text{ff}}$	-	169.58
		$U_{\text{eff,ff}}$	-	165.33
		$\tau_{0,\text{ff}}$	-	185.89
$T_{\text{B3}}$	27	$U_{\text{eff,ff}}$ , $\tau_{0,\text{ff}}$	$U_{\text{eff,ff}}$ , $\tau_{0,\text{ff}}$	88.5
		$U_{\text{eff,ff}}$	$U_{\text{eff,ff}}$	91.51
		$\tau_{0,\text{ff}}$	-	137.25
$T_{\text{B3H}}$	23	$U_{\text{eff,ff}}$ , $\tau_{0,\text{ff}}$	$U_{\text{eff,ff}}$	74.62
		$U_{\text{eff,ff}}$	$U_{\text{eff,ff}}$	73.54
		$\tau_{0,\text{ff}}$	-	116.81
Hyst	67	$U_{\text{eff,ff}}$ , $\tau_{0,\text{ff}}$	-	137.57
		$U_{\text{eff,ff}}$	-	131.57
		$\tau_{0,\text{ff}}$	-	156.68
$T_{\text{hyst}}$	36	$U_{\text{eff,ff}}$ , $\tau_{0,\text{ff}}$	$U_{\text{eff,ff}}$	102.08
		$U_{\text{eff,ff}}$	$U_{\text{eff,ff}}$	102.72
		$\tau_{0,\text{ff}}$	-	191.68

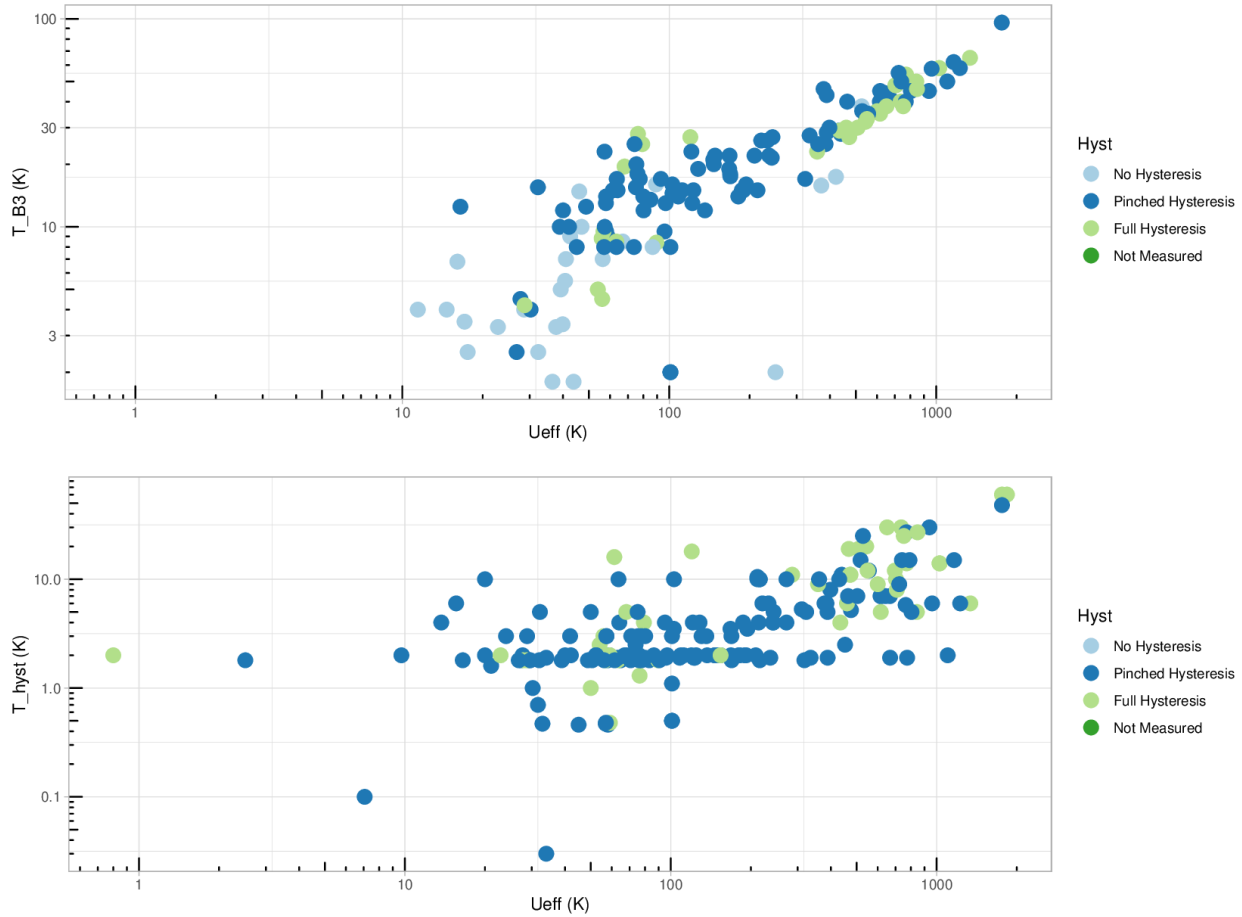
Supplementary Table 4 contains the same analysis but including only  $U_{\text{eff,ff}}$  and  $\tau_{0,\text{ff}}$ , *i.e.* a more complete model that should be closer to reality. The modelling employing  $U_{\text{eff,ff}}$  is almost as good as in the case of  $U_{\text{eff}}$ . However, since information about  $U_{\text{eff,ff}}$  is available in less samples,  $U_{\text{eff}}$  is statistically preferable.

To visualize these correlations, see Supplementary Figs. 22 and 23. The relations between  $U_{\text{eff}}$ ,  $\tau_0$ ,  $\chi''_{\text{max}}$ ,  $T_{\text{B3H}}$  are represented in Supplementary Fig. 22. Within a wide dispersion, a (log-log) inverse linear relation is apparent between (log-log)  $U_{\text{eff}}$  and  $\tau_0$  (more on this on Supplementary Figs. 24.1 and 24.2) and a (log-log) linear relation is apparent between  $T_{\text{B3H}}$  and  $U_{\text{eff}}$ . These graphs also show how samples with higher values of  $U_{\text{eff}}$  systematically present a maximum in  $T_{\text{B3}}$ , and in contrast samples where no frequency-dependent  $\chi''$  is measured tend to display lower values of  $U_{\text{eff}}$ . To complete the picture, we represent the relations between  $U_{\text{eff}}$ , *Hyst*,  $T_{\text{hyst}}$ ,  $T_{\text{B3}}$  (Supplementary Fig. 23). A (log-log) linear tendency is apparent when plotting  $T_{\text{B3}}$  vs  $U_{\text{eff}}$ ; this is obscured in the case of  $T_{\text{hyst}}$  vs  $U_{\text{eff}}$  by the abundance of samples where the hysteresis was characterized only at 2 K. Like in the case of the ac susceptibility, there is a large dispersion of behaviours by samples with longer magnetic memory, in this case meaning the ones presenting whole hysteresis, tend to be grouped around higher values of  $U_{\text{eff}}$ , with samples presenting no

hysteresis tend to present lower values of  $U_{\text{eff}}$  and samples with pinched hysteresis presenting typically intermediate values.



**Supplementary Figure 22 | Scatterplots depicting the relation of  $U_{\text{eff}}$  with  $\tau_0$ ,  $\chi''_{\text{max}}$ ,  $T_{\text{B3H}}$ .  $\tau_0$  vs  $U_{\text{eff}}$ , colored by  $\chi''_{\text{max}}$  (up);  $T_{\text{B3H}}$  vs  $U_{\text{eff}}$ , colored by  $\chi''_{\text{max}}$  (down).**



**Supplementary Figure 23 | Scatterplots depicting the relation of  $U_{\text{eff}}$  with  $Hyst$ ,  $T_{\text{hyst}}$ ,  $T_{B3}$ ,  $T_{B3}$  vs  $U_{\text{eff}}$ , colored by  $Hyst$  (top);  $T_{\text{hyst}}$  vs  $U_{\text{eff}}$ , colored by  $Hyst$  (down).**

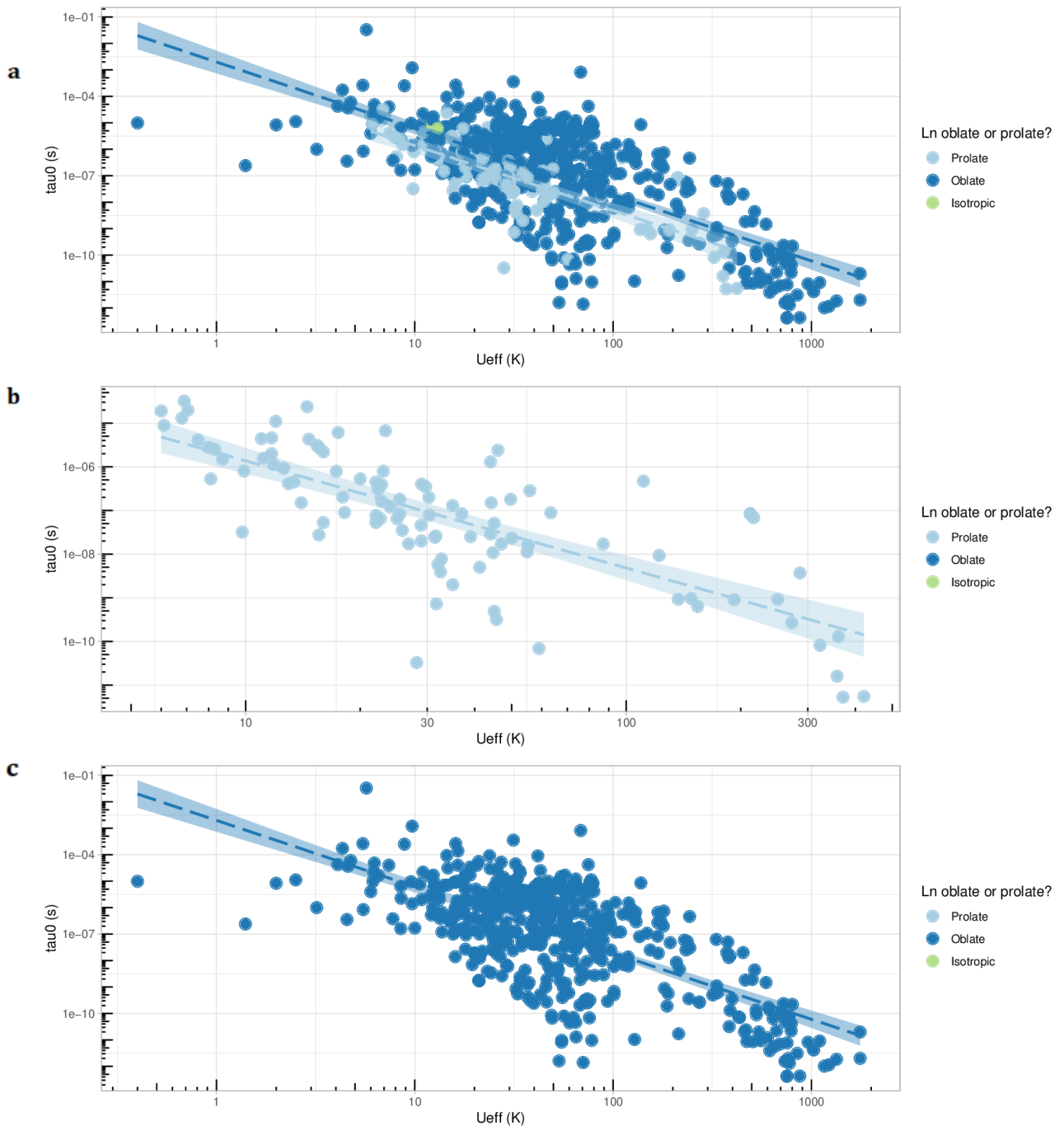
The main conclusion of the study is that  $U_{\text{eff}}$  derived from a simplistic Arrhenius plot is currently the best single predictor for physical behaviour. This means that, whether we are discussing in terms of the presence of maximum in out-of-phase component of the ac susceptibility ( $\chi''_{\text{max}}$ ) or the temperature of said maximum ( $T_{B3}$ ,  $T_{B3H}$ ),  $U_{\text{eff}}$  is a better predictor than  $\tau_0$  or  $U_{\text{eff},2}$  (note that the number of studies with  $U_{\text{eff},2}$  is too small). Also the number of studies deriving  $U_{\text{eff},\text{ff}}$  from a full fit considering the other physical processes is very low. Furthermore, the correlation between  $U_{\text{eff},\text{ff}}$  and  $U_{\text{eff}}$  is very high. The combination of the two facts mean that there is no statistical argument for the qualitative observation that  $U_{\text{eff},\text{ff}}$  from a full fit is a better predictor for  $T_{\text{hyst}}$ .

Finally, let us represent the available data in terms of  $\tau_0$  vs  $U_{\text{eff}}$ . Note that the slopes are identical but the constant term is higher for oblate ions compared with prolate ions: at a given  $U_{\text{eff}}$  the expected  $\tau_0$  for oblate ions is ten times higher than  $\tau_0$  for prolate ions, meaning an equivalent  $U_{\text{eff}}$  relaxation will be substantially slower in oblate ions (Supplementary Fig. 21.4). Within the two main oblate ions ( $\text{Dy}^{3+}$  and  $\text{Tb}^{3+}$ ), the slope is slightly higher for  $\text{Dy}^{3+}$ , meaning a dramatic

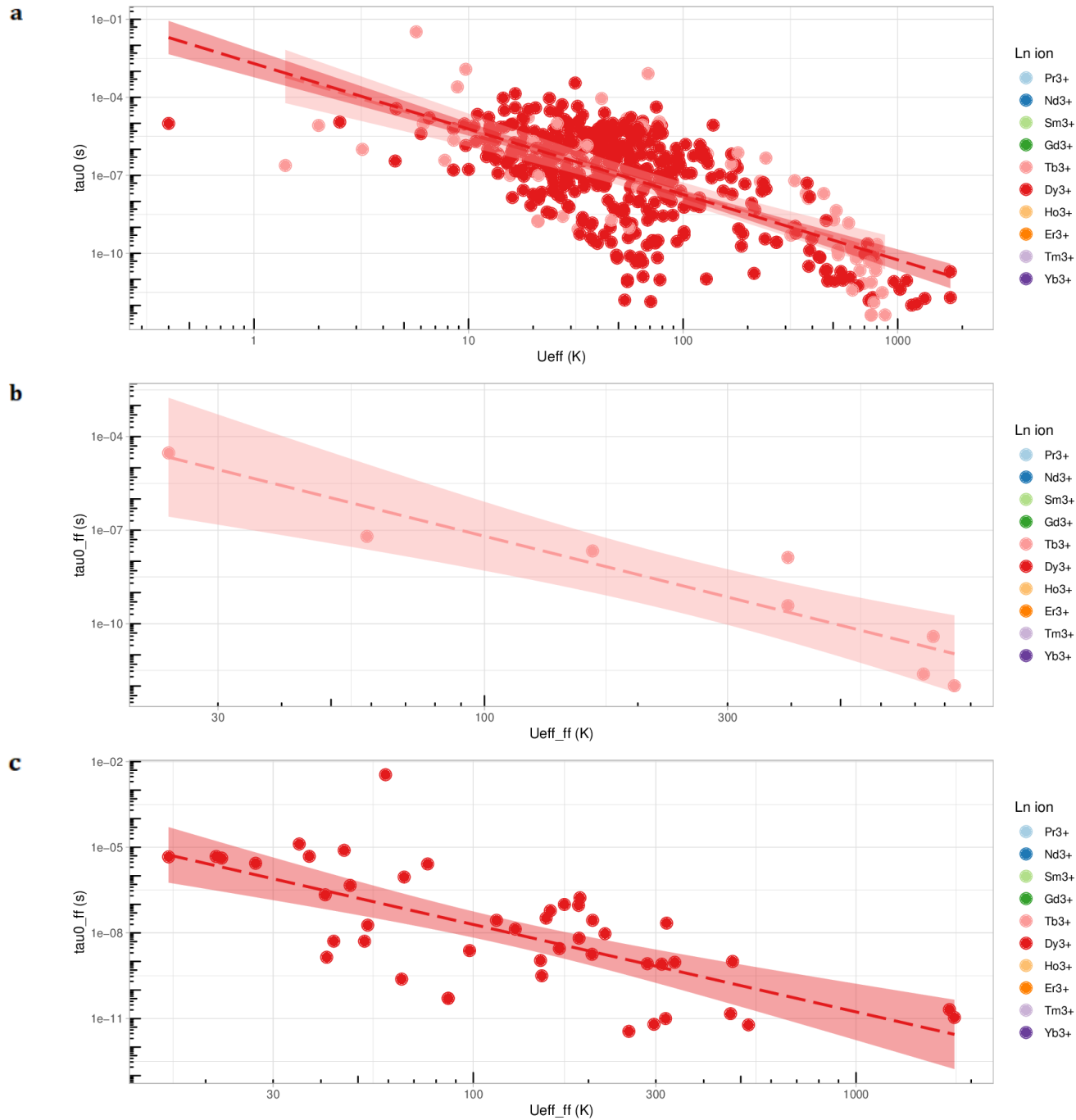
increase in  $U_{\text{eff}}$  is somewhat more beneficial for  $\text{Tb}^{3+}$  compared with  $\text{Dy}^{3+}$  (Supplementary Fig. 21.2).

**Supplementary Table 5 | Least squares fits of  $\ln(U_{\text{eff}})$  vs  $-\ln(\tau_0)$  and  $\ln(U_{\text{eff,ff}})$  vs  $-\ln(\tau_{0,\text{ff}})$ .**

Data	Intercept ( $R_{\text{Or}}$ )	Slope ( $n$ )
All	839.4	2.437
Prolate	2557.5	2.454
Oblate	504.3	2.506
$\text{Tb}^{3+}$	700.5	2.415
$\text{Dy}^{3+}$	504.0	2.515
Full fit	151.2	2.957



**Supplementary Figure 24.1**  $\tau_0$  vs  $U_{\text{eff}}$ , for prolate and oblate ions. **a**, Comparison between both. **b**, Only prolate ions. **c**, Only oblate ions.



**Supplementary Figure 24.2 |  $\tau_0$  vs  $U_{\text{eff}}$  and  $\tau_{0,\text{ff}}$  vs  $U_{\text{eff,ff}}$  for  $\text{Tb}^{3+}$  and  $\text{Dy}^{3+}$ .** **a**, Comparison between both. **b**, Only  $\text{Tb}^{3+}$  complexes. **c**, Only  $\text{Dy}^{3+}$  complexes.

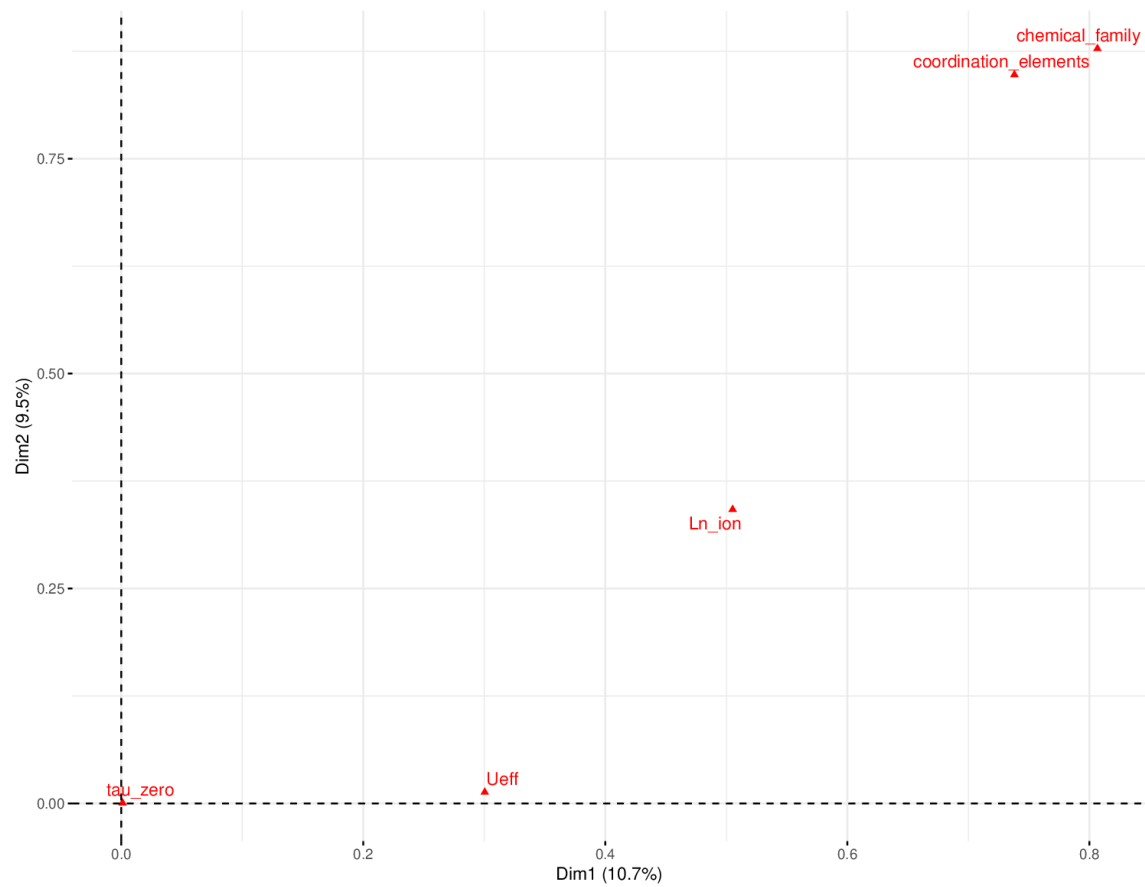
## Supplementary Section 6. FAMD and magnetostructural clustering

For all the statistical studies of the physical variables that follow in Supplementary Section 6, we performed the analysis two times, to check for consistency and robustness of the results. In particular, we performed the analysis of the full dataset (~1400 samples) and repeated it independently employing only the data subset in the timeframe 2003-2017 (~1000 samples). We found that all major qualitative results presented here are robust and independently obtained whether one considers the whole set 2003-2019 or the 2003-2017 subset. Furthermore, quantitative data were found to be within a 25% deviation, with a shift towards higher values of  $U_{\text{eff}}$ ,  $T_{\text{B}3}$  and  $T_{\text{hyst}}$  in the 2003-2019 set when compared with the 2003-2017 subset.

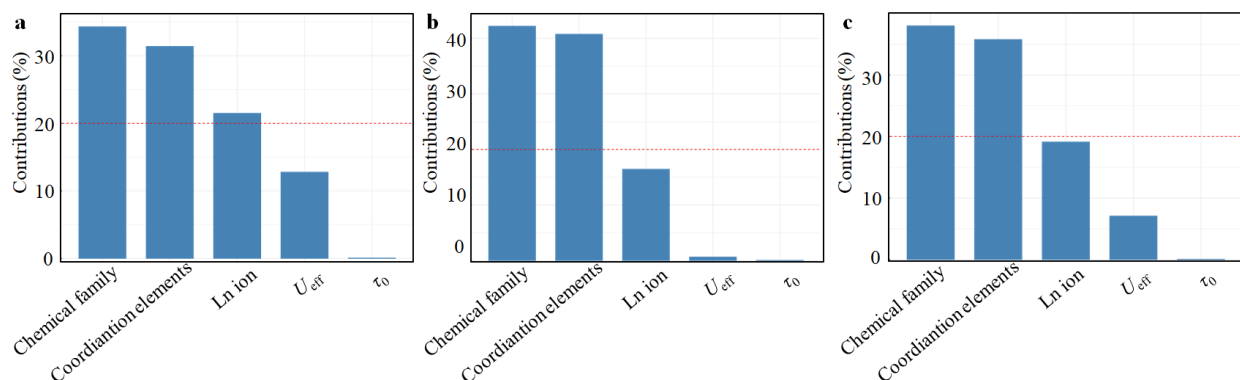
Factorial analysis of mixed data (FAMD) is a factorial method appropriate to analyse data containing both quantitative and qualitative variables. FAMD is a versatile method that acts as Principal Component Analysis for quantitative variables, and as Multiple Correspondence Analysis for qualitative variables. Qualitative and quantitative variables are normalized during the analysis to equilibrate the influence of each in the variable set. In this case this allows us a simultaneous analysis of physical and chemical properties, to perform a hierarchical clustering of samples with the goal of producing a magnetostructural taxonomy in our Ln-based SIMs catalogue. By grouping the samples by taking into consideration their molecular structure and their magnetic behaviour, we can aspire to obtain information on the main relation between form and function. To perform this analysis and data representation we employed R packages FactoMineR<sup>56</sup> and factoextra.<sup>60</sup>

We found that the chemical family, the lanthanide ion and the coordination elements are the best chemical predictors, as  $U_{\text{eff}}$  among the physical parameters. Only 608 samples in the dataset contain quantitative  $U_{\text{eff}}$  and  $\tau_0$  data. We initially worked just with these 608 samples, and later repeated the analysis with all samples, obtaining the same result.

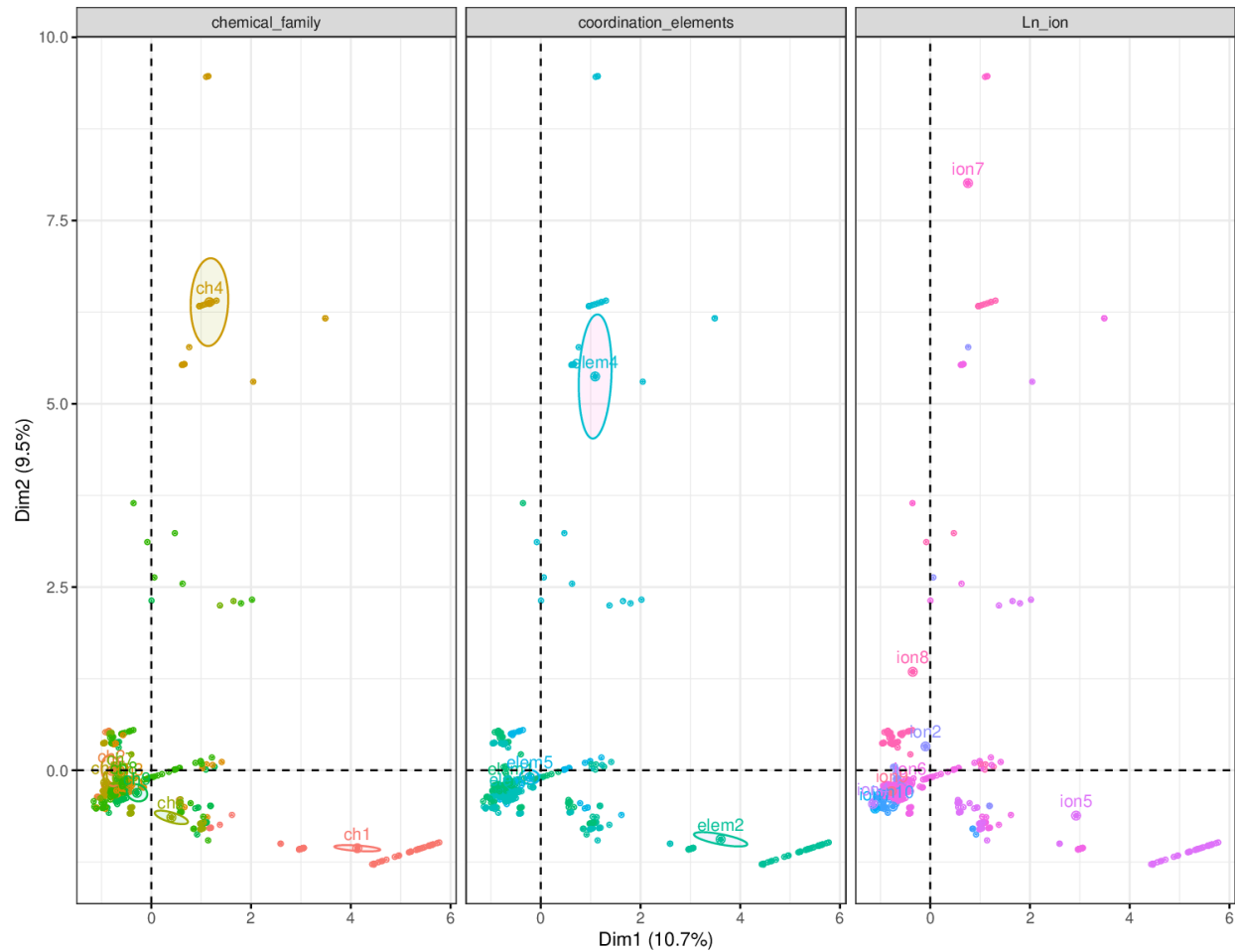
Let us start with representing the relation between the two main FAMD dimensions and the main physical and chemical variables (Supplementary Figs. 25, 26 and 27). Analyzing the contribution from the main chemical and physical variables to the main FAMD dimensions (Supplementary Figs. 25 and 26), one can see that the distinctive traits for both dimension 1 and dimension 2 are the variables “chemical family” and “coordination elements”, with the “Ln ion” choice appears in a distant third place, while “ $U_{\text{eff}}$ ” participates only in dimension 1. This is similar to what was seen in Supplementary Section 4.2. The FAMD factor map (Supplementary Fig. 27) provides additional information on the actual values of the variables presented by the samples and their relation to the two main dimensions.



**Supplementary Figure 25 | Representation of the physical and chemical variables according to a FAMD method.**



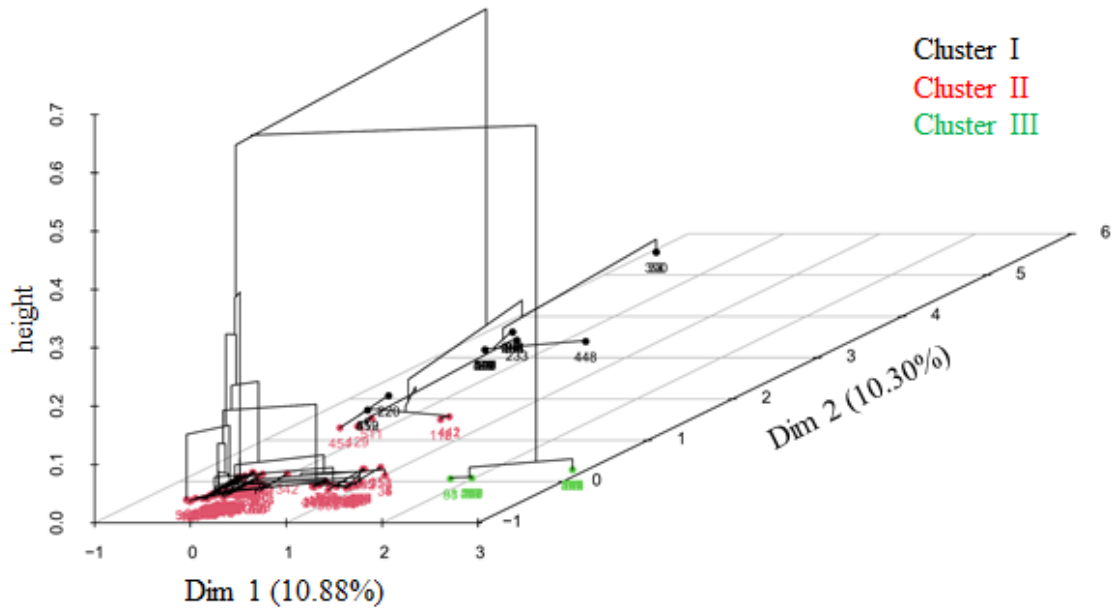
**Supplementary Figure 26 | Contribution from the main chemical and physical variables to the main FAMD dimensions.** **a**, Contributions to the dimension 1. **b**, Contributions to dimension 2. **c**, Combined contributions to dimensions 1 and 2.



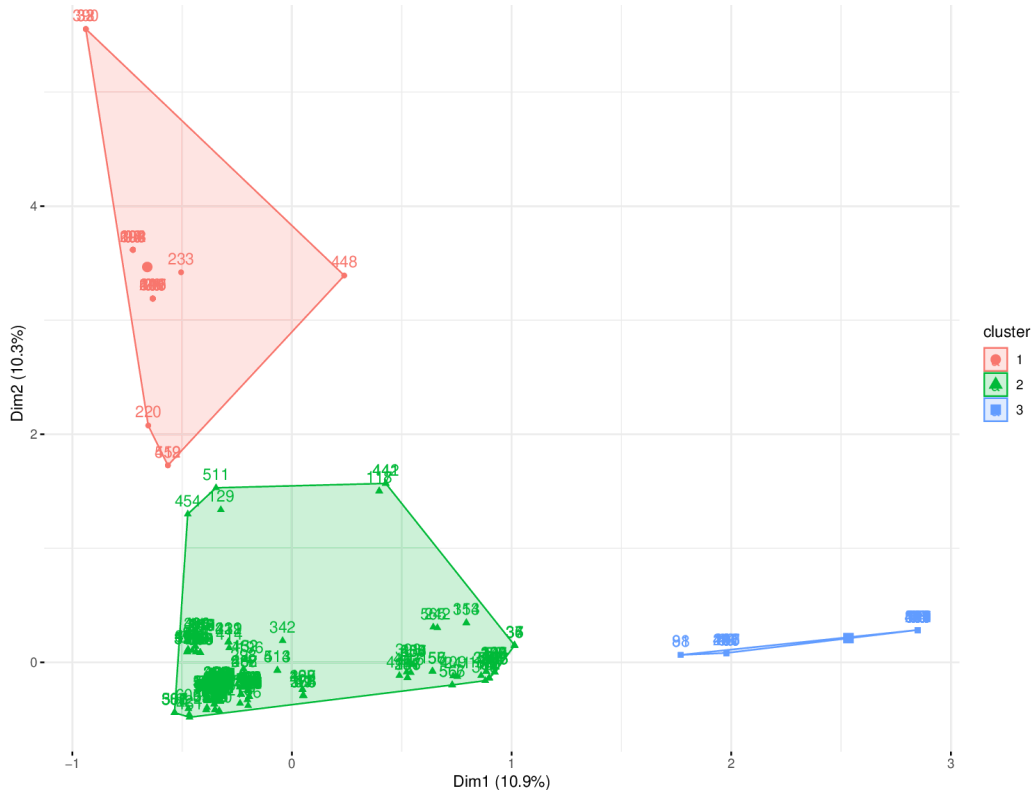
**Supplementary Figure 27 | FAMD factor map.** The groupings of the different values for the three main chemical variables is shown. See numbering convention for the categories of variables in Supplementary Section 1.

## 6.1. Magnetostructural clusters

We proceed to analyze the magnetostructural hierarchical clustering. This is comparable with the molecular clustering presented in Supplementary Section 4.2, but considering both physical and chemical variables. Dendrograms are represented in Supplementary Figs. 28 and 29, and a description of the different clusters follows.



**Supplementary Figure 28 | Dendrogram depicting the hierarchical clustering on the factor map.** The numbers in the plot represent sample\_IDs.



**Supplementary Figure 29 | Alternate view of the calculated hierarchical clustering on the factor map.** The numbers in the plot represent sample\_IDs.

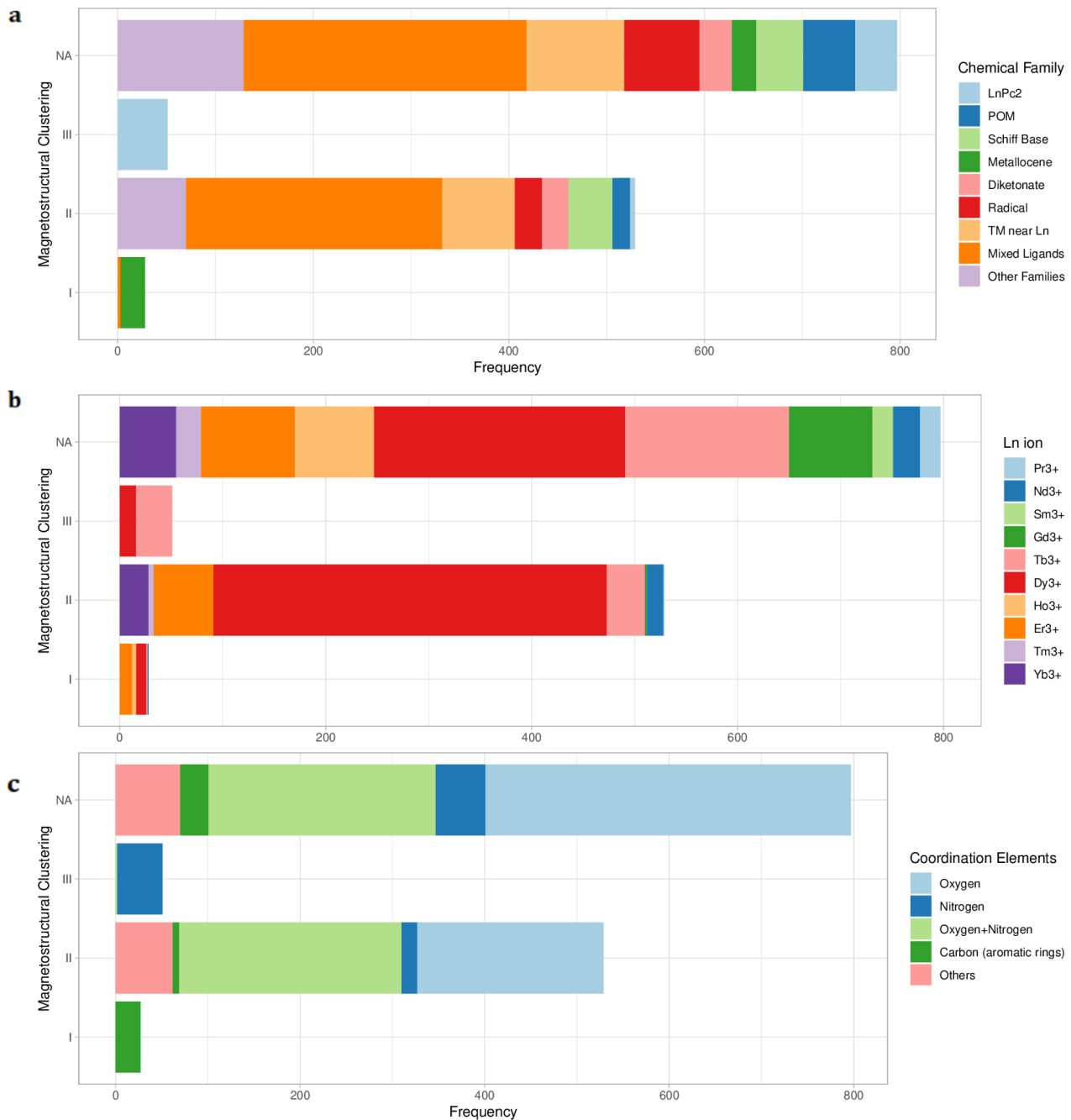
The main results from these analysis are as follows:

- Cluster I:  $U_{\text{eff}}$  is the most associated variable in cluster I. The average value of  $U_{\text{eff}}$  (252 K) in cluster I is considerably higher than the general average of  $U_{\text{eff}}$  (117 K). In addition, the average value of  $T_{\text{hyst}}$  in cluster I (9.9 K) is also significantly above the average value of  $T_{\text{hyst}}$  (5.5 K). Indeed, cluster I is characterised by higher-than-average values of  $U_{\text{eff}}$  and  $T_{\text{hyst}}$ .
- Cluster II is characterised by close-to-average values of  $T_{\text{B}3}$  (18.5 K < 19.2 K) and  $T_{\text{hyst}}$  (5.2 K < 5.5 K), and lower-than average  $U_{\text{eff}}$  (87 K < 117 K).
- Cluster III, like cluster I but less intensely, is characterised by higher-than-average values for  $U_{\text{eff}}$  (353 K > 117 K) and  $T_{\text{B}3}$  (26 K > 19 K).

A partial clustering taking into account of the first 1000 data points (*i.e.* discarding data from 2018 and 2019) results in a very similar classification, but primarily characterizes cluster I by higher-than-average values for  $U_{\text{eff}}$  and  $T_{\text{B}3}$  and cluster III by higher-than-average values for  $T_{\text{hyst}}$  and  $U_{\text{eff}}$ . As a notable difference, discarding recent data results in a significant decrease in the average value for cluster III down to  $U_{\text{eff}} = 199$  K.

This general “magnetostructural” clustering classification, when described strictly from the point of view of the chemical variables, is depicted in Supplementary Fig. 30 and can be simplified to:

- cluster I: metallocene-type sandwiches, carbon as donor atoms, with  $\text{Ho}^{3+}$  and  $\text{Er}^{3+}$  as the most abundant ions.
- cluster II: predominantly mixed ligands, *i.e.* a mixture of different coordination ligands, predominantly  $\text{Dy}^{3+}$  ion, and either only oxygens or a mixture of nitrogen and oxygen as donor atoms. This is by far the most abundant class of compounds with reported  $U_{\text{eff}}$ .
- cluster III:  $\text{Tb}^{3+}$  ion (followed by  $\text{Dy}^{3+}$ ),  $\text{LnPc}_2$  family, nitrogens as donor atoms. These values for these variables are partially overlapping.

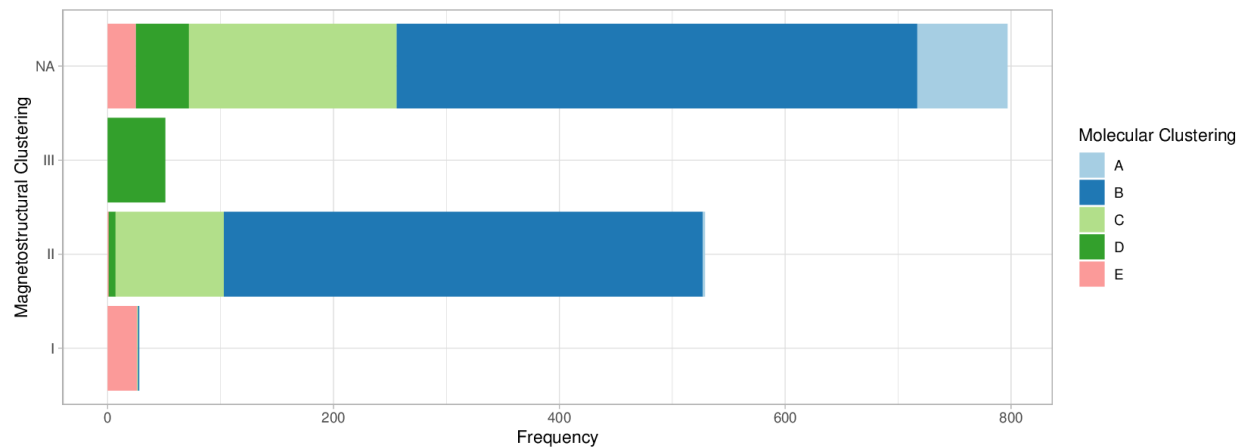


**Supplementary Figure 30 | Bar charts for magnetoostructural clusters and their relation with the main chemical variables.** From top to down, the bar charts are filled according to: **(a)** chemical family, **(b)** lanthanide ion and **(c)** coordination elements in the coordination sphere.

The correlation between the magnetoostructural clusters I-II-III and the chemical clusters A-B-C-D-E is depicted in Supplementary Fig. 31, and can be summarized as follows:

-cluster I is mostly composed of samples from cluster E

- cluster II is a mixture of samples from cluster B and C, and as well some from cluster D, but mostly from B
- cluster III is mainly samples of cluster D
- samples outside the I-II-III classification (not assigned), meaning samples with no recorded value of  $U_{\text{eff}}$  are a mixture of all of the A-B-C-D-E cases, notably including all of the cases of cluster A ( $\text{Gd}^{3+}$  complexes), and are, in order of relative abundance: B, C, A, D, E.



**Supplementary Figure 31 | Bar charts for magnetostuctural clusters and their relation with the molecular (chemical) clusters.** NA stands for not assigned samples, *i.e.* samples that do not belong in any of the 3 magnetostuctural clusters I-III.

Note that the dataset downloadable from the SIMDAVIS dashboard includes an alternate lower cut to the same hierarchical clustering (mag\_struct\_cluster\_2 in the dataset), finding up to 8 distinct magnetostuctural clusters.

## Supplementary Section 7. Annex: articles included in the study

1. Ishikawa, N., Sugita, M., Ishikawa, T., Koshihara, S. & Kaizu, Y. Lanthanide Double-Decker Complexes Functioning as Magnets at the Single-Molecular Level. *Journal of the American Chemical Society* **125**, 8694–8695 (2003).
2. Ishikawa, N., Sugita, M., Ishikawa, T., Koshihara, S. & Kaizu, Y. Mononuclear Lanthanide Complexes with a Long Magnetization Relaxation Time at High Temperatures: A New Category of Magnets at the Single-Molecular Level. *The Journal of Physical Chemistry B* **108**, 11265–11271 (2004).
3. Ishikawa, N. *et al.* Upward Temperature Shift of the Intrinsic Phase Lag of the Magnetization of Bis(phthalocyaninato)terbium by Ligand Oxidation Creating an  $S=1/2$  Spin. *Inorganic Chemistry* **43**, 5498–5500 (2004).
4. Ishikawa, N., Otsuka, S. & Kaizu, Y. The Effect of the  $f-f$  Interaction on the Dynamic Magnetism of a Coupled 4f8 System in a Dinuclear Terbium Complex with Phthalocyanines. *Angewandte Chemie International Edition* **44**, 731–733 (2005).
5. Ishikawa, N., Sugita, M. & Wernsdorfer, W. Nuclear Spin Driven Quantum Tunneling of Magnetization in a New Lanthanide Single-Molecule Magnet: Bis(Phthalocyaninato)holmium Anion. *Journal of the American Chemical Society* **127**, 3650–3651 (2005).
6. Ishikawa, N., Sugita, M. & Wernsdorfer, W. Quantum Tunneling of Magnetization in Lanthanide Single-Molecule Magnets: Bis(phthalocyaninato)terbium and Bis(phthalocyaninato)dysprosium Anions. *Angewandte Chemie International Edition* **44**, 2931–2935 (2005).
7. Sugita, M., Ishikawa, N., Ishikawa, T., Koshihara, S. & Kaizu, Y. Static Magnetic-Field-Induced Phase Lag in the Magnetization Response of Tris(dipicolinato)lanthanides. *Inorganic Chemistry* **45**, 1299–1304 (2006).
8. Ueki, S., Nogami, T., Ishida, T. & Tamura, M. ET and TTF Salts with Lanthanide Complex Ions Showing Frequency-Dependent ac Magnetic Susceptibility. *Molecular Crystals and Liquid Crystals* **455**, 129–134 (2006).
9. Poneti, G. *et al.* A rational approach to the modulation of the dynamics of the magnetisation in a dysprosium–nitronyl–nitroxide radical complex. *Chem. Commun.* 1807–1809 (2007).
10. Takamatsu, S., Ishikawa, T., Koshihara, S. & Ishikawa, N. Significant Increase of the Barrier Energy for Magnetization Reversal of a Single-4f-Ionic Single-Molecule Magnet by a Longitudinal Contraction of the Coordination Space. *Inorganic Chemistry* **46**, 7250–7252 (2007).
11. Zhang, W., Zhao, F., Liu, T. & Gao, S. Syntheses, structures and magnetic properties of a family of one-dimensional M(II)-lanthanide(III) (M = Ni(II) and Zn(II)) coordination polymers. *Science in China Series B: Chemistry* **50**, 308–317 (2007).
12. AlDamen, M. A., Clemente-Juan, J. M., Coronado, E., Martí-Gastaldo, C. & Gaita-Ariño, A. Mononuclear Lanthanide Single-Molecule Magnets Based on Polyoxometalates. *Journal of the American Chemical Society* **130**, 8874–8875 (2008).
13. Ishikawa, N., Mizuno, Y., Takamatsu, S., Ishikawa, T. & Koshihara, S. Effects of Chemically Induced Contraction of a Coordination Polyhedron on the Dynamical Magnetism of Bis(phthalocyaninato)dysprosium, a Single-4f-Ionic Single-Molecule Magnet with a Kramers Ground State. *Inorganic Chemistry* **47**, 10217–10219 (2008).
14. AlDamen, M. A. *et al.* Mononuclear Lanthanide Single Molecule Magnets Based on the Polyoxometalates  $[\text{Ln}(\text{W}_5\text{O}_{18})_2]^{9-}$  and  $[\text{Ln}(\beta_2\text{-SiW}_{11}\text{O}_{39})_2]^{13-}$  ( $\text{Ln}^{\text{III}} = \text{Tb, Dy, Ho, Er, Tm, and Yb}$ ). *Inorganic Chemistry* **48**, 3467–3479 (2009).
15. Gonidec, M. *et al.* A Liquid-Crystalline Single-Molecule Magnet with Variable Magnetic Properties. *Angewandte Chemie International Edition* **49**, 1623–1626 (2010).
16. Li, D.-P. *et al.* Single-ion magnets based on mononuclear lanthanide complexes with chiral Schiff base ligands  $[\text{Ln}(\text{FTA})_3\text{L}]$  ( $\text{Ln} = \text{Sm, Eu, Gd, Tb and Dy}$ ). *Chemical Communications* **46**, 2929 (2010).
17. Wang, X.-L., Li, L.-C. & Liao, D.-Z. Slow Magnetic Relaxation in Lanthanide Complexes with Chelating Nitronyl Nitroxide Radical. *Inorganic Chemistry* **49**, 4735–4737 (2010).
18. Wang, Y., Li, X.-L., Wang, T.-W., Song, Y. & You, X.-Z. Slow Relaxation Processes and Single-Ion Magnetic Behaviors in Dysprosium-Containing Complexes. *Inorganic Chemistry* **49**, 969–976 (2010).
19. Bi, Y. *et al.* Capping Ligand Perturbed Slow Magnetic Relaxation in Dysprosium Single-Ion Magnets.

*Chemistry - A European Journal* **17**, 12476–12481 (2011).

20. Chen, G.-J. *et al.* Coordination-perturbed single-molecule magnet behaviour of mononuclear dysprosium complexes. *Dalton Transactions* **40**, 5579 (2011).
21. Feltham, H. L. C. *et al.* A family of 13 tetrานuclear zinc(II)-lanthanide(III) complexes of a [3 + 3] Schiff-base macrocycle derived from 1,4-diformyl-2,3-dihydroxybenzene. *Dalton Transactions* **40**, 11425 (2011).
22. Feltham, H. L. C. *et al.* A Non-sandwiched Macroyclic Monolanthanide Single-Molecule Magnet: The Key Role of Axiality. *Chemistry - A European Journal* **17**, 4362–4365 (2011).
23. Jeletic, M. *et al.* An Organometallic Sandwich Lanthanide Single-Ion Magnet with an Unusual Multiple Relaxation Mechanism. *Journal of the American Chemical Society* **133**, 19286–19289 (2011).
24. Jiang, S.-D., Wang, B.-W., Sun, H.-L., Wang, Z.-M. & Gao, S. An Organometallic Single-Ion Magnet. *Journal of the American Chemical Society* **133**, 4730–4733 (2011).
25. Li, D.-P. *et al.* Distinct magnetic dynamic behavior for two polymorphs of the same Dy(III) complex. *Chemical Communications* **47**, 6867 (2011).
26. Meihaus, K. R., Rinehart, J. D. & Long, J. R. Dilution-Induced Slow Magnetic Relaxation and Anomalous Hysteresis in Trigonal Prismatic Dysprosium(III) and Uranium(III) Complexes. *Inorganic Chemistry* **50**, 8484–8489 (2011).
27. Okazawa, A., Nojiri, H., Ishida, T. & Kojima, N. Single-molecule magnet behavior enhanced by magnetic coupling between 4f and 3d spins. *Polyhedron* **30**, 3140–3144 (2011).
28. Wang, X.-L. *et al.* Slow magnetic relaxation in lanthanide complexes with chelating imino nitroxide radicals. *Inorganic Chemistry Communications* **14**, 1728–1731 (2011).
29. Watanabe, A., Yamashita, A., Nakano, M., Yamamura, T. & Kajiwara, T. Multi-Path Magnetic Relaxation of Mono-Dysprosium(III) Single-Molecule Magnet with Extremely High Barrier. *Chemistry - A European Journal* **17**, 7428–7432 (2011).
30. Yamashita, A. *et al.* Wheel-Shaped  $\text{Er}^{\text{III}}\text{Zn}^{\text{II}}_3$  Single-Molecule Magnet: A Macroyclic Approach to Designing Magnetic Anisotropy. *Angewandte Chemie International Edition* **50**, 4016–4019 (2011).
31. Bhunia, A. *et al.* From a Dy(III) Single Molecule Magnet (SMM) to a Ferromagnetic  $[\text{Mn}(\text{II})\text{Dy}(\text{III})\text{Mn}(\text{II})]$  Trinuclear Complex. *Inorganic Chemistry* **51**, 9589–9597 (2012).
32. Boulon, M.-E. *et al.* Magnetic Anisotropy and Spin-Parity Effect Along the Series of Lanthanide Complexes with DOTA. *Angewandte Chemie International Edition* **52**, 350–354 (2012).
33. Cardona-Serra, S. *et al.* Lanthanoid Single-Ion Magnets Based on Polyoxometalates with a 5-fold Symmetry: The Series  $[\text{LnP}_5\text{W}_{30}\text{O}_{110}]^{12-}$  ( $\text{Ln}^{3+} = \text{Tb, Dy, Ho, Er, Tm, and Yb}$ ). *Journal of the American Chemical Society* **134**, 14982–14990 (2012).
34. Gonidec, M., Amabilino, D. B. & Veciana, J. Novel double-decker phthalocyaninato terbium(III) single molecule magnets with stabilised redox states. *Dalton Transactions* **41**, 13632 (2012).
35. Habib, F. *et al.* Supramolecular architectures for controlling slow magnetic relaxation in field-induced single-molecule magnets. *Chemical Science* **3**, 2158 (2012).
36. Hu, P. *et al.* Single-molecule magnets based on rare earth complexes with chelating benzimidazole-substituted nitronyl nitroxide radicals. *Dalton Transactions* **41**, 14651 (2012).
37. Jiang, S.-D. *et al.* Series of Lanthanide Organometallic Single-Ion Magnets. *Inorganic Chemistry* **51**, 3079–3087 (2012).
38. Katoh, K. *et al.* Multiple-decker phthalocyaninato dinuclear lanthanoid(III) single-molecule magnets with dual-magnetic relaxation processes. *Dalton Transactions* **41**, 13582 (2012).
39. Katoh, K., Umetsu, K., Brian, K. B. & Yamashita, M. Magnetic relaxation behavior of a spatially closed dysprosium(III) phthalocyaninato double-decker complex. *Science China Chemistry* **55**, 918–925 (2012).
40. Li, X.-L. *et al.* Modulation of Homochiral  $\text{Dy}^{\text{III}}$  Complexes: Single-Molecule Magnets with Ferroelectric Properties. *Chemistry - A European Journal* **18**, 14632–14637 (2012).
41. Lin, P.-H., Korobkov, I., Burchell, T. J. & Murugesu, M. Connecting single-ion magnets through ligand dimerisation. *Dalton Transactions* **41**, 13649 (2012).
42. Liu, J.-L. *et al.* A Six-Coordinate Ytterbium Complex Exhibiting Easy-Plane Anisotropy and Field-Induced Single-Ion Magnet Behavior. *Inorganic Chemistry* **51**, 8538–8544 (2012).
43. Liu, Q.-Y. *et al.* Diversity of Lanthanide(III)-Organic Extended Frameworks with a 4,8-Disulfonyl-2,6-naphthalenedicarboxylic Acid Ligand: Syntheses, Structures, and Magnetic and Luminescent Properties. *Inorganic Chemistry* **51**, 2381–2392 (2012).

44. Mei, X.-L. *et al.* Modulating spin dynamics of cyclic  $\text{Ln}^{\text{III}}$ -radical complexes ( $\text{Ln}^{\text{III}} = \text{Tb}, \text{Dy}$ ) by using phenyltrifluoroacetylacetone coligand. *Dalton Transactions* **41**, 2904 (2012).

45. Mei, X.-L., Ma, Y., Li, L.-C. & Liao, D.-Z. Ligand field-tuned single-molecule magnet behaviour of  $2p$ - $4f$  complexes. *Dalton Trans.* **41**, 505–511 (2012).

46. Menelaou, M. *et al.* Dy $^{\text{III}}$ - and Yb $^{\text{III}}$ -Curcuminoid Compounds: Original Fluorescent Single-Ion Magnet and Magnetic Near-IR Luminescent Species. *Chemistry - A European Journal* **18**, 11545–11549 (2012).

47. Pointillart, F., Bernot, K., Poneti, G. & Sessoli, R. Crystal Packing Effects on the Magnetic Slow Relaxation of Tb(III)-Nitronyl Nitroxide Radical Cyclic Dinuclear Clusters. *Inorganic Chemistry* **51**, 12218–12229 (2012).

48. Rinehart, J. D. & Long, J. R. Slow magnetic relaxation in homoleptic trispyrazolylborate complexes of neodymium(iii) and uranium(iii). *Dalton Transactions* **41**, 13572 (2012).

49. Ruiz, J. *et al.* Field and dilution effects on the slow relaxation of a luminescent Dy $^{\text{III}}$  low-symmetry single-ion magnet. *Chemical Communications* **48**, 7916 (2012).

50. Sakaue, S., Fuyuhiro, A., Fukuda, T. & Ishikawa, N. Dinuclear single-molecule magnets with porphyrin–phthalocyanine mixed triple-decker ligand systems giving SAP and SP coordination polyhedra. *Chemical Communications* **48**, 5337 (2012).

51. Wang, C. *et al.* Two new lanthanide–radical complexes: synthesis, structure, and magnetic properties. *Journal of Coordination Chemistry* **65**, 2830–2838 (2012).

52. Wang, H., Liu, T., Wang, K., Duan, C. & Jiang, J. Tetrakis(phthalocyaninato) Rare-Earth-Cadmium-Rare-Earth Quadruple-Decker Sandwich SMMs: Suppression of QTM by Long-Distance f-f Interactions. *Chemistry - A European Journal* **18**, 7691–7694 (2012).

53. Williams, U. J. *et al.* A comparison of the effects of symmetry and magnetoanisotropy on paramagnetic relaxation in related dysprosium single ion magnets. *Chemical Communications* **48**, 5593 (2012).

54. Yao, M.-X. *et al.* Field-induced slow magnetic relaxation in chiral seven-coordinated mononuclear lanthanide complexes. *Dalton Transactions* **41**, 13682 (2012).

55. Anwar, M. U., Dawe, L. N., Tandon, S. S., Bunge, S. D. & Thompson, L. K. Polynuclear lanthanide (Ln) complexes of a tri-functional hydrazone ligand – mononuclear (Dy), dinuclear (Yb, Tm), tetranuclear (Gd), and hexanuclear (Gd, Dy, Tb) examples. *Dalton Transactions* **42**, 7781 (2013).

56. Bartolomé, E. *et al.*  $\{\text{Dy}(\alpha\text{-fur})_3\}_n$ : from double relaxation single-ion magnet behavior to 3D ordering. *Dalton Transactions* **42**, 10153 (2013).

57. Blagg, R. J. *et al.* Magnetic relaxation pathways in lanthanide single-molecule magnets. *Nature Chemistry* **5**, 673–678 (2013).

58. Cameron, J. M. *et al.* Synthesis and characterisation of a lanthanide-capped dodecavanadate cage. *Chemical Communications* **49**, 3395 (2013).

59. Campbell, V. E. *et al.* Subcomponent Self-Assembly of Rare-Earth Single-Molecule Magnets. *Inorganic Chemistry* **52**, 5194–5200 (2013).

60. Cao, D.-K., Gu, Y.-W., Feng, J.-Q., Cai, Z.-S. & Ward, M. D. Mononuclear lanthanide complexes incorporating an anthracene group: structural modification, slow magnetic relaxation and multicomponent fluorescence emissions in Dy compounds. *Dalton Transactions* **42**, 11436 (2013).

61. Chandrasekhar, V., Chakraborty, A. & Sañudo, E. C. Ferrocene-based compartmental ligand for the assembly of neutral Zn $^{\text{II}}$ /Ln $^{\text{III}}$  heterometallic complexes. *Dalton Transactions* **42**, 13436 (2013).

62. Chilton, N. F. *et al.* Single molecule magnetism in a family of mononuclear  $\beta$ -diketonate lanthanide(iii) complexes: rationalization of magnetic anisotropy in complexes of low symmetry. *Chemical Science* **4**, 1719 (2013).

63. Cosquer, G., Pointillart, F., Golhen, S., Cador, O. & Ouahab, L. Slow Magnetic Relaxation in Condensed versus Dispersed Dysprosium(III) Mononuclear Complexes. *Chemistry - A European Journal* **19**, 7895–7903 (2013).

64. Feltham, H. L. C. *et al.* By Design: A Macroyclic 3d–4f Single-Molecule Magnet with Quantifiable Zero-Field Slow Relaxation of Magnetization. *Inorganic Chemistry* **52**, 3236–3240 (2013).

65. Fortea-Pérez, F. R. *et al.* Slow Magnetic Relaxation in a Hydrogen-Bonded 2D Array of Mononuclear Dysprosium(III) Oxamates. *Inorganic Chemistry* **52**, 4777–4779 (2013).

66. Fukuda, T., Matsumura, K. & Ishikawa, N. Influence of Intramolecular f-f Interactions on Nuclear Spin Driven Quantum Tunneling of Magnetizations in Quadruple-Decker Phthalocyanine Complexes Containing Two Terbium or Dysprosium Magnetic Centers. *The Journal of Physical Chemistry A* **117**, 10447–10454 (2013).

(2013).

67. Gao, F. *et al.* Seven-Coordinate Lanthanide Sandwich-Type Complexes with a Tetrathiafulvalene-Fused Schiff Base Ligand. *Inorganic Chemistry* **52**, 11164–11172 (2013).
68. Gao, F., Cui, L., Song, Y., Li, Y.-Z. & Zuo, J.-L. Calix[4]arene-Supported Mononuclear Lanthanide Single-Molecule Magnet. *Inorganic Chemistry* **53**, 562–567 (2013).
69. Gao, F. *et al.* Syntheses, Structures, and Magnetic Properties of seven-coordinate Lanthanide Porphyrinate or Phthalocyaninate Complexes with Kläui's Tripodal Ligand. *Inorganic Chemistry* **52**, 6407–6416 (2013).
70. Gao, Y. *et al.* A novel nitronyl nitroxide radical and its Gd(III), Tb(III), Dy(III) complexes: Synthesis, structure and magnetic properties. *Inorganic Chemistry Communications* **27**, 31–35 (2013).
71. Gonidec, M. *et al.* Highly Reduced Double-Decker Single-Molecule Magnets Exhibiting Slow Magnetic Relaxation. *Inorganic Chemistry* **52**, 4464–4471 (2013).
72. Goswami, S., Adhikary, A., Jena, H. S. & Konar, S. Lanthanide based coordination polymers chill, relax under magnetic field and also fluoresce. *Dalton Transactions* **42**, 9813 (2013).
73. Hu, P. *et al.* Lanthanide–radical linear chain compounds based on 2,4,4,5,5-pentamethylimidazoline-1-oxyl-3-oxide: Structure and magnetic properties. *Inorganica Chimica Acta* **398**, 136–140 (2013).
74. Kan, J. *et al.* Sandwich-Type Mixed Tetrapyrrole Rare-Earth Triple-Decker Compounds. Effect of the Coordination Geometry on the Single-Molecule-Magnet Nature. *Inorganic Chemistry* **52**, 8505–8510 (2013).
75. Li, Q.-W. *et al.* Fluorescent single-ion magnets: molecular hybrid  $(\text{HNEt}_3)[\text{Dy}_x\text{Yb}_{1-x}(\text{bpyda})_2]$  ( $x = 0.135\text{--}1$ ). *Dalton Transactions* **42**, 11262 (2013).
76. Li, X.-L. *et al.* Luminescent, magnetic and ferroelectric properties of noncentrosymmetric chain-like complexes composed of nine-coordinate lanthanide ions. *Dalton Transactions* **42**, 15317 (2013).
77. Li, Y.-Y., Gao, F., Beves, J. E., Li, Y.-Z. & Zuo, J.-L. A giant metallo-supramolecular cage encapsulating a single-molecule magnet. *Chemical Communications* **49**, 3658 (2013).
78. Liu, J.-L. *et al.* Switching the anisotropy barrier of a single-ion magnet by symmetry change from quasi- $D_{3h}$  to quasi- $O_h$ . *Chemical Science* **4**, 3310 (2013).
79. Liu, R. N., Zhao, S. P. & Xiong, C. X. Syntheses, crystal structures, and magnetic properties of two monometallic tri-spin complexes involving nitronyl nitroxide radicals-lanthanide ions. *Russian Journal of Coordination Chemistry* **39**, 808–812 (2013).
80. Martín-Ramos, P. *et al.* Single-Ion Magnetism in a Luminescent  $\text{Er}^{3+}$   $\beta$ -Diketonato Complex with Multiple Relaxation Mechanisms. *European Journal of Inorganic Chemistry* **2014**, 511–517 (2013).
81. Meihaus, K. R. & Long, J. R. Magnetic Blocking at 10 K and a Dipolar-Mediated Avalanche in Salts of the Bis( $\eta^8$ -cyclooctatetraenide) Complex  $[\text{Er}(\text{COT})_2]$ . *Journal of the American Chemical Society* **135**, 17952–17957 (2013).
82. Meng, Y. *et al.* Ionothermal synthesis of two oxalate-bridged lanthanide(III) chains with slow magnetization relaxation by using a deep eutectic solvent. *Dalton Transactions* **42**, 12853 (2013).
83. Murakami, R., Ishida, T., Yoshii, S. & Nojiri, H. Single-molecule magnet  $[\text{Tb}(\text{hfac})_3(2\text{pyNO})]$  ( $2\text{pyNO} = \text{t-butyl 2-pyridyl nitroxide}$ ) with a relatively high barrier of magnetization reversal. *Dalton Transactions* **42**, 13968 (2013).
84. Na, B., Wang, Y.-X., Han, T., Shi, W. & Cheng, P. A rare one-dimensional Dy(III) complex exhibiting slow magnetic relaxation. *Inorganic Chemistry Communications* **35**, 19–21 (2013).
85. Palacios, M. A. *et al.* Bifunctional  $\text{Zn}^{\text{II}}\text{Ln}^{\text{III}}$  Dinuclear Complexes Combining Field Induced SMM Behavior and Luminescence: Enhanced NIR Lanthanide Emission by 9-Anthracene Carboxylate Bridging Ligands. *Inorganic Chemistry* **53**, 1465–1474 (2013).
86. Pointillart, F. *et al.* A Series of Tetrathiafulvalene-Based Lanthanide Complexes Displaying Either Single Molecule Magnet or Luminescence—Direct Magnetic and Photo-Physical Correlations in the Ytterbium Analogue. *Inorganic Chemistry* **52**, 5978–5990 (2013).
87. Roy, J. J. L. *et al.* An Organometallic Building Block Approach To Produce a Multidecker 4/ $f$  Single-Molecule Magnet. *Journal of the American Chemical Society* **135**, 3502–3510 (2013).
88. Sato, R., Suzuki, K., Sugawa, M. & Mizuno, N. Heterodinuclear Lanthanoid-Containing Polyoxometalates: Stepwise Synthesis and Single-Molecule Magnet Behavior. *Chemistry - A European Journal* **19**, 12982–12990 (2013).
89. Völcker, F., Lan, Y., Powell, A. K. & Roesky, P. W. Slow magnetic relaxation in tris(diphosphanylarnido) and tetra(phosphanoamido) dysprosium complexes. *Dalton Transactions* **42**, 11471 (2013).

90. Vrábel, P. *et al.* Slow spin relaxation induced by magnetic field in  $[\text{NdCo}(\text{bpdo})(\text{H}_2\text{O})_4(\text{CN})_6]\cdot 3\text{H}_2\text{O}$ . *Journal of Physics: Condensed Matter* **25**, 186003 (2013).

91. Wang, K. *et al.* Binuclear Phthalocyanine-Based Sandwich-Type Rare Earth Complexes: Unprecedented Two  $\pi$ -Bridged Biradical-Metal Integrated SMMs. *Chemistry - A European Journal* **19**, 11162–11166 (2013).

92. Wang, Y.-L. *et al.* Syntheses, crystal structures, magnetic and luminescence properties of five novel lanthanide complexes of nitronyl nitroxide radical. *Journal of Solid State Chemistry* **202**, 276–281 (2013).

93. Wang, Y.-L. *et al.* Syntheses, Structures, and Magnetic and Luminescence Properties of a New Dy<sup>III</sup>-Based Single-Ion Magnet. *Inorganic Chemistry* **52**, 7380–7386 (2013).

94. Wu, S.-Q. *et al.* Supramolecular lanthanide metallogrids exhibiting field-induced single-ion magnetic behavior. *Dalton Transactions* **42**, 4369 (2013).

95. Xu, W. *et al.* Crystal Structure, Multiplex Photoluminescence, and Magnetic Properties of a Series of Lanthanide Coordination Polymers Based on Quinoline Carboxylate Ligand. *Crystal Growth & Design* **13**, 5420–5432 (2013).

96. Zhang, P., Zhang, L., Lin, S.-Y. & Tang, J. Tetranuclear  $[\text{MDy}]_2$  Compounds and Their Dinuclear  $[\text{MDy}]$  ( $\text{M} = \text{Zn}/\text{Cu}$ ) Building Units: Their Assembly, Structures, and Magnetic Properties. *Inorganic Chemistry* **52**, 6595–6602 (2013).

97. Zhou, W. *et al.* New polyoxometalate-based mononuclear lanthanide complexes with slow relaxation of magnetization. *Inorganica Chimica Acta* **394**, 770–775 (2013).

98. Zhu, J., Song, H.-F., Yan, P.-F., Hou, G.-F. & Li, G.-M. Slow relaxation processes of salen type Dy<sub>2</sub> complex and 1D ionic spiral Dyn coordination polymer. *CrystEngComm* **15**, 1747 (2013).

99. Bag, P. *et al.* Oxalato-Bridged Neutral Octanuclear Heterometallic Complexes  $[\text{Ln}_4\text{K}_4(\text{L})_4(\mu\text{-H}_2\text{O})_4(\text{NO}_3)_2(\mu\text{-Ox})]$  ( $\text{Ln} = \text{Dy}(\text{III}), \text{Gd}(\text{III}), \text{Tb}(\text{III}), \text{Ho}(\text{III})$ ;  $\text{LH}_3 = \text{N}[\text{CH}_2\text{CH}_2\text{N}=\text{CH-C}_6\text{H}_3\text{-2-OH-3-OMe}]_3$ ;  $\text{Ox} = (\text{C}_2\text{O}_4)^{2-}$ ): Synthesis, Structure, Magnetic and Luminescent Properties. *Crystal Growth & Design* **14**, 4583–4592 (2014).

100. Baldoví, J. J. *et al.* Construction of a General Library for the Rational Design of Nanomagnets and Spin Qubits Based on Mononuclear f-Block Complexes. The Polyoxometalate Case. *Inorganic Chemistry* **53**, 9976–9980 (2014).

101. Baldoví, J. J. *et al.* A SIM-MOF: Three-Dimensional Organisation of Single-Ion Magnets with Anion-Exchange Capabilities. *Chemistry - A European Journal* **20**, 10695–10702 (2014).

102. Biswas, S., Jena, H. S., Adhikary, A. & Konar, S. Two Isostructural 3D Lanthanide Coordination Networks ( $\text{Ln} = \text{Gd}^{3+}, \text{Dy}^{3+}$ ) with Squashed Cuboid-Type Nanoscopic Cages Showing Significant Cryogenic Magnetic Refrigeration and Slow Magnetic Relaxation. *Inorganic Chemistry* **53**, 3926–3928 (2014).

103. Campbell, V. E. *et al.* Structural and Electronic Dependence of the Single-Molecule-Magnet Behavior of Dysprosium(III) Complexes. *Inorganic Chemistry* **53**, 2598–2605 (2014).

104. Demir, S., Zadrozny, J. M. & Long, J. R. Large Spin-Relaxation Barriers for the Low-Symmetry Organolanthanide Complexes  $[\text{Cp}^*_2\text{Ln}(\text{BPh}_4)]$  ( $\text{Cp}^* = \text{pentamethylcyclopentadienyl}$ ;  $\text{Ln} = \text{Tb}, \text{Dy}$ ). *Chemistry - A European Journal* **20**, 9524–9529 (2014).

105. Dreiser, J. *et al.* The Metallofullerene Field-Induced Single-Ion Magnet  $\text{HoSc}_2\text{N}@\text{C}_{80}$ . *Chemistry - A European Journal* **20**, 13536–13540 (2014).

106. Fukuda, T., Shigeyoshi, N., Yamamura, T. & Ishikawa, N. Magnetic Relaxations Arising from Spin-Phonon Interactions in the Nonthermally Activated Temperature Range for a Double-Decker Terbium Phthalocyanine Single Molecule Magnet. *Inorganic Chemistry* **53**, 9080–9086 (2014).

107. Giménez-Agulló, N. *et al.* Single-Molecule-Magnet Behavior in the Family of  $[\text{Ln}(\text{OETAP})_2]$  Double-Decker Complexes ( $\text{Ln} = \text{Lanthanide}$ , OETAP=Octa(ethyl)tetraazaporphyrin). *Chemistry - A European Journal* **20**, 12817–12825 (2014).

108. Girginova, P. I., Pereira, L. C. J., Coutinho, J. T., Santos, I. C. & Almeida, M. Slow magnetic relaxation in lanthanide ladder type coordination polymers. *Dalton Trans.* **43**, 1897–1905 (2014).

109. Guo, Y.-N. *et al.* An NCN-pincer ligand dysprosium single-ion magnet showing magnetic relaxation via the second excited state. *Scientific Reports* **4**, (2014).

110. Hu, P. *et al.* Magnetic relaxation in mononuclear Tb complex involving a nitronyl nitroxide ligand. *New J. Chem.* **38**, 4716–4721 (2014).

111. Hu, P. *et al.* A new family of Ln–radical chains ( $\text{Ln} = \text{Nd}, \text{Sm}, \text{Gd}, \text{Tb}$  and  $\text{Dy}$ ): synthesis, structure, and magnetic properties. *Dalton Trans.* **43**, 2234–2243 (2014).

112. Jung, J. *et al.* Magnetic Studies of Redox-Active Tetrathiafulvalene-Based Complexes: Dysprosium vs.

Ytterbium Analogues. *European Journal of Inorganic Chemistry* **2014**, 3888–3894 (2014).

113. Katoh, K. *et al.* Effect of f-f interactions on quantum tunnelling of the magnetization: mono- and dinuclear Dy(III) phthalocyaninato triple-decker single-molecule magnets with the same octacoordination environment. *Dalton Transactions* **43**, 7716 (2014).

114. Klyatskaya, S., Eichhöfer, A. & Wernsdorfer, W. X-ray Crystallographic Analysis of a Tailor-Made Bis(phthalocyaninato)-Tb<sup>III</sup> Single-Molecule Magnet as a Fundamental Unit for Supramolecular Spintronic Devices. *European Journal of Inorganic Chemistry* **2014**, 4179–4185 (2014).

115. König, S. N. *et al.* Fast magnetic relaxation in an octahedral dysprosium tetramethyl-aluminate complex. *Dalton Trans.* **43**, 3035–3038 (2014).

116. Lannes, A., Intissar, M., Suffren, Y., Reber, C. & Luneau, D. Terbium(III) and Yttrium(III) Complexes with Pyridine-Substituted Nitronyl Nitroxide Radical and Different  $\beta$ -Diketonate Ligands. Crystal Structures and Magnetic and Luminescence Properties. *Inorganic Chemistry* **53**, 9548–9560 (2014).

117. Liu, C.-M., Zhang, D.-Q., Hao, X. & Zhu, D.-B. Trinuclear [Co<sup>III</sup><sub>2</sub>-Ln<sup>III</sup>] (Ln=Tb, Dy) Single-Ion Magnets with Mixed 6-Chloro-2-Hydroxypyridine and Schiff Base Ligands. *Chemistry - An Asian Journal* **9**, 1847–1853 (2014).

118. Liu, J.-F. *et al.* Syntheses, Structure, and Properties of Mixed Cp–Amidinate Rare-Earth-Metal(III) Complexes. *Organometallics* **33**, 1374–1381 (2014).

119. Liu, Q.-Y. *et al.* Urothermal synthesis of mononuclear lanthanide compounds: slow magnetization relaxation observed in Dy analogue. *CrystEngComm* **16**, 585–590 (2014).

120. Liu, S.-S. *et al.* A half-sandwich organometallic single-ion magnet with hexamethylbenzene coordinated to the Dy(III) ion. *Chem. Commun.* **50**, 11418–11420 (2014).

121. Long, J. *et al.* A High-Temperature Molecular Ferroelectric Zn/Dy Complex Exhibiting Single-Ion-Magnet Behavior and Lanthanide Luminescence. *Angewandte Chemie International Edition* **54**, 2236–2240 (2014).

122. Lucaccini, E., Sorace, L., Perfetti, M., Costes, J.-P. & Sessoli, R. Beyond the anisotropy barrier: slow relaxation of the magnetization in both easy-axis and easy-plane Ln(trensal) complexes. *Chem. Commun.* **50**, 1648–1651 (2014).

123. Maxim, C. *et al.* Cyanomethylene-bis(phosphonate)-Based Lanthanide Complexes: Structural, Photophysical, and Magnetic Investigations. *Inorganic Chemistry* **53**, 2708–2717 (2014).

124. Oyarzabal, I. *et al.* Rational Electrostatic Design of Easy-Axis Magnetic Anisotropy in a Zn<sup>II</sup>-Dy<sup>III</sup>-Zn<sup>II</sup> Single-Molecule Magnet with a High Energy Barrier. *Chemistry - A European Journal* **20**, 14262–14269 (2014).

125. Meihaus, K. R. *et al.* Influence of Pyrazolate vs N-Heterocyclic Carbene Ligands on the Slow Magnetic Relaxation of Homoleptic Trischelate Lanthanide(III) and Uranium(III) Complexes. *Journal of the American Chemical Society* **136**, 6056–6068 (2014).

126. Na, B. *et al.* Six-Coordinate Lanthanide Complexes: Slow Relaxation of Magnetization in the Dysprosium(III) Complex. *Chemistry - A European Journal* **20**, 15975–15980 (2014).

127. Nayak, S., Novitchi, G., Hołyńska, M. & Dehnen, S. Two Heterometallic Ionic Compounds with Isolated [3d] and [4f] Complex Units: Field-Induced Single-Ion Magnet (SIM) Behavior Observed from a Mononuclear Dysprosium(III) Complex. *European Journal of Inorganic Chemistry* **2014**, 3065–3071 (2014).

128. Norel, L. *et al.* Redox Modulation of Magnetic Slow Relaxation in a 4f-Based Single-Molecule Magnet with a 4d Carbon-Rich Ligand. *Inorganic Chemistry* **53**, 2361–2363 (2014).

129. Pedersen, K. S. *et al.* Modifying the properties of 4f single-ion magnets by peripheral ligand functionalisation. *Chem. Sci.* **5**, 1650–1660 (2014).

130. Qiao, X.-M., Zhang, C.-X., Kong, Y.-K., Wang, Q.-L. & Zhang, Y.-Y. Two Mononuclear Tri-Spin Compounds based on the Lanthanide-Nitronyl Nitroxide Radicals: Synthesis, Crystal Structure, and Magnetic Properties. *Zeitschrift für anorganische und allgemeine Chemie* **640**, 1684–1687 (2014).

131. Shintoyo, S. *et al.* Crystal Field Splitting of the Ground State of Terbium(III) and Dysprosium(III) Complexes with a Triimidazolyl Tripod Ligand and an Acetate Determined by Magnetic Analysis and Luminescence. *Inorganic Chemistry* **53**, 10359–10369 (2014).

132. Silva, M. R., Martin-Ramos, P., Coutinho, J. T., Pereira, L. C. J. & Martin-Gil, J. Effect of the capping ligand on luminescent erbium(III)  $\beta$ -diketonate single-ion magnets. *Dalton Transactions* **43**, 6752 (2014).

133. Sun, W.-B. *et al.* The slow magnetic relaxation regulated by ligand conformation of a lanthanide single-ion magnet [He<sub>x</sub>4N][Dy(DBM)4]. *Inorg. Chem. Front.* **1**, 503–509 (2014).

134. Tretyakov, E. V. *et al.* Complexes of lanthanides with spin-labeled pyrazolylquinoline. *Russian Chemical Bulletin* **63**, 1459–1464 (2014).

135. Ungur, L., Le Roy, J. J., Korobkov, I., Murugesu, M. & Chibotaru, L. F. Fine-tuning the Local Symmetry to Attain Record Blocking Temperature and Magnetic Remanence in a Single-Ion Magnet. *Angewandte Chemie International Edition* **53**, 4413–4417 (2014).

136. Upadhyay, A. *et al.* Enhancing the effective energy barrier of a Dy(III) SMM using a bridged diamagnetic Zn(II) ion. *Chem. Commun.* **50**, 8838–8841 (2014).

137. Xie, Q.-W. *et al.* Heterodinuclear  $M^{II}$ – $Ln^{III}$  single molecule magnets constructed from exchange-coupled single ion magnets. *Dalton Transactions* **43**, 11309 (2014).

138. Xiong, G. *et al.* New strategy to construct single-ion magnets: a unique  $Dy@Zn_6$  cluster exhibiting slow magnetic relaxation. *Chem. Commun.* **50**, 4255–4257 (2014).

139. Yamauchi, S. *et al.* Synthesis, Structure, Luminescence, and Magnetic Properties of a Single-Ion Magnet “mer”-[Tris(N-[(imidazol-4-yl)-methylidene]-dl-phenylalaninato)terbium(III) and Related “fac”-dl-Alaninato Derivative. *Inorganic Chemistry* **53**, 5961–5971 (2014).

140. Yi, X. *et al.* Unraveling the Crystal Structure of Lanthanide-Murexide Complexes: Use of an Ancient Complexometry Indicator as a Near-Infrared-Emitting Single-Ion Magnet. *Chemistry - A European Journal* **20**, 1569–1576 (2014).

141. Zeng, D., Ren, M., Bao, S.-S., Li, L. & Zheng, L.-M. A luminescent heptanuclear  $DyIr_6$  complex showing field-induced slow magnetization relaxation. *Chemical Communications* **50**, 8356 (2014).

142. Zeng, D., Ren, M., Bao, S.-S. & Zheng, L.-M. Tuning the Coordination Geometries and Magnetic Dynamics of  $[Ln(hfac)_4]$ -through Alkali Metal Counterions. *Inorganic Chemistry* **53**, 795–801 (2014).

143. Zhang, P. *et al.* Equatorially Coordinated Lanthanide Single Ion Magnets. *Journal of the American Chemical Society* **136**, 4484–4487 (2014).

144. Zhao, J. *et al.* Rectangle versus Square Oxalate-Connective Tetralanthanide Cluster Anchored in Lacunary Lindqvist Isopolytungstates: Syntheses, Structures, and Properties. *Crystal Growth & Design* **14**, 5495–5505 (2014).

145. Zhu, J. *et al.* Local Coordination Geometry Perturbed  $\beta$ -Diketone Dysprosium Single-Ion Magnets. *Inorganic Chemistry* **53**, 8895–8901 (2014).

146. Anastasiadis, N. C. *et al.* Dinuclear lanthanide(III)/zinc(II) complexes with methyl 2-pyridyl ketone oxime. *Dalton Transactions* **44**, 19791–19795 (2015).

147. Brown, A. J., Pinkowicz, D., Saber, M. R. & Dunbar, K. R. A Trigonal-Pyramidal Erbium(III) Single-Molecule Magnet. *Angewandte Chemie* **127**, 5962–5966 (2015).

148. Cao, W. *et al.* Rational enhancement of the energy barrier of bis(tetrapyrrole) dysprosium SMMs via replacing atom of porphyrin core. *Chemical Science* **6**, 5947–5954 (2015).

149. Chen, P. *et al.* Crystallization of triple- and quadruple-stranded dinuclear bis- $\beta$ -diketonate-Dy(iii) helicates: single molecule magnetic behavior. *CrystEngComm* **17**, 7227–7232 (2015).

150. Chen, P. *et al.* Anion-dependent assembly of Dy complexes: structures and magnetic behaviors. *CrystEngComm* **17**, 5066–5073 (2015).

151. Chien, Y.-L. *et al.* New salen-type dysprosium(III) double-decker and triple-decker complexes. *Polyhedron* **102**, 8–15 (2015).

152. Costes, J. P. *et al.* Analysis of the Role of Peripheral Ligands Coordinated to  $Zn^{II}$  in Enhancing the Energy Barrier in Luminescent Linear Trinuclear Zn-Dy-Zn Single-Molecule Magnets. *Chemistry - A European Journal* **21**, 15785–15796 (2015).

153. Coutinho, J. T. *et al.* Field-induced single-ion magnetic behaviour in a highly luminescent  $Er^{3+}$  complex. *Materials Chemistry and Physics* **160**, 429–434 (2015).

154. Das, C. *et al.* Origin of SMM behaviour in an asymmetric Er(III) Schiff base complex: a combined experimental and theoretical study. *Chemical Communications* **51**, 6137–6140 (2015).

155. Das, S. *et al.* Amending the Anisotropy Barrier and Luminescence Behavior of Heterometallic Trinuclear Linear  $[M^{II}Ln^{III}M^{II}]$  ( $Ln^{III}$ =Gd, Tb, Dy;  $M^{II}$ =Mg/Zn) Complexes by Change from Divalent Paramagnetic to Diamagnetic Metal Ions. *Chemistry - A European Journal* **21**, 6449–6464 (2015).

156. Dolai, M., Ali, M., Titiš, J. & Boča, R. Cu(II)–Dy(III) and Co(III)–Dy(III) based single molecule magnets with multiple slow magnetic relaxation processes in the Cu(II)–Dy(III) complex. *Dalton Transactions* **44**, 13242–13249 (2015).

157. Dong, Y., Yan, P., Zou, X. & Li, G. Azacyclo-auxiliary ligand-tuned SMMs of dibenzoylmethane Dy(III)

complexes. *Inorganic Chemistry Frontiers* **2**, 827–836 (2015).

158. Dong, Y., Yan, P., Zou, X., Liu, T. & Li, G. Exploiting single-molecule magnets of  $\beta$ -diketone dysprosium complexes with  $C_{3v}$  symmetry: suppression of quantum tunneling of magnetization. *Journal of Materials Chemistry C* **3**, 4407–4415 (2015).

159. Duan, F., Liu, L., Qiao, C. & Yang, H. Self-assembly and magnetic behavior of 2-aldehyde-8-hydroxyquinolinate-based lanthanide complex. *Inorganic Chemistry Communications* **55**, 120–122 (2015).

160. Feng, H.-K., Huang, P.-J. & Tsai, H.-L. One-dimensional lanthanide coordination polymers: synthesis, structures, and single-ion magnetic behaviour. *Dalton Transactions* **44**, 3764–3772 (2015).

161. Feng, M. *et al.* Multiple Single-Molecule Magnet Behaviors in Dysprosium Dinuclear Complexes Involving a Multiple Functionalized Tetrathiafulvalene-Based Ligand. *Inorganic Chemistry* **54**, 4021–4028 (2015).

162. Feng, M. *et al.* Dysprosium- and Ytterbium-Based Complexes Involving Tetrathiafulvalene Derivatives Functionalised with 2,2'-Bipyridine or 2,6-Di(pyrazol-1-yl)-4-pyridine. *European Journal of Inorganic Chemistry* **2016**, 2039–2050 (2015).

163. Gao, F., Yang, F.-L., Zhu, G.-Z. & Zhao, Y. Syntheses, structures, and magnetic properties of homodinuclear lanthanide complexes based on dinucleating Schiff base ligands. *Dalton Transactions* **44**, 20232–20241 (2015).

164. Gavey, E. L. *et al.* Placing a crown on Dy<sup>III</sup> – a dual property LnIII crown ether complex displaying optical properties and SMM behaviour. *Journal of Materials Chemistry C* **3**, 7738–7747 (2015).

165. Gavrilita, A. *et al.* Osmium-Nitrosyl Oxalato-Bridged Lanthanide-Centered Pentanuclear Complexes – Synthesis, Crystal Structures and Magnetic Properties. *European Journal of Inorganic Chemistry* **2015**, 1616–1624 (2015).

166. Goura, J., Brambleby, J., Goddard, P. & Chandrasekhar, V. A Single-Ion Magnet Based on a Heterometallic Co<sup>III</sup><sub>2</sub>Dy<sup>III</sup> Complex. *Chemistry - A European Journal* **21**, 4926–4930 (2015).

167. Han, S.-D., Wang, Q.-L., Xu, J. & Bu, X.-H. Anion-Triggered Modulation of Structure and Magnetic Properties of Copper(I)-Dysprosium(III) Complexes Derived from 1-Hydroxybenzotriazolate. *European Journal of Inorganic Chemistry* **2015**, 5379–5386 (2015).

168. Han, T. *et al.* Field and dilution effects on the magnetic relaxation behaviours of a 1D dysprosium(III)-carboxylate chain built from chiral ligands. *Dalton Transactions* **44**, 13480–13484 (2015).

169. Horii, Y., Katoh, K., Yasuda, N., Breedlove, B. K. & Yamashita, M. Effects of *f-f* Interactions on the Single-Molecule Magnet Properties of Terbium(III)-Phthalocyaninato Quintuple-Decker Complexes. *Inorganic Chemistry* **54**, 3297–3305 (2015).

170. Hu, K.-Q. *et al.* A trimetallic strategy towards Zn<sup>II</sup><sub>4</sub>Dy<sup>III</sup><sub>2</sub>Cr<sup>III</sup><sub>2</sub> and Zn<sup>II</sup><sub>4</sub>Dy<sup>III</sup><sub>2</sub>Co<sup>III</sup><sub>2</sub> single-ion magnets. *Dalton Transactions* **44**, 15413–15416 (2015).

171. Jung, J. *et al.* Analysis of the electrostatics in Dy<sup>III</sup> single-molecule magnets: the case study of Dy(Murex)<sub>3</sub>. *Dalton Transactions* **44**, 18270–18275 (2015).

172. Kanetomo, T., Yoshii, S., Nojiri, H. & Ishida, T. Single-molecule magnet involving strong exchange coupling in terbium(iii) complex with 2,2'-bipyridin-6-yl tert-butyl nitroxide. *Inorganic Chemistry Frontiers* **2**, 860–866 (2015).

173. Lannes, A. & Luneau, D. New Family of Lanthanide-Based Complexes with Different Scorpionate-Type Ligands: A Rare Case Where Dysprosium and Ytterbium Analogues Display Single-Ion-Magnet Behavior. *Inorganic Chemistry* **54**, 6736–6743 (2015).

174. Li, L.-L., Liu, S., Zhang, Y., Shi, W. & Cheng, P. Three new mononuclear tri-spin lanthanide-nitronyl nitroxide radical compounds: syntheses, structures and magnetic properties. *Dalton Transactions* **44**, 6118–6125 (2015).

175. Li, L., Liu, S., Zhang, Y., Xu, N. & Cheng, P. Two new mononuclear tri-spin lanthanide-nitronyl nitroxide radical complexes: Syntheses, structure and magnetic properties. *Inorganic Chemistry Communications* **57**, 51–53 (2015).

176. Li, Q.-W. *et al.* “Half-sandwich” Yb<sup>III</sup> single-ion magnets with metallacrowns. *Chemical Communications* **51**, 10291–10294 (2015).

177. Lin, S.-Y., Wang, C., Zhao, L., Wu, J. & Tang, J. Chiral mononuclear lanthanide complexes and the field-induced single-ion magnet behaviour of a Dy analogue. *Dalton Transactions* **44**, 223–229 (2015).

178. Liu, S.-S. *et al.* Half-Sandwich Complexes of Dy<sup>III</sup>: A Janus-Motif with Facile Tunability of Magnetism.

*Inorganic Chemistry* **54**, 5162–5168 (2015).

179. Meihaus, K. R., Fieser, M. E., Corbey, J. F., Evans, W. J. & Long, J. R. Record High Single-Ion Magnetic Moments Through 4fn5d1 Electron Configurations in the Divalent Lanthanide Complexes  $[(C_5H_4SiMe_3)_3Ln]$ . *Journal of the American Chemical Society* **137**, 9855–9860 (2015).

180. Mondal, A. K., Goswami, S. & Konar, S. Influence of the coordination environment on slow magnetic relaxation and photoluminescence behavior in two mononuclear dysprosium(III) based single molecule magnets. *Dalton Transactions* **44**, 5086–5094 (2015).

181. Pointillart, F. *et al.* Luminescence and Single-Molecule Magnet Behavior in Lanthanide Complexes Involving a Tetrathiafulvalene-Fused Dipyridophenazine Ligand. *Inorganic Chemistry* **54**, 5384–5397 (2015).

182. Pointillart, F. *et al.* Magnetic and Photo-Physical Properties of Lanthanide Dinuclear Complexes Involving the 4,5-Bis(2-Pyridyl-N-Oxidemethylthio)-4',5'-Dicarboxylic Acid-Tetrathiafulvalene-, Dimethyl Ester Ligand. *Inorganics* **3**, 554–572 (2015).

183. Qian, K. *et al.* Does the thermal evolution of molecular structures critically affect the magnetic anisotropy? *Chemical Science* **6**, 4587–4593 (2015).

184. Rechkemmer, Y. *et al.* Comprehensive Spectroscopic Determination of the Crystal Field Splitting in an Erbium Single-Ion Magnet. *Journal of the American Chemical Society* **137**, 13114–13120 (2015).

185. Ren, M. *et al.* Lanthanide phosphonates with pseudo-D5h local symmetry exhibiting magnetic and luminescence bifunctional properties. *Inorganic Chemistry Frontiers* **2**, 558–566 (2015).

186. Roy, J. J. L., Gorelsky, S. I., Korobkov, I. & Murugesu, M. Slow Magnetic Relaxation in Uranium(III) and Neodymium(III) Cyclooctatetraenyl Complexes. *Organometallics* **34**, 1415–1418 (2015).

187. Shan, P.-Y. *et al.* Synthesis, Crystal Structure, and Single-Molecule Magnetic Properties of a Salen-type Zn-Dy-Zn Complex. *Zeitschrift für anorganische und allgemeine Chemie* **641**, 1119–1124 (2015).

188. Soussi, K. *et al.* Magnetic and photo-physical investigations into Dy<sup>III</sup> and Yb<sup>III</sup> complexes involving tetrathiafulvalene ligand. *Inorganic Chemistry Frontiers* **2**, 1105–1117 (2015).

189. Takehara, C. *et al.* Slow magnetic relaxation of light lanthanide-based linear LnZn<sub>2</sub> trinuclear complexes. *Dalton Transactions* **44**, 18276–18283 (2015).

190. Wang, X., Zhu, M., Wang, J. & Li, L. Unusual Gd–nitronyl nitroxide antiferromagnetic coupling and slow magnetic relaxation in the corresponding Tb analogue. *Dalton Transactions* **44**, 13890–13896 (2015).

191. Wu, J., Zhao, L., Guo, M. & Tang, J. Constructing supramolecular grids: from 4f square to 3d–4f grid. *Chemical Communications* **51**, 17317–17320 (2015).

192. Wu, J. *et al.* Linear 3d–4f compounds: synthesis, structure, and determination of the *d*–*f* magnetic interaction. *Dalton Transactions* **44**, 11935–11942 (2015).

193. Yue, Y., Sun, J., Yan, P. & Li, G. Single molecule magnet of flexible Salen-type dysprosium coordination polymer with 1D ionic chain structure. *Inorganic Chemistry Communications* **51**, 42–45 (2015).

194. Zeng, D. *et al.* pH-controlled polymorphism in a layered dysprosium phosphonate and its impact on the magnetization relaxation. *Chemical Communications* **51**, 2649–2652 (2015).

195. Zhang, C.-X. *et al.* Two Lanthanide–nitronyl nitroxide radicals compounds with slow magnetic relaxation behavior. *Journal of Molecular Structure* **1081**, 348–354 (2015).

196. Zhang, X.-J. *et al.* An unusual three-dimensional Dy–Cd<sub>2</sub> framework exhibiting single-ion magnet behavior. *Dalton Transactions* **44**, 7757–7760 (2015).

197. Zhang, Y. *et al.* Tuning the Origin of Magnetic Relaxation by Substituting the 3d or Rare-Earth Ions into Three Isostructural Cyano-Bridged 3d–4f Heterodinuclear Compounds. *Inorganic Chemistry* **54**, 10316–10322 (2015).

198. Zhou, S. Y. *et al.* A series of heterospin complexes based on lanthanides and pyridine biradicals: synthesis, structure and magnetic properties. *RSC Advances* **5**, 17131–17139 (2015).

199. Zou, X., Yan, P., Dong, Y., Luan, F. & Li, G. Magnetic dynamics of two salen type Dy<sub>2</sub> complexes modulated by coordination geometry. *RSC Advances* **5**, 96573–96579 (2015).

200. Amjad, A., Figuerola, A., Caneschi, A. & Sorace, L. Multiple Magnetization Reversal Channels Observed in a 3d-4f Single Molecule Magnet. *Magnetochemistry* **2**, 27 (2016).

201. Amjad, A., Madalan, A. M., Andruh, M., Caneschi, A. & Sorace, L. Slow Relaxation of Magnetization in an Isostructural Series of Zinc-Lanthanide Complexes: An Integrated EPR and AC Susceptibility Study. *Chemistry - A European Journal* **22**, 12849–12858 (2016).

202. Antal, P., Drahoš, B., Herchel, R. & Trávníček, Z. Muffin-like lanthanide complexes with an N<sub>5</sub>O<sub>2</sub>-donor macrocyclic ligand showing field-induced single-molecule magnet behaviour. *Dalton Transactions* **45**,

15114–15121 (2016).

203. Baldoví, J. J. *et al.* Single ion magnets based on lanthanoid polyoxomolybdate complexes. *Dalton Transactions* **45**, 16653–16660 (2016).

204. Baldoví, J. J. *et al.* Rational Design of Lanthanoid Single-Ion Magnets: Predictive Power of the Theoretical Models. *Chemistry - A European Journal* **22**, 13532–13539 (2016).

205. Bi, Y. *et al.* Thermostability and photoluminescence of Dy(III) single-molecule magnets under a magnetic field. *Chem. Sci.* **7**, 5020–5031 (2016).

206. Boadi, N. O. *et al.* The deposition of PbS and PbSe thin films from lead dichalcogenoimidophosphinates by AACVD. *Inorganica Chimica Acta* **453**, 439–442 (2016).

207. Chen, Y.-C. *et al.* Symmetry-Supported Magnetic Blocking at 20 K in Pentagonal Bipyramidal Dy(III) Single-Ion Magnets. *Journal of the American Chemical Society* **138**, 2829–2837 (2016).

208. Chorazy, S., Rams, M., Nakabayashi, K., Sieklucka, B. & Ohkoshi, S. White Light Emissive Dy<sup>III</sup> Single-Molecule Magnets Sensitized by Diamagnetic [Co<sup>III</sup>(CN)<sub>6</sub>]<sup>3-</sup> Linkers. *Chemistry - A European Journal* **22**, 7371–7375 (2016).

209. Chorazy, S., Wang, J. & Ohkoshi, S. Yellow to greenish-blue colour-tunable photoluminescence and 4f-centered slow magnetic relaxation in a cyanido-bridged Dy<sup>III</sup>(4-hydroxypyridine)-Co<sup>III</sup> layered material. *Chemical Communications* **52**, 10795–10798 (2016).

210. Dickie, C. M. & Nippe, M. Magnetization dynamics of a heterometallic Dy-isocarbonyl complex. *Inorganic Chemistry Frontiers* **3**, 97–103 (2016).

211. Ding, Y.-S. *et al.* Syntheses, structures and magnetic properties of a series of mono- and di-nuclear dysprosium(III)-crown-ether complexes: effects of a weak ligand-field and flexible cyclic coordination modes. *Inorganic Chemistry Frontiers* **3**, 798–807 (2016).

212. Dong, Y. *et al.* Auxiliary ligand field dominated single-molecule magnets of a series of indole-derivative  $\beta$ -diketone mononuclear Dy(III) complexes. *Dalton Transactions* **45**, 9148–9157 (2016).

213. Fernandez-Garcia, G. *et al.* Slow Magnetic Relaxation in Chiral Helicene-Based Coordination Complex of Dysprosium. *Magnetochemistry* **3**, 2 (2016).

214. Gao, C., Yang, Q., Wang, B.-W., Wang, Z.-M. & Gao, S. Evaporable lanthanide single-ion magnet. *CrystEngComm* **18**, 4165–4171 (2016).

215. Gao, R.-C. *et al.* Two 3D Isostructural Ln(III)-MOFs: Displaying the Slow Magnetic Relaxation and Luminescence Properties in Detection of Nitrobenzene and Cr<sub>2</sub>O<sub>7</sub><sup>2-</sup>. *Inorganic Chemistry* **55**, 11323–11330 (2016).

216. Goswami, S., Biswas, S., Tomar, K. & Konar, S. Tuning the Magnetoluminescence Behavior of Lanthanide Complexes Having Sphenocorona and Cubic Coordination Geometries. *European Journal of Inorganic Chemistry* **2016**, 2774–2782 (2016).

217. Goura, J. *et al.* Heterometallic trinuclear {Co<sup>III</sup><sub>2</sub>Ln<sup>III</sup>} (Ln = Gd, Tb, Ho and Er) complexes in a bent geometry. Field-induced single-ion magnetic behavior of the Er<sup>III</sup> and Tb<sup>III</sup> analogues. *Dalton Transactions* **45**, 9235–9249 (2016).

218. Gregson, M. *et al.* A monometallic lanthanide bis(methanediide) single molecule magnet with a large energy barrier and complex spin relaxation behaviour. *Chemical Science* **7**, 155–165 (2016).

219. Gupta, S. K., Rajeshkumar, T., Rajaraman, G. & Murugavel, R. An air-stable Dy(III) single-ion magnet with high anisotropy barrier and blocking temperature. *Chemical Science* **7**, 5181–5191 (2016).

220. Gupta, S. K., Rajeshkumar, T., Rajaraman, G. & Murugavel, R. An unprecedented zero field neodymium(III) single-ion magnet based on a phosphonic diamide. *Chemical Communications* **52**, 7168–7171 (2016).

221. Gutiérrez, A., Perpiñán, M. F., Sánchez, A. E., Torralba, M. C. & González, V. Water inclusion mediated structural diversity and the role of H-bonds in molecular assemblies of manganese(III) bicompartimental Schiff-base complexes. *Inorganica Chimica Acta* **453**, 169–178 (2016).

222. Hamada, D. *et al.* Luminescent Dy<sup>III</sup> single ion magnets with same N6O3 donor atoms but different donor atom arrangements, 'fac'-[Dy<sup>III</sup>(HLDL-ala)<sub>3</sub>]<sup>·</sup>8H<sub>2</sub>O and 'mer'-[Dy<sup>III</sup>(HLDL-phe)<sub>3</sub>]<sup>·</sup>7H<sub>2</sub>O. *Polyhedron* **109**, 120–128 (2016).

223. Hazra, S., Titiš, J., Valigura, D., Boča, R. & Mohanta, S. Bis-phenoxido and bis-acetato bridged heteronuclear {Co<sup>III</sup>Dy<sup>III</sup>} single molecule magnets with two slow relaxation branches. *Dalton Transactions* **45**, 7510–7520 (2016).

224. Holmberg, R. J., Korobkov, I. & Murugesu, M. Enchaining EDTA-chelated lanthanide molecular

magnets into ordered 1D networks. *RSC Advances* **6**, 72510–72518 (2016).

225. Holmberg, R. J., Polovkova, M. A., Martynov, A. G., Gorbunova, Y. G. & Murugesu, M. Impact of the coordination environment on the magnetic properties of single-molecule magnets based on homo- and hetero-dinuclear terbium(III) heteroleptic tris(crownphthalocyaninate). *Dalton Transactions* **45**, 9320–9327 (2016).

226. Horii, Y., Katoh, K., Cosquer, G., Breedlove, B. K. & Yamashita, M. Weak Dy<sup>III</sup>–Dy<sup>III</sup> Interactions in Dy<sup>III</sup>–Phthalocyaninato Multiple-Decker Single-Molecule Magnets Effectively Suppress Magnetic Relaxation. *Inorganic Chemistry* **55**, 11782–11790 (2016).

227. Huang, W. *et al.* Metallogrid Single-Molecule Magnet: Solvent-Induced Nuclearity Transformation and Magnetic Hysteresis at 16 K. *Inorganic Chemistry* **55**, 5476–5484 (2016).

228. Janzen, D. E. *et al.* Trigonal (-3) symmetry octahedral lanthanide(III) complexes of zwitterionic tripodal ligands: luminescence and magnetism. *Supramolecular Chemistry* **28**, 125–140 (2016).

229. Jia, Y.-Q., Feng, S.-S., Shen, M.-L. & Lu, L.-P. Construction of multifunctional materials based on Tb<sup>3+</sup> and croconic acid, directed by K<sup>+</sup> cations: synthesis, structures, fluorescence, magnetic and ferroelectric behaviors. *CrystEngComm* **18**, 5344–5352 (2016).

230. Jiang, Z.-X. *et al.* Lanthanoid single-ion magnets with the LnN10 coordination geometry. *Chemical Communications* **52**, 6261–6264 (2016).

231. Jiménez, J.-R. *et al.* Lanthanide Tetrazolate Complexes Combining Single-Molecule Magnet and Luminescence Properties: The Effect of the Replacement of Tetrazolate N<sub>3</sub> by β-Diketonate Ligands on the Anisotropy Energy Barrier. *Chemistry - A European Journal* **22**, 14548–14559 (2016).

232. Karbowiak, M., Rudowicz, C., Nakamura, T., Murakami, R. & Ishida, T. Spectroscopic and magnetic studies of erbium(III)-TEMPO complex as a potential single-molecule magnet: Interplay of the crystal-field and exchange coupling effects. *Chemical Physics Letters* **662**, 163–168 (2016).

233. Klementyeva, S. V. *et al.* Mono- and Dinuclear Rare-Earth Chlorides Ligated by a Mesityl-Substituted β-Diketiminate. *European Journal of Inorganic Chemistry* **2016**, 3666–3672 (2016).

234. Koroteev, P. S., Dobrokhotova, Z. V., Ilyukhin, A. B., Efimov, N. N. & Novotortsev, V. M. Synthesis, structure, and magnetic properties of lanthanide ferrocenoylacetones with nitrate and 2,2'-bipyridine ligands. *Journal of Coordination Chemistry* **69**, 2723–2735 (2016).

235. Koroteev, P. S. *et al.* Synthesis, structure, and physical properties of new rare earth ferrocenoylacetones. *Dalton Transactions* **45**, 6405–6417 (2016).

236. Lan, Y., Magri, A., Fuhr, O. & Ruben, M. Phenalenyl-based mononuclear dysprosium complexes. *Beilstein Journal of Nanotechnology* **7**, 995–1009 (2016).

237. Li, C. *et al.* From Monomeric Species to One-Dimensional Chain: Enhancing Slow Magnetic Relaxation through Coupling Mononuclear Fragments in Ln-rad System. *Crystal Growth & Design* **16**, 7155–7162 (2016).

238. Li, H., Chen, P., Sun, W., Zhang, L. & Yan, P. Solvent triggered structural diversity of triple-stranded helicates: single molecular magnets. *Dalton Transactions* **45**, 3175–3181 (2016).

239. Li, T. *et al.* Modulating spin dynamics of Ln<sup>III</sup>-radical complexes by using different coligands. *RSC Advances* **6**, 3058–3067 (2016).

240. Li, W.-J. *et al.* Syntheses, Crystal Structures and Magnetic Properties of Two Nitrophenyl Substituted Nitronyl Nitroxide Radical-lanthanide Complexes. *China Academic Journals* **35**, 1787–1796 (2016).

241. Li, Y., Zhang, C., Yu, J.-W., Yang, E.-C. & Zhao, X.-J. Transition metal ion-directed magnetic behaviors observed in an isostructural heterobinuclear system. *Inorganica Chimica Acta* **445**, 110–116 (2016).

242. Lim, K. S. *et al.* Switching of Slow Magnetic Relaxation Dynamics in Mononuclear Dysprosium(III) Compounds with Charge Density. *Inorganic Chemistry* **55**, 5398–5404 (2016).

243. Liu, D. *et al.* Novel binuclear manganese(III), cobalt(III) and chromium(III) complexes for the alternating ring-opening copolymerization of cyclohexene oxide and maleic anhydride. *Inorganica Chimica Acta* **453**, 222–229 (2016).

244. Liu, J. *et al.* A Stable Pentagonal Bipyramidal Dy(III) Single-Ion Magnet with a Record Magnetization Reversal Barrier over 1000 K. *Journal of the American Chemical Society* **138**, 5441–5450 (2016).

245. Liu, S.-S. *et al.* A distinct magnetic anisotropy enhancement in mononuclear dysprosium–sulfur complexes by controlling the Dy-ligand bond length. *Dalton Transactions* **45**, 8149–8153 (2016).

246. Long, J. *et al.* Study of the influence of magnetic dilution over relaxation processes in a Zn/Dy single-ion magnet by correlation between luminescence and magnetism. *RSC Advances* **6**, 108810–108818 (2016).

247. Lucaccini, E. *et al.* Relaxation Dynamics and Magnetic Anisotropy in a Low-Symmetry Dy<sup>III</sup> Complex. *Chemistry - A European Journal* **22**, 5552–5562 (2016).

248. Ma, P. *et al.* Magnetic double-tartaric bridging mono-lanthanide substituted phosphotungstates with photochromic and switchable luminescence properties. *Journal of Materials Chemistry C* **4**, 5424–5433 (2016).

249. Mamontova, E. *et al.* Magneto-Luminescence Correlation in the Textbook Dysprosium(III) Nitrate Single-Ion Magnet. *Magnetochemistry* **2**, 41 (2016).

250. Meng, Y.-S. *et al.* Can Non-Kramers Tm<sup>III</sup> Mononuclear Molecules be Single-Molecule Magnets (SMMs)? *Chemistry - A European Journal* **22**, 4704–4708 (2016).

251. Meng, Y.-S. *et al.* (Boratabenzene)(cyclooctatetraenyl) lanthanide complexes: a new type of organometallic single-ion magnet. *Inorganic Chemistry Frontiers* **3**, 828–835 (2016).

252. Mihalcea, I. *et al.* Spin Helicity in Chiral Lanthanide Chains. *Inorganic Chemistry* **55**, 10068–10074 (2016).

253. Mondal, A., Parmar, V. & Konar, S. Modulating the Slow Relaxation Dynamics of Binuclear Dysprosium(III) Complexes through Coordination Geometry. *Magnetochemistry* **2**, 35 (2016).

254. Ou-Yang, J.-K. *et al.* Improved slow magnetic relaxation in optically pure helicene-based Dy<sup>III</sup> single molecule magnets. *Chemical Communications* **52**, 14474–14477 (2016).

255. Reis, S. G. *et al.* First coordination compounds based on a bis(imino nitroxide) biradical and 4f metal ions: synthesis, crystal structures and magnetic properties. *Dalton Transactions* **45**, 2936–2944 (2016).

256. Reis, S. G. *et al.* Binuclear Lanthanide-Radical Complexes Featuring Two Centers with Different Magnetic and Luminescence Properties. *Inorganic Chemistry* **55**, 11676–11684 (2016).

257. Ren, M. *et al.* Lanthanide salen-type complexes exhibiting single ion magnet and photoluminescent properties. *Dalton Transactions* **45**, 2974–2982 (2016).

258. Selvanathan, P. *et al.* Highly Axial Magnetic Anisotropy in a N<sub>3</sub>O<sub>5</sub> Dysprosium(III) Coordination Environment Generated by a Merocyanine Ligand. *Chemistry - A European Journal* **22**, 15222–15226 (2016).

259. Sun, H., Liu, M. & Zhang, B. Two dysprosium complexes based on 8-hydroxyquinoline Schiff base: Structures, luminescence properties and single-molecule magnets behaviors. *Inorganica Chimica Acta* **453**, 681–686 (2016).

260. Sun, L. *et al.* Fine-Tuning of the Coordination Environment To Regulate the Magnetic Behavior in Solvent/Anion-Dependent Dy<sup>III</sup> Compounds: Synthesis, Structure, Magnetism, and Ab Initio Calculations. *Inorganic Chemistry* **55**, 10587–10596 (2016).

261. Sun, O. *et al.* A series of dinuclear lanthanide(III) complexes constructed from Schiff base and \$\\upbeta\$-diketonate ligands: synthesis, structure, luminescence and SMM behavior. *CrystEngComm* **18**, 4627–4635 (2016).

262. Sun, W.-B. *et al.* High symmetry or low symmetry, that is the question – high performance Dy(III) single-ion magnets by electrostatic potential design. *Chemical Science* **7**, 684–691 (2016).

263. Tang, X. *et al.* Four ColI-GdIII mixed-metal phosphonate clusters as molecular magnetic refrigerants. *Inorganica Chimica Acta* **453**, 142–148 (2016).

264. Vonci, M. *et al.* Magnetic Excitations in Polyoxotungstate-Supported Lanthanoid Single-Molecule Magnets: An Inelastic Neutron Scattering and ab Initio Study. *Inorganic Chemistry* **56**, 378–394 (2016).

265. Wada, H., Ooka, S., Iwasawa, D., Hasegawa, M. & Kajiwara, T. Slow Magnetic Relaxation of Lanthanide(III) Complexes with a Helical Ligand. *Magnetochemistry* **2**, 43 (2016).

266. Wada, H., Ooka, S., Yamamura, T. & Kajiwara, T. Light Lanthanide Complexes with Crown Ether and Its Aza Derivative Which Show Slow Magnetic Relaxation Behaviors. *Inorganic Chemistry* **56**, 147–155 (2016).

267. Wang, S. *et al.* Solvent- and metal-directed lanthanide-organic frameworks based on pamoic acid: observation of slow magnetization relaxation, magnetocaloric effect and luminescent sensing. *Science China Chemistry* **59**, 948–958 (2016).

268. Wu, J. *et al.* *Cis-trans* isomerism modulates the magnetic relaxation of dysprosium single-molecule magnets. *Chemical Science* **7**, 3632–3639 (2016).

269. Wu, J. *et al.* Macroscopic Hexagonal Tubes of 3d-4f Metallocycles. *Angewandte Chemie International Edition* **55**, 15574–15578 (2016).

270. Wu, J. *et al.* Metallosupramolecular Coordination Complexes: The Design of Heterometallic 3d–4f Gridlike Structures. *Inorganic Chemistry* **55**, 5514–5519 (2016).

271. Zhang, J.-W., Jiang, Y., Xie, Y.-R., Chu, J. & Liu, B.-Q. Syntheses, structures, photoluminescence, and

magnetism of a series of discrete heavy lanthanide complexes based on a tricarboxylic acid. *Inorganica Chimica Acta* **453**, 257–262 (2016).

272. Zhang, P., Jung, J., Zhang, L., Tang, J. & Guennic, B. L. Elucidating the Magnetic Anisotropy and Relaxation Dynamics of Low-Coordinate Lanthanide Compounds. *Inorganic Chemistry* **55**, 1905–1911 (2016).

273. Zhang, S. *et al.* Dysprosium(III) complexes with a square-antiprism configuration featuring mononuclear single-molecule magnetic behaviours based on different  $\beta$ -diketonate ligands and auxiliary ligands. *Dalton Transactions* **45**, 5310–5320 (2016).

274. Zhang, S. *et al.* Magnetization Dynamics Changes of Dysprosium(III) Single-Ion Magnets Associated with Guest Molecules. *Inorganic Chemistry* **55**, 3865–3871 (2016).

275. Amjad, A., Figuerola, A. & Sorace, L. Tm(III) complexes undergoing slow relaxation of magnetization: exchange coupling and aging effects. *Dalton Transactions* **46**, 3848–3856 (2017).

276. Biswas, S. *et al.* Mononuclear Lanthanide Complexes: Energy-Barrier Enhancement by Ligand Substitution in Field-Induced Dy<sup>III</sup> SIMs. *Inorganic Chemistry* **56**, 7985–7997 (2017).

277. Boča, R. *et al.* Slow magnetic relaxations in a ladder-type Dy(III) complex and its dinuclear analogue. *Dalton Transactions* **46**, 5344–5351 (2017).

278. Cen, P.-P. *et al.* Electrostatic Potential Determined Magnetic Dynamics Observed in Two Mononuclear  $\beta$ -Diketone Dysprosium(III) Single-Molecule Magnets. *Inorganic Chemistry* **56**, 3644–3656 (2017).

279. Chen, L., Zhou, J., Yuan, A. & Song, Y. Slow magnetic relaxation in luminescent mononuclear dysprosium(III) and erbium(III) pentanitrate complexes with the same LnO<sub>10</sub> coordination geometry. *Dalton Transactions* **46**, 15812–15818 (2017).

280. Chen, Y.-C. *et al.* Dynamic Magnetic and Optical Insight into a High Performance Pentagonal Bipyramidal DyIII Single-Ion Magnet. *Chemistry - A European Journal* **23**, 5708–5715 (2017).

281. Chen, Y.-C. *et al.* Hyperfine-Interaction-Driven Suppression of Quantum Tunneling at Zero Field in a Holmium(III) Single-Ion Magnet. *Angewandte Chemie International Edition* **56**, 4996–5000 (2017).

282. Chen, Y. *et al.* A New Bis(phthalocyaninato) Terbium Single-Ion Magnet with an Overall Excellent Magnetic Performance. *Inorganic Chemistry* **56**, 13889–13896 (2017).

283. Chen, Y. *et al.* Novel bis(phthalocyaninato) rare earth complexes with the bulky and strong electron-donating dibutylamino groups: synthesis, spectroscopy, and SMM properties. *Inorganic Chemistry Frontiers* **4**, 1465–1471 (2017).

284. Chorazy, S., Rams, M., Wang, J., Sieklucka, B. & Ohkoshi, S. Octahedral Yb(III) complexes embedded in [Co<sup>III</sup>(CN)<sub>6</sub>]-bridged coordination chains: combining sensitized near-infrared fluorescence with slow magnetic relaxation. *Dalton Transactions* **46**, 13668–13672 (2017).

285. Craze, A. R. *et al.* Synthesis and characterisation of new tripodal lanthanide complexes and investigation of their optical and magnetic properties. *Dalton Transactions* **46**, 12177–12184 (2017).

286. Demir, S. *et al.* Slow Magnetic Relaxation in a Dysprosium Ammonia Metallocene Complex. *Inorganic Chemistry* **56**, 15049–15056 (2017).

287. Dolinar, B. S., Gómez-Coca, S., Alexandropoulos, D. I. & Dunbar, K. R. An air stable radical-bridged dysprosium single molecule magnet and its neutral counterpart: redox switching of magnetic relaxation dynamics. *Chemical Communications* **53**, 2283–2286 (2017).

288. Dong, Y., Li, W., Zou, X., Hou, G. & Li, G. Electron-donating effect dominated 5,6-dimethoxy-2-(2,2,2-trifluoroethyl)-1-indone dysprosium SMM. *Inorganica Chimica Acta* **466**, 599–603 (2017).

289. Dunstan, M. A. *et al.* Slow magnetisation relaxation in tetraoxolene-bridged rare earth complexes. *Dalton Trans.* **46**, 13756–13767 (2017).

290. Fondo, M. *et al.* Designing Ligands to Isolate ZnLn and Zn<sub>2</sub>Ln Complexes: Field-Induced Single-Ion Magnet Behavior of the ZnDy, Zn<sub>2</sub>Dy, and Zn<sub>2</sub>Er Analogue. *Inorganic Chemistry* **56**, 5646–5656 (2017).

291. Fondo, M. *et al.* Improving the SMM and luminescence properties of lanthanide complexes with LnO<sub>9</sub> cores in the presence of Zn<sup>II</sup>: an emissive Zn<sub>2</sub>Dy single ion magnet. *Dalton Transactions* **46**, 17000–17009 (2017).

292. Gao, F. *et al.* Half-sandwich lanthanide crown ether complexes with the slow relaxation of magnetization and photoluminescence behaviors. *Dalton Transactions* **46**, 1317–1323 (2017).

293. Gao, X., Li, H., Chen, P., Sun, W. & Yan, P. A series of triple-stranded lanthanide(III) helicates: Syntheses, structures and single molecular magnets. *Polyhedron* **126**, 1–7 (2017).

294. Goodwin, C. A. P., Ortú, F., Reta, D., Chilton, N. F. & Mills, D. P. Molecular magnetic hysteresis at 60 kelvin in dysprosocenium. *Nature* **548**, 439–442 (2017).

295. Goodwin, C. A. P., Reta, D., Ortú, F., Chilton, N. F. & Mills, D. P. Synthesis and Electronic Structures of Heavy Lanthanide Metallocenium Cations. *Journal of the American Chemical Society* **139**, 18714–18724 (2017).

296. Griffiths, K. *et al.* Four New Families of Polynuclear Zn-Ln Coordination Clusters. Synthetic, Topological, Magnetic, and Luminescent Aspects. *Crystal Growth & Design* **17**, 1524–1538 (2017).

297. Guettas, D. *et al.* Fine Control of the Metal Environment within Dysprosium-Based Mononuclear Single-Molecule Magnets. *European Journal of Inorganic Chemistry* **2018**, 333–339 (2017).

298. Guo, F.-S. *et al.* A Dysprosium Metallocene Single-Molecule Magnet Functioning at the Axial Limit. *Angewandte Chemie International Edition* **56**, 11445–11449 (2017).

299. Guseva, E. V. & Buslaeva, T. M. Complexes of rhodium and platinum with 4,6-dinitro-5,7-dihydroxybenzo[1,2-c][1,2,5]oxadiazole 1-oxide. *Inorganica Chimica Acta* **455**, 455–464 (2017).

300. Harriman, K. L. M., Brosmer, J. L., Ungur, L., Diaconescu, P. L. & Murugesu, M. Pursuit of Record Breaking Energy Barriers: A Study of Magnetic Axiality in Diamide Ligated Dy<sup>III</sup> Single-Molecule Magnets. *Journal of the American Chemical Society* **139**, 1420–1423 (2017).

301. Harriman, K. L. M., Korobkov, I. & Murugesu, M. From a Piano Stool to a Sandwich: A Stepwise Route for Improving the Slow Magnetic Relaxation Properties of Thulium. *Organometallics* **36**, 4515–4518 (2017).

302. Horii, Y., Katoh, K., Breedlove, B. K. & Yamashita, M. Elongation of magnetic relaxation times in a single-molecule magnet through intermetallic interactions: a clamshell-type dinuclear terbium(III)-phthalocyaninato quadruple-decker complex. *Chemical Communications* **53**, 8561–8564 (2017).

303. Hu, P. *et al.* One mononuclear single-molecule magnet derived from Dy(III) and dmby (dmby = 4,4'-dimethyl-2,2'-dipyridyl). *Inorganic Chemistry Communications* **84**, 207–211 (2017).

304. Ishida, T. Spin-Parity Behavior in the Exchange-Coupled Lanthanoid-Nitroxide Molecular Magnets. *IOP Conference Series: Materials Science and Engineering* **202**, 012001 (2017).

305. Ishikawa, R. *et al.* Field-Induced Slow Magnetic Relaxation of Mono- and Dinuclear Dysprosium(III) Complexes Coordinated by a Chloranilate with Different Resonance Forms. *Inorganics* **6**, 7 (2017).

306. Jin, Z. *et al.* A new series of mononuclear lanthanide single molecule magnets based on sandwich-type germanomolybdates  $[\text{Ln}(\text{GeMo}_{11}\text{O}_{39})_2]^{13-}$  ( $\text{Ln} = \text{Er}^{\text{III}}$ ,  $\text{Gd}^{\text{III}}$ ,  $\text{Dy}^{\text{III}}$  or  $\text{Tb}^{\text{III}}$ ). *New Journal of Chemistry* **41**, 13490–13494 (2017).

307. Kanetomo, T., Yasui, M. & Ishida, T. Exchange-coupled terbium-radical complex Tb-phNO showing slow reversal of magnetization. *Polyhedron* **136**, 30–34 (2017).

308. Kishi, Y. *et al.* Luminescence and Single-Molecule-Magnet Behaviour in Lanthanide Coordination Complexes Involving Benzothiazole-Based Tetrathiafulvalene Ligands. *European Journal of Inorganic Chemistry* **2018**, 458–468 (2017).

309. Latendresse, T. P., Bhuvanesh, N. S. & Nippe, M. Slow Magnetic Relaxation in a Lanthanide-[1]Metallocenophane Complex. *Journal of the American Chemical Society* **139**, 8058–8061 (2017).

310. Li, J. *et al.* Magnetic Anisotropy along a Series of Lanthanide Polyoxometalates with Pentagonal Bipyramidal Symmetry. *Inorganic Chemistry* **56**, 7835–7841 (2017).

311. Li, X., Li, T., Shi, X. J. & Tian, L. A family of 2p-4f complexes based on indazole radical: Syntheses, structures and magnetic properties. *Inorganica Chimica Acta* **456**, 216–223 (2017).

312. Liang, Z. *et al.* Proton Control of the Lanthanoid Single-Ion Magnet Behavior of a Double-Decker Complex with an Indolenine-Substituted Annulene Ligand. *Inorganic Chemistry* **56**, 6512–6521 (2017).

313. Lim, K. S. *et al.* Custom Coordination Environments for Lanthanoids: Tripodal Ligands Achieve Near-Perfect Octahedral Coordination for Two Dysprosium-Based Molecular Nanomagnets. *Inorganic Chemistry* **56**, 4911–4917 (2017).

314. Lim, K. S. *et al.* Slow relaxation dynamics of a mononuclear Er(III) complex surrounded by a ligand environment with anisotropic charge density. *Dalton Transactions* **46**, 739–744 (2017).

315. Liu, L., Li, Y., Deng, S.-X. & Zhang, Y.-P. A dysprosium(III) complex based on Schiff-base ligand exhibiting two magnetic relaxation processes. *Inorganica Chimica Acta* **457**, 1–6 (2017).

316. Liu, M.-J. *et al.* Chiral six-coordinate Dy(III) and Tb(III) complexes of an achiral ligand: structure, fluorescence, and magnetism. *Dalton Transactions* **46**, 13035–13042 (2017).

317. Liu, S.-S. *et al.* A Six-Coordinate Dysprosium Single-Ion Magnet with Trigonal-Prismatic Geometry. *Inorganic Chemistry* **56**, 7320–7323 (2017).

318. Lorenz, V. *et al.* Lanthanide(III) Sandwich and Half-Sandwich Complexes with Bulky Cyclooctatetraenyl Ligands: Synthesis, Structures, and Magnetic Properties. *European Journal of Inorganic Chemistry* **2017**, 4840–4849 (2017).

319. Lucaccini, E. *et al.* Electronic Structure and Magnetic Anisotropy in Lanthanoid Single-Ion Magnets with  $C_3$  Symmetry: The Ln(trenovan) Series. *Inorganic Chemistry* **56**, 4728–4738 (2017).

320. Ma, P. *et al.* Magnetoluminescent Bifunctional Dysprosium-Based Phosphotungstates with Synthesis and Correlations between Structures and Properties. *Crystal Growth & Design* **17**, 1947–1956 (2017).

321. Marinho, M. V. *et al.* Photoluminescent and Slow Magnetic Relaxation Studies on Lanthanide(III)-2,5-pyrazinedicarboxylate Frameworks. *Inorganic Chemistry* **56**, 2108–2123 (2017).

322. Moilanen, J. O. *et al.* Thermal expansion and magnetic properties of benzoquinone-bridged dinuclear rare-earth complexes. *Dalton Trans.* **46**, 13582–13589 (2017).

323. Petrosyants, S. P. *et al.* Mononuclear Dysprosium Thiocyanate Complexes with 2,2'-Bipyridine and 1,10-Phenanthroline: Synthesis, Crystal Structures, SIM Behavior, and Solid-Phase Transformations. *European Journal of Inorganic Chemistry* **2017**, 3561–3569 (2017).

324. Skvortsov, G. G. *et al.* Rare-Earth Complexes Coordinated by ansa -Bis(amidinate) Ligands with m -Phenylene, 2,6-Pyridinediyl, and SiMe<sub>2</sub> Linkers. *European Journal of Inorganic Chemistry* **2017**, 4275–4284 (2017).

325. Speed, S. *et al.* Lanthanide complexes involving multichelating TTF-based ligands. *Inorganic Chemistry Frontiers* **4**, 604–617 (2017).

326. Speed, S. *et al.* Photophysical and Magnetic Properties in Complexes Containing 3d/4f Elements and Chiral Phenanthroline-Based Helicate-Like Ligands. *European Journal of Inorganic Chemistry* **2017**, 2100–2111 (2017).

327. Upadhyay, A. *et al.* Role of the Diamagnetic Zinc(II) Ion in Determining the Electronic Structure of Lanthanide Single-Ion Magnets. *Chemistry - A European Journal* **23**, 4903–4916 (2017).

328. Upadhyay, A. *et al.* Influence of the Ligand Field on the Slow Relaxation of Magnetization of Unsymmetrical Monomeric Lanthanide Complexes: Synthesis and Theoretical Studies. *Inorganic Chemistry* **56**, 14260–14276 (2017).

329. Wang, X. *et al.* Two Families of Rare-Earth-Substituted Dawson-type Monomeric and Dimeric Phosphotungstates Functionalized by Carboxylic Ligands. *Crystal Growth & Design* **17**, 5295–5308 (2017).

330. Wen, H.-R. *et al.* 3d–4f heterometallic trinuclear complexes derived from amine-phenol tripodal ligands exhibiting magnetic and luminescent properties. *Dalton Transactions* **46**, 1153–1162 (2017).

331. Wen, H.-R. *et al.* Mononuclear Dy(III) complex based on bipyridyl-tetrazolate ligand with field-induced single-ion magnet behavior and luminescent properties. *Inorganic Chemistry Communications* **79**, 41–45 (2017).

332. Wu, D.-Q. *et al.* Single-ion magnetism in seven-coordinate Yb<sup>III</sup> complexes with distorted D5h coordination geometry. *Dalton Transactions* **46**, 12884–12892 (2017).

333. Wu, J. *et al.* Axial Ligand Field in D4d Coordination Symmetry: Magnetic Relaxation of Dy SMMs Perturbed by Counteranions. *Inorganic Chemistry* **56**, 11211–11219 (2017).

334. Yamabayashi, T., Katoh, K., Breedlove, B. & Yamashita, M. Molecular Orientation of a Terbium(III)-Phthalocyaninato Double-Decker Complex for Effective Suppression of Quantum Tunneling of the Magnetization. *Molecules* **22**, 999 (2017).

335. Yao, B. *et al.* Single-molecule magnet behavior in a mononuclear dysprosium(III) complex with 1-methylimidazole. *RSC Advances* **7**, 2766–2772 (2017).

336. Yoshida, T. *et al.* Multiple Magnetic Relaxation Pathways and Dual-Emission Modulated by a Heterometallic Tb-Pt Bonding Environment. *Chemistry - A European Journal* **23**, 10527–10531 (2017).

337. Yue, Y., Hou, G., Yao, X. & Li, G. Single molecular magnet of lanthanide coordination polymer with 1D helical-like chain based on flexible Salen-type ligand. *Polyhedron* **129**, 157–163 (2017).

338. Zabala-Lekuona, A. *et al.* Rational design of triple-bridged dinuclear Zn<sup>II</sup>Ln<sup>III</sup>-based complexes: a structural, magnetic and luminescence study. *CrystEngComm* **19**, 256–264 (2017).

339. Alexandropoulos, D. I., Schulte, K. A., Vignesh, K. R. & Dunbar, K. R. Slow magnetic dynamics in a family of mononuclear lanthanide complexes exhibiting the rare cubic coordination geometry. *Chemical Communications* **54**, 10136–10139 (2018).

340. Bar, A. K., Kalita, P., Sutter, J.-P. & Chandrasekhar, V. Pentagonal-Bipyramidal Ln(III) Complexes Exhibiting Single-Ion-Magnet Behavior: A Rational Synthetic Approach for a Rigid Equatorial Plane. *Inorganic Chemistry* **57**, 2398–2401 (2018).

341. Bazhina, E. S. *et al.* Lanthanide(III) (Eu, Gd, Tb, Dy) Complexes Derived from 4-(Pyridin-2-yl)methyleneamino-1,2,4-triazole: Crystal Structure, Magnetic Properties, and Photoluminescence. *Chemistry - An Asian Journal* **13**, 2060–2068 (2018).

342. Béreau, V., Dhers, S., Costes, J.-P., Duhayon, C. & Sutter, J.-P. Syntheses, Structures, and Magnetic Properties of Symmetric and Dissymmetric Ester-Functionalized 3d-4f Schiff Base Complexes. *European Journal of Inorganic Chemistry* **2018**, 66–73 (2018).

343. Canaj, A. B., Singh, M. K., Wilson, C., Rajaraman, G. & Murrie, M. Chemical and *in silico* tuning of the magnetisation reversal barrier in pentagonal bipyramidal Dy(III) single-ion magnets. *Chemical Communications* **54**, 8273–8276 (2018).

344. Cañon-Mancisidor, W. *et al.* Sublimable Single Ion Magnets Based on Lanthanoid Quinolinate Complexes: The Role of Intermolecular Interactions on Their Thermal Stability. *Inorganic Chemistry* **57**, 14170–14177 (2018).

345. Chen, S.-M. *et al.* A soft phosphorus atom to “harden” an erbium(III) single-ion magnet. *Chemical Science* **9**, 7540–7545 (2018).

346. Chen, X.-X. *et al.* A neutral auxiliary ligand enhanced dysprosium(III) single molecule magnet. *Dalton Transactions* **47**, 7395–7398 (2018).

347. Chen, Y.-C., Huang, X.-S., Liu, J.-L. & Tong, M.-L. Magnetic Dynamics of a Neodymium(III) Single-Ion Magnet. *Inorganic Chemistry* **57**, 11782–11787 (2018).

348. Chen, Y. *et al.* Fabricating Bis(phthalocyaninato) Terbium SIM into Tetrakis(phthalocyaninato) Terbium SMM with Enhanced Performance through Sodium Coordination. *Chemistry - A European Journal* **24**, 8066–8070 (2018).

349. Chorazy, S., Charytanowicz, T., Wang, J., Ohkoshi, S. & Sieklucka, B. Hybrid organic–inorganic connectivity of Nd<sup>III</sup>(pyrazine-N,N'-dioxide)[Co<sup>III</sup>(CN)<sub>6</sub>]<sup>3-</sup> coordination chains for creating near-infrared emissive Nd(III) showing field-induced slow magnetic relaxation. *Dalton Transactions* **47**, 7870–7874 (2018).

350. Chorazy, S., Zychowicz, M., Ohkoshi, S. & Sieklucka, B. Wide-Range UV-to-Visible Excitation of Near-Infrared Emission and Slow Magnetic Relaxation in Ln<sup>III</sup>(4,4'-Azopyridine-1,1'-dioxide)[Co<sup>III</sup>(CN)<sub>6</sub>]<sup>3-</sup> Layered Frameworks. *Inorganic Chemistry* **58**, 165–179 (2018).

351. Day, B. M. *et al.* Rare-Earth Cyclobutadienyl Sandwich Complexes: Synthesis, Structure and Dynamic Magnetic Properties. *Chemistry - A European Journal* **24**, 16779–16782 (2018).

352. Demir, S., Meihaus, K. R. & Long, J. R. Slow magnetic relaxation in a neodymium metallocene tetraphenylborate complex. *Journal of Organometallic Chemistry* **857**, 164–169 (2018).

353. Feltham, H. L. C. *et al.* The Effect of Modifying the Macroyclic Ring Size on Zn<sub>3</sub>Ln (Ln= Dy, Er, and Yb) Single-Molecule Magnet Behavior. *Zeitschrift für anorganische und allgemeine Chemie* **644**, 775–779 (2018).

354. Fondo, M. *et al.* Field-Induced Single Molecule Magnets of Phosphine- and Arsine-Oxides. *Frontiers in Chemistry* **6**, (2018).

355. Fondo, M. *et al.* Tb<sub>2</sub>, Dy<sub>2</sub>, and Zn<sub>2</sub>Dy<sub>4</sub> Complexes Showing the Unusual Versatility of a Hydrazone Ligand toward Lanthanoid Ions: a Structural and Magnetic Study. *Inorganic Chemistry* **57**, 10100–10110 (2018).

356. Ge, J.-Y. *et al.* Thiocalix[4]arene-supported mononuclear lanthanide compounds: slow magnetic relaxation in dysprosium and erbium analogues. *New Journal of Chemistry* **42**, 17968–17974 (2018).

357. Gonzalez, J. F. *et al.* Field-Induced Dysprosium Single-Molecule Magnet Involving a Fused o-Semiquinone-Extended-Tetrathiafulvalene-o-Semiquinone Bridging Triad. *Inorganics* **6**, 45 (2018).

358. Gonzalez, J. F. *et al.* Slow Relaxation of the Magnetization in Bis-Decorated Chiral Helicene-Based Coordination Complexes of Lanthanides. *Magnetochemistry* **4**, 39 (2018).

359. Goodwin, C. A. P. *et al.* Terboceneum: completing a heavy lanthanide metallocenium cation family with an alternative anion abstraction strategy. *Chemical Communications* **54**, 9182–9185 (2018).

360. Gorczyński, A. *et al.* New field-induced single ion magnets based on prolate Er(III) and Yb(III) ions: tuning the energy barrier U<sub>eff</sub> by the choice of counterions within an N3-tridentate Schiff-base scaffold. *Inorganic Chemistry Frontiers* **5**, 605–618 (2018).

361. Guo, M. & Tang, J. Six-Coordinate Ln(III) Complexes with Various Coordination Geometries Showing

Distinct Magnetic Properties. *Inorganics* **6**, 16 (2018).

362. Guo, M., Zhang, Y.-Q., Zhu, Z. & Tang, J. Dysprosium Compounds with Hula-Hoop-like Geometries: The Influence of Magnetic Anisotropy and Magnetic Interactions on Magnetic Relaxation. *Inorganic Chemistry* **57**, 12213–12221 (2018).

363. Guo, S., Lv, X.-C., Gao, X.-H., Li, C.-L. & Zhang, X.-F. Structures, Magnetic and Thermodynamic Properties of a 3d–4f Mixed Metal Cluster  $[\text{ErZn}_6(\mu_3\text{-O})_3(\mu_3\text{-C}_2\text{H}_4\text{NO}_2)_6(\text{H}_2\text{O})_9]^{6+}$ . *Journal of Cluster Science* **29**, 975–980 (2018).

364. He, M. *et al.* Enantiopure Benzamidinate/Cyclooctatetraene Complexes of the Rare-Earth Elements: Synthesis, Structure, and Magnetism. *Organometallics* **37**, 3708–3717 (2018).

365. Hilgar, J. D., Bernbeck, M. G., Flores, B. S. & Rinehart, J. D. Metal–ligand pair anisotropy in a series of mononuclear Er–COT complexes. *Chemical Science* **9**, 7204–7209 (2018).

366. Horii, Y. *et al.* Supramolecular Approach for Enhancing Single-Molecule Magnet Properties of Terbium(III)-Phthalocyaninato Double-Decker Complexes with Crown Moieties. *Chemistry - A European Journal* **24**, 4320–4327 (2018).

367. Huang, G. *et al.* Closing the Circle of the Lanthanide-Murexide Series: Single-Molecule Magnet Behavior and Near-Infrared Emission of the Nd<sup>III</sup> Derivative. *Magnetochemistry* **4**, 44 (2018).

368. Huang, X.-D. *et al.* Reversible SC-SC Transformation involving [4 + 4] Cycloaddition of Anthracene: A Single-Ion to Single-Molecule Magnet and Yellow-Green to Blue-White Emission. *Angewandte Chemie* **130**, 8713–8717 (2018).

369. Ji, C.-L. *et al.* Field-induced Slow Magnetic Relaxation Behavior in a Mononuclear Dy(III) Complex based on 8-Hydroxyquinoline Derivate Ligand. *Zeitschrift für anorganische und allgemeine Chemie* **644**, 1635–1640 (2018).

370. Jiang, Z. *et al.* Excess axial electrostatic repulsion as a criterion for pentagonal bipyramidal Dy<sup>III</sup> single-ion magnets with high Ueff and TB. *Journal of Materials Chemistry C* **6**, 4273–4280 (2018).

371. Langley, S. *et al.* Mononuclear Dysprosium(III) Complexes with Triphenylphosphine Oxide Ligands: Controlling the Coordination Environment and Magnetic Anisotropy. *Inorganics* **6**, 61 (2018).

372. Latendresse, T. P. *et al.* Magnetic Properties of a Terbium-[1]Ferrocenophane Complex: Analogies between Lanthanide–Ferrocenophane and Lanthanide–Bis-phthalocyanine Complexes. *Angewandte Chemie* **130**, 8296–8301 (2018).

373. Li, M. *et al.* Two  $\{\text{Zn}^{\text{II}}_2\text{Dy}^{\text{III}}\}$  complexes supported by monophenoxydodicarboxylate bridges with multiple relaxation processes: carboxylato ancillary ligand-controlled magnetic anisotropy in square antiprismatic Dy<sup>III</sup> species. *Dalton Transactions* **47**, 9482–9491 (2018).

374. Li, X.-L. *et al.* An intense luminescent Dy(III) single-ion magnet with the acylpyrazolone ligand showing two slow magnetic relaxation processes. *New Journal of Chemistry* **42**, 16992–16998 (2018).

375. Liu, W. *et al.* Hemiporphyrazine-Involved Sandwich Dysprosium Double-Decker Single-Ion Magnets. *Inorganic Chemistry* **57**, 12347–12353 (2018).

376. Long, J. *et al.* Dysprosium Single-Molecule Magnets with Bulky Schiff Base Ligands: Modification of the Slow Relaxation of the Magnetization by Substituent Change. *Chemistry - A European Journal* **25**, 474–478 (2018).

377. Long, J. *et al.* Synthesis, structure and magnetic properties of tris(pyrazolyl)methane lanthanide complexes: effect of the anion on the slow relaxation of magnetization. *Dalton Transactions* **47**, 5153–5156 (2018).

378. Long, Q.-Q. *et al.* Field-induced single molecule magnet behavior of a Dy<sup>III</sup>-Na<sup>+</sup> one-dimensional chain extended by acetate ions. *Inorganic Chemistry Communications* **98**, 127–131 (2018).

379. Lutter, J. C., Eliseeva, S. V., Kampf, J. W., Petoud, S. & Pecoraro, V. L. A Unique Ln<sup>III</sup>  $\{[3.3.1]\text{Ga}^{\text{III}}$  Metallacryptate} Series That Possesses Properties of Slow Magnetic Relaxation and Visible/Near-Infrared Luminescence. *Chemistry - A European Journal* **24**, 10773–10783 (2018).

380. Maniaki, D. *et al.* Slow magnetic relaxation and luminescence properties in lanthanide(iii)/anil complexes. *Dalton Transactions* **47**, 11859–11872 (2018).

381. Maxwell, L., Amoza, M. & Ruiz, E. Mononuclear Lanthanide Complexes with 18-Crown-6 Ether: Synthesis, Characterization, Magnetic Properties, and Theoretical Studies. *Inorganic Chemistry* **57**, 13225–13234 (2018).

382. Meng, Y.-S. *et al.* Low-Coordinate Single-Ion Magnets by Intercalation of Lanthanides into a Phenol Matrix. *Angewandte Chemie* **130**, 4763–4766 (2018).

383. Miralles, S. G. *et al.* Sublimable chloroquinolinate lanthanoid single-ion magnets deposited on ferromagnetic electrodes. *Chemical Science* **9**, 199–208 (2018).

384. Morita, T. *et al.* Comparison of the Magnetic Anisotropy and Spin Relaxation Phenomenon of Dinuclear Terbium(III) Phthalocyaninato Single-Molecule Magnets Using the Geometric Spin Arrangement. *Journal of the American Chemical Society* **140**, 2995–3007 (2018).

385. Mylonas-Margaritis, I. *et al.* Mononuclear Lanthanide(III)-Salicylideneaniline Complexes: Synthetic, Structural, Spectroscopic, and Magnetic Studies. *Magnetochemistry* **4**, 45 (2018).

386. Norel, L. *et al.* A Terminal Fluoride Ligand Generates Axial Magnetic Anisotropy in Dysprosium Complexes. *Angewandte Chemie* **130**, 1951–1956 (2018).

387. Øvre, A. *et al.* Chiral, Heterometallic Lanthanide–Transition Metal Complexes by Design. *Inorganics* **6**, 72 (2018).

388. Peng, G. *et al.* Single molecule magnetic behaviour in lanthanide naphthalenesulfonate complexes. *Dalton Transactions* **47**, 17349–17356 (2018).

389. Perfetti, M. *et al.* Magnetic Anisotropy Switch: Easy Axis to Easy Plane Conversion and Vice Versa. *Advanced Functional Materials* **28**, 1801846 (2018).

390. Petrosyants, S. P., Ilyukhin, A. B., Efimov, N. N., Gavrikov, A. V. & Novotortsev, V. M. Self-assembly and SMM properties of lanthanide cyanocobaltate chain complexes with terpyridine as blocking ligand. *Inorganica Chimica Acta* **482**, 813–820 (2018).

391. Qiao, S. *et al.* Field-induced single-molecule magnet (SMM) behavior of dinuclear Dy<sup>III</sup> system. *Inorganica Chimica Acta* **469**, 57–65 (2018).

392. Rousset, E. *et al.* Slow Magnetic Relaxation in Lanthanoid Crown Ether Complexes: Interplay of Raman and Anomalous Phonon Bottleneck Processes. *Chemistry - A European Journal* **24**, 14768–14785 (2018).

393. Sasnovskaya, V. D. *et al.* Slow magnetic relaxation in mononuclear complexes of Tb, Dy, Ho and Er with the pentadentate (N<sub>3</sub>O<sub>2</sub>) Schiff-base dapsc ligand. *New Journal of Chemistry* **42**, 14883–14893 (2018).

394. Selvanathan, P. *et al.* trans to cis photo-isomerization in merocyanine dysprosium and yttrium complexes. *Dalton Transactions* **47**, 4139–4148 (2018).

395. Shen, F.-X. *et al.* Heterometallic M<sup>II</sup>Ln<sup>III</sup> (M = Co/Zn; Ln = Dy/Y) Complexes with Pentagonal Bipyramidal 3d Centers: Syntheses, Structures, and Magnetic Properties. *Inorganic Chemistry* **57**, 15526–15536 (2018).

396. Skvortsov, G. G., Cherkasov, A. V., Long, J., Larionova, J. & Trifonov, A. A. Synthesis, structure and magnetic properties of the dinuclear complex [1,3-C<sub>6</sub>H<sub>4</sub>{NC(Ph)N(SiMe<sub>3</sub>)<sub>2</sub>}<sub>2</sub>]<sub>3</sub>Dy<sub>2</sub> coordinated by ansa-bis(amidinate) ligands with a m-phenylene linker. *Mendeleev Communications* **28**, 521–523 (2018).

397. Sun, J., Yang, M., Xi, L., Ma, Y. & Li, L. Magnetic relaxation in [Ln(hfac)<sub>4</sub>]<sup>-</sup> anions with [Cu(hfac)-radical]<sub>n</sub><sup>n+</sup> cation chains as counterions. *Dalton Transactions* **47**, 8142–8148 (2018).

398. Taylor, R. *et al.* Homoleptic Lanthanide Complexes Containing a Redox-Active Ligand and the Investigation of Their Electronic and Photophysical Properties. *Inorganics* **6**, 56 (2018).

399. Wang, H.-L. *et al.* Mixed chelating ligands used to regulate the luminescence of Ln(III) complexes and single-ion magnet behavior in Dy-based analogues. *Dalton Transactions* **47**, 15929–15940 (2018).

400. Wang, J., Chorazy, S., Nakabayashi, K., Sieklucka, B. & Ohkoshi, S. Achieving white light emission and increased magnetic anisotropy by transition metal substitution in functional materials based on dinuclear Dy<sup>III</sup>(4-pyridone)[M<sup>III</sup>(CN)<sub>6</sub>]<sup>3-</sup> (M = Co, Rh) molecules. *Journal of Materials Chemistry C* **6**, 473–481 (2018).

401. Wang, Y.-X. *et al.* Observation of Magnetodielectric Effect in a Dysprosium-Based Single-Molecule Magnet. *Journal of the American Chemical Society* **140**, 7795–7798 (2018).

402. Wen, H.-R. *et al.* Chiral mononuclear Dy(III) complex based on pyrrolidine-dithiocarboxylate S-donors with field-induced single-ion magnet behavior. *Inorganica Chimica Acta* **473**, 145–151 (2018).

403. Wu, J. *et al.* From double-shelled grids to supramolecular frameworks. *Chemical Communications* **54**, 12097–12100 (2018).

404. Xiao, Z.-X. *et al.* A family of lanthanide compounds with reduced nitronyl nitroxide diradical: syntheses, structures and magnetic properties. *Dalton Transactions* **47**, 7925–7933 (2018).

405. Xiong, X. *et al.* The Exploration and Analysis of the Magnetic Relaxation Behavior in Three Isostructural Cyano-Bridged 3d–4f Linear Heterotrinuclear Compounds. *Inorganics* **6**, 36 (2018).

406. Xu, M.-X. *et al.* Magnetic anisotropy investigation on light lanthanide complexes. *Dalton Transactions* **47**, 1966–1971 (2018).

407. Yang, J.-W. *et al.* Modulation of the Coordination Environment around the Magnetic Easy Axis Leads to

Significant Magnetic Relaxations in a Series of 3d-4f Schiff Complexes. *Inorganic Chemistry* **57**, 8065–8077 (2018).

408. Yao, X. *et al.* Investigation of magneto-structural correlation based on a series of seven-coordinated  $\beta$ -diketonate Dy(III) single-ion magnets with  $C_{2v}$  and  $C_{3v}$  local symmetry. *Dalton Transactions* **47**, 3976–3984 (2018).

409. Zhang, P. *et al.* Exchange coupling and single molecule magnetism in redox-active tetraoxolene-bridged dilanthanide complexes. *Chemical Science* **9**, 1221–1230 (2018).

410. Zhang, S. *et al.* The slow magnetic relaxation regulated by the coordination, configuration and intermolecular dipolar field in two mononuclear Dy<sup>III</sup> single-molecule magnets (SMMs). *Dalton Transactions* **47**, 12393–12405 (2018).

411. Bazhin, D. N. *et al.* Dinuclear lanthanide–lithium complexes based on fluorinated  $\beta$ -diketonate with acetal group: magnetism and effect of crystal packing on mechanoluminescence. *Inorganic Chemistry Frontiers* **6**, 40–49 (2019).

412. Bhattacharya, S., Bala, S. & Mondal, R. Ln-MOFs using a compartmental ligand with a unique combination of hard–soft terminals and their magnetic, gas adsorption and luminescence properties. *CrystEngComm* **21**, 5665–5672 (2019).

413. Boulkedid, A.-L. *et al.* Synthesis, structure and magnetic properties of a series of dinuclear heteroleptic Zn<sup>2+</sup>Ln<sup>3+</sup> Schiff base complexes: effect of lanthanide ions on the slow relaxation of magnetization. *Dalton Transactions* **48**, 11637–11641 (2019).

414. Cañón-Mancisidor, W. *et al.* Hybrid organic–inorganic mononuclear lanthanoid single ion magnets. *Chemical Communications* **55**, 14992–14995 (2019).

415. Cen, P. *et al.* Capping N-Donor Ligands Modulate the Magnetic Dynamics of Dy<sup>III</sup>  $\beta$ -Diketonate Single-Ion Magnets with  $D_{4a}$  Symmetry. *Chemistry – A European Journal* **25**, 3884–3892 (2019).

416. Chen, Y.-C., Peng, Y.-Y., Liu, J.-L. & Tong, M.-L. Field-induced slow magnetic relaxation in a mononuclear Gd(III) complex. *Inorganic Chemistry Communications* **107**, 107449 (2019).

417. Cheng, L.-W., Zhang, C.-L., Wei, J.-Y. & Lin, P.-H. Mononuclear and trinuclear Dy<sup>III</sup> SMMs with Schiff-base ligands modified by nitro-groups: first triangular complex with a N–N pathway. *Dalton Transactions* **48**, 17331–17339 (2019).

418. Cunha, T. T. da *et al.* Slow magnetic relaxation in mononuclear gadolinium(III) and dysprosium(III) oxamato complexes. *Polyhedron* **169**, 102–113 (2019).

419. Echenique-Errandonea, E. *et al.* Effect of the change of the ancillary carboxylate bridging ligand on the SMM and luminescence properties of a series of carboxylate-diphenoxido triply bridged dinuclear ZnLn and tetrานuclear Zn<sub>2</sub>Ln<sub>2</sub> complexes (Ln = Dy, Er). *Dalton Transactions* **48**, 190–201 (2019).

420. Evans, P., Reta, D., Whitehead, G. F. S., Chilton, N. F. & Mills, D. P. Bis-Monophospholyl Dysprosium Cation Showing Magnetic Hysteresis at 48 K. *Journal of the American Chemical Society* **141**, 19935–19940 (2019).

421. Fang, Y. *et al.* Determination of the magnetic principal axes of a dysprosium complex with slow relaxation on a single crystal. *Journal of Magnetism and Magnetic Materials* **490**, 165475 (2019).

422. Gonzalez, J. F., Pointillart, F. & Cador, O. Hyperfine coupling and slow magnetic relaxation in isotopically enriched Dy<sup>III</sup> mononuclear single-molecule magnets. *Inorganic Chemistry Frontiers* **6**, 1081–1086 (2019).

423. Gould, C. A. *et al.* Synthesis and Magnetism of Neutral, Linear Metallocene Complexes of Terbium(II) and Dysprosium(II). *Journal of the American Chemical Society* **141**, 12967–12973 (2019).

424. Han, M., Zhang, H., Wang, J., Feng, S. & Lu, L. Three chiral one-dimensional lanthanide–ditoluoyl-tartrate bifunctional polymers exhibiting luminescence and magnetic behaviors. *RSC Advances* **9**, 32288–32295 (2019).

425. Horii, Y. *et al.* Detailed Analysis of the Crystal Structures and Magnetic Properties of a Dysprosium(III) Phthalocyaninato Sextuple-Decker Complex: Weak *f*–*f* Interactions Suppress Magnetic Relaxation. *Chemistry – A European Journal* (2019) doi:10.1002/chem.201805368.

426. Kalita, P. *et al.* Mononuclear lanthanide complexes assembled from a tridentate NNO donor ligand: design of a Dy<sup>III</sup> single-ion magnet. *Dalton Transactions* **48**, 4857–4866 (2019).

427. Konarev, D. V. *et al.* Effect of One- and Two-Electron Reduction of Terbium(III) Double-Decker Phthalocyanine on Single-Ion Magnet Behavior and NIR Absorption. *Inorganic Chemistry* **58**, 5058–5068 (2019).

428. Kühne, I. A. *et al.* Comparison of two field-induced Er<sup>III</sup> single ion magnets. *Dalton Transactions* **48**, 15679–15686 (2019).

429. Li, L.-L., Su, H.-D., Liu, S., Xu, Y.-C. & Wang, W.-Z. A new air- and moisture-stable pentagonal-bipyramidal Dy<sup>III</sup> single-ion magnet based on the HMPA ligand. *Dalton Transactions* **48**, 2213–2219 (2019).

430. Li, Z.-H., Zhai, Y.-Q., Chen, W.-P., Ding, Y.-S. & Zheng, Y.-Z. Air-Stable Hexagonal Bipyramidal Dysprosium(III) Single-Ion Magnets with Nearly Perfect  $D_{6h}$  Local Symmetry. *Chemistry – A European Journal* **25**, 16219–16224 (2019).

431. Lu, G. *et al.* Single-ion magnet and luminescent properties in a Dy(III) triangular dodecahedral complex. *Inorganic Chemistry Communications* **102**, 16–19 (2019).

432. Mayans, J., Sorace, L., Font-Bardia, M. & Escuer, A. Chiral mononuclear lanthanide complexes derived from chiral Schiff bases: Structural and magnetic studies. *Polyhedron* **170**, 264–270 (2019).

433. Mayans, J., Saez, Q., Font-Bardia, M. & Escuer, A. Enhancement of magnetic relaxation properties with 3d diamagnetic cations in [Zn<sup>II</sup>Ln<sup>III</sup>] and [Ni<sup>II</sup>Ln<sup>III</sup>], Ln<sup>III</sup>= Kramers lanthanides. *Dalton Transactions* **48**, 641–652 (2019).

434. Münzfeld, L. *et al.* Synthesis, structures and magnetic properties of  $[(\eta^9\text{-C}_9\text{H}_9)\text{Ln}(\eta^8\text{-C}_8\text{H}_8)]$  super sandwich complexes. *Nature Communications* **10**, (2019).

435. Petrosyants, S. P. *et al.* Towards comparative investigation of Er- and Yb-based SMMs: the effect of the coordination environment configuration on the magnetic relaxation in the series of heteroleptic thiocyanate complexes. *Dalton Transactions* **48**, 12644–12655 (2019).

436. Petrosyants, S. P. *et al.* Luminescent and magnetic properties of mononuclear lanthanide thiocyanates with terpyridine as auxiliary ligand. *Inorganica Chimica Acta* **486**, 499–505 (2019).

437. Prytula-Kurkunova, A. Y., Pichon, C., Duhayon, C., Amirkhanov, V. M. & Sutter, J.-P. Mononuclear Lanthanide Complexes Containing [O-O]-Chelating Sulfonylamidophosphate Type Ligands. *European Journal of Inorganic Chemistry* **2019**, 4592–4596 (2019).

438. Wang, H.-L. *et al.* A series of dysprosium-based hydrogen-bonded organic frameworks (Dy–HOFs): thermally triggered off → on conversion of a single-ion magnet. *Inorganic Chemistry Frontiers* **6**, 2906–2913 (2019).

439. Wen, H.-R. *et al.* Multifunctional Lanthanide Complexes Based on Tetraazacyclolamidophenol Ligand with Field-Induced Slow Magnetic Relaxation, Luminescent and SHG Properties. *European Journal of Inorganic Chemistry* **2019**, 1406–1412 (2019).

440. Wen, H.-R. *et al.* Tb<sup>III</sup>/3d–Tb<sup>III</sup> clusters derived from a 1,4,7-triazacyclononane-based hexadentate ligand with field-induced slow magnetic relaxation and oxygen-sensitive luminescence. *New Journal of Chemistry* **43**, 4067–4074 (2019).

441. Xémard, M. *et al.* Divalent Thulium Crown Ether Complexes with Field-Induced Slow Magnetic Relaxation. *Inorganic Chemistry* **58**, 2872–2880 (2019).

442. Yang, H. *et al.* Magnetic properties and theoretical calculations of mononuclear lanthanide complexes with a Schiff base coordinated to Ln(III) ion in a monodentate coordination mode. *Inorganica Chimica Acta* **494**, 8–12 (2019).

443. Yin, C.-L. *et al.* Single molecule magnet behaviors of Zn<sub>4</sub>Ln<sub>2</sub> (Ln = Dy<sup>III</sup>, Tb<sup>III</sup>) complexes with multidentate organic ligands formed by absorption of CO<sub>2</sub> in air through in situ reactions. *Dalton Transactions* **48**, 512–522 (2019).

444. Yu, S. *et al.* Two mononuclear dysprosium(III) complexes with their slow magnetic relaxation behaviors tuned by coordination geometry. *Dalton Transactions* **48**, 16679–16686 (2019).

445. Zakrzewski, J. J., Chorazy, S., Nakabayashi, K., Ohkoshi, S. & Sieklucka, B. Photoluminescent Lanthanide(III) Single-Molecule Magnets in Three-Dimensional Polycyanidocuprate(I)-Based Frameworks. *Chemistry – A European Journal* **25**, 11820–11825 (2019).

446. Zeng, D. *et al.* Octahedral erbium and ytterbium ion encapsulated in phosphorescent iridium complexes showing field-induced magnetization relaxation. *Journal of Magnetism and Magnetic Materials* **484**, 139–145 (2019).

447. Zhang, S. *et al.* Regulation of Substituent Effects on Configurations and Magnetic Performances of Mononuclear Dy<sup>III</sup> Single-Molecule Magnets. *Inorganic Chemistry* **58**, 15330–15343 (2019).

448. Zhang, S. *et al.* Ligand ratio/solvent-influenced syntheses, crystal structures, and magnetic properties of polydentate Schiff base ligand-Dy(III) compounds with  $\beta$ -diketonate ligands as co-ligands. *Dalton Transactions* **48**, 15679–15686 (2019).

*Transactions* **48**, 12466–12481 (2019).

449. Zhi, Q. *et al.* Single-Ion Magnet Investigation of ABAB-Type Tetrachloro- and Tetraalkoxy-Substituted Bis(phthalocyaninato) Terbium Double-Decker with  $D_2$  Symmetrical Ligand Field. *European Journal of Inorganic Chemistry* **2019**, 1329–1334 (2019).

450. Zou, H.-H. *et al.* Bifunctional Mononuclear Dysprosium Complexes: Single-Ion Magnet Behaviors and Antitumor Activities. *Inorganic Chemistry* **58**, 2286–2298 (2019).

451. Zou, Q., Huang, X.-D., Liu, J.-C., Bao, S.-S. & Zheng, L.-M. Lanthanide anthracene complexes: slow magnetic relaxation and luminescence in  $Dy^{III}$ ,  $Er^{III}$  and  $Yb^{III}$  based materials. *Dalton Transactions* **48**, 2735–2740 (2019).

## Supplementary References

- (1) Ishikawa, N.; Sugita, M.; Ishikawa, T.; Koshihara, S.; Kaizu, Y. Lanthanide double-decker complexes functioning as magnets at the single-molecular level. *J. Am. Chem. Soc.* **2003**, *125* (29), 8694–8695. <https://doi.org/10.1021/ja029629n>.
- (2) AlDamen, M. A.; Clemente-Juan, J. M.; Coronado, E.; Martí-Gastaldo, C.; Gaita-Ariño, A. Mononuclear lanthanide single-molecule magnets based on polyoxometalates. *J. Am. Chem. Soc.* **2008**, *130* (28), 8874–8875. <https://doi.org/10.1021/ja801659m>.
- (3) AlDamen, M. A.; Cardona-Serra, S.; Clemente-Juan, J. M.; Coronado, E.; Gaita-Ariño, A.; Martí-Gastaldo, C.; Luis, F.; Montero, O. Mononuclear lanthanide single molecule magnets based on the polyoxometalates  $[\text{Ln}(\text{W}_5\text{O}_{18})^2]^{9-}$  and  $[\text{Ln}(\beta_2\text{-SiW}_{11}\text{O}_{39})^2]^{13-}$  ( $\text{Ln}^{\text{III}} = \text{Tb}, \text{Dy}, \text{Ho}, \text{Er}, \text{Tm}, \text{and} \text{Yb}$ ). *Inorg. Chem.* **2009**, *48* (8), 3467–3479. <https://doi.org/10.1021/ic801630z>.
- (4) Cardona-Serra, S.; Clemente-Juan, J. M.; Coronado, E.; Gaita-Ariño, A.; Camón, A.; Evangelisti, M.; Luis, F.; Martínez-Pérez, M. J.; Sesé, J. Lanthanoid single-ion magnets based on polyoxometalates with a 5-fold symmetry: the series  $[\text{LnP}_5\text{W}_{30}\text{O}_{110}]^{12-}$  ( $\text{Ln}^{3+} = \text{Tb}, \text{Dy}, \text{Ho}, \text{Er}, \text{Tm}, \text{and} \text{Yb}$ ). *J. Am. Chem. Soc.* **2012**, *134* (36), 14982–14990. <https://doi.org/10.1021/ja305163t>.
- (5) Li, D.-P.; Wang, T.-W.; Li, C.-H.; Liu, D.-S.; Li, Y.-Z.; You, X.-Z. Single-ion magnets based on mononuclear lanthanide complexes with chiral schiff base ligands  $[\text{Ln}(\text{FTA})_3\text{L}]$  ( $\text{Ln} = \text{Sm}, \text{Eu}, \text{Gd}, \text{Tb} \text{ and} \text{ Dy}$ ). *Chem. Commun.* **2010**, *46* (17), 2929–2931. <https://doi.org/10.1039/B924547B>.
- (6) Li, X.; Li, T.; Shi, X. J.; Tian, L. A family of  $2p\text{-}4f$  complexes based on indazole radical: syntheses, structures and magnetic properties. *Inorganica Chim. Acta* **2017**, *456*, 216–223. <https://doi.org/10.1016/j.ica.2016.11.002>.
- (7) Wang, Y.; Li, X.-L.; Wang, T.-W.; Song, Y.; You, X.-Z. Slow relaxation processes and single-ion magnetic behaviors in dysprosium-containing complexes. *Inorg. Chem.* **2010**, *49* (3), 969–976. <https://doi.org/10.1021/ic901720a>.
- (8) Mei, X.-L.; Ma, Y.; Li, L.-C.; Liao, D.-Z. Ligand field-tuned single-molecule magnet behaviour of  $2p\text{-}4f$  complexes. *Dalton Trans.* **2011**, *41* (2), 505–511. <https://doi.org/10.1039/C1DT11795E>.
- (9) Mei, X.-L.; Liu, R.-N.; Wang, C.; Yang, P.-P.; Li, L.-C.; Liao, D.-Z. Modulating spin dynamics of cyclic  $\text{Ln}^{\text{III}}$ -radical complexes ( $\text{Ln}^{\text{III}} = \text{Tb}, \text{Dy}$ ) by using phenyltrifluoroacetylacetone coligand. *Dalton Trans.* **2012**, *41* (10), 2904. <https://doi.org/10.1039/c2dt11671e>.
- (10) Hu, P.; Zhu, M.; Mei, X.; Tian, H.; Ma, Y.; Li, L.; Liao, D. Single-molecule magnets based on rare earth complexes with chelating benzimidazole-substituted nitronyl nitroxide radicals. *Dalton Trans.* **2012**, *41* (48), 14651. <https://doi.org/10.1039/c2dt31806g>.
- (11) Murakami, R.; Ishida, T.; Yoshii, S.; Nojiri, H. Single-molecule magnet  $[\text{Tb}(\text{Hfac})_3(2\text{pyNO})]$  ( $2\text{pyNO} = t\text{-butyl 2-pyridyl nitroxide}$ ) with a relatively high barrier of magnetization reversal. *Dalton Trans.* **2013**, *42* (38), 13968. <https://doi.org/10.1039/c3dt51784e>.
- (12) Hu, P.; Wang, X.; Ma, Y.; Wang, Q.; Li, L.; Liao, D. A new family of  $\text{Ln}$ -radical chains ( $\text{Ln} = \text{Nd}, \text{Sm}, \text{Gd}, \text{Tb} \text{ and} \text{ Dy}$ ): Synthesis, Structure, and Magnetic Properties. *Dalton Trans.* **2014**, *43* (5), 2234–2243. <https://doi.org/10.1039/c3dt52959b>.
- (13) Tretyakov, E. V.; Fokin, S. V.; Zueva, E. M.; Tkacheva, A. O.; Romanenko, G. V.; Bogomyakov, A. S.; Larionov, S. V.; Popov, S. A.; Ovcharenko, V. I. Complexes of lanthanides with spin-labeled pyrazolylquinoline. *Russ. Chem. Bull.* **2014**, *63* (7), 1459–1464. <https://doi.org/10.1007/s11172-014-0621-8>.
- (14) Li, C.; Sun, J.; Yang, M.; Sun, G.; Guo, J.; Ma, Y.; Li, L. From monomeric species to one-dimensional chain: enhancing slow magnetic relaxation through coupling mononuclear fragments in  $\text{Ln}$ -rad system. *Cryst. Growth Des.* **2016**, *16* (12), 7155–7162. <https://doi.org/10.1021/acs.cgd.6b01369>.

(15) Dolinar, B. S.; Gómez-Coca, S.; Alexandropoulos, D. I.; Dunbar, K. R. An air stable radical-bridged dysprosium single molecule magnet and its neutral counterpart: redox switching of magnetic relaxation dynamics. *Chem. Commun.* **2017**, *53* (14), 2283–2286. <https://doi.org/10.1039/c6cc09824j>.

(16) Sun, W.-B.; Yan, B.; Zhang, Y.-Q.; Wang, B.-W.; Wang, Z.-M.; Jia, J.-H.; Gao, S. The slow magnetic relaxation regulated by ligand conformation of a lanthanide single-ion magnet  $[\text{Hex}_4\text{N}][\text{Dy(DBM)}_4]$ . *Inorg. Chem. Front.* **2014**, *1* (6), 503–509. <https://doi.org/10.1039/C4QI00057A>.

(17) Zeng, D.; Ren, M.; Bao, S.-S.; Zheng, L.-M. Tuning the coordination geometries and magnetic dynamics of  $[\text{Ln}(\text{Hfac})_4]^-$  through alkali metal counterions. *Inorg. Chem.* **2014**, *53* (2), 795–801. <https://doi.org/10.1021/ic402111v>.

(18) Cen, P.; Liu, X.; Ferrando-Soria, J.; Zhang, Y.-Q.; Xie, G.; Chen, S.; Pardo, E. Capping N-donor ligands modulate the magnetic dynamics of  $\text{Dy}^{\text{III}}$   $\beta$ -Diketonate single-ion magnets with  $D_{4\text{d}}$  symmetry. *Chem. – Eur. J.* **2019**, *25* (15), 3884–3892. <https://doi.org/10.1002/chem.201805608>.

(19) Wang, H.; Wang, B.-W.; Bian, Y.; Gao, S.; Jiang, J. Single-molecule magnetism of tetrapyrrole lanthanide compounds with sandwich multiple-decker structures. *Coord. Chem. Rev.* **2016**, *306*, 195–216. <https://doi.org/10.1016/j.ccr.2015.07.004>.

(20) Ishikawa, N.; Mizuno, Y.; Takamatsu, S.; Ishikawa, T.; Koshihara, S. Effects of chemically induced contraction of a coordination polyhedron on the dynamical magnetism of bis(phthalocyaninato)dysprosium, a single-4f-ionic single-molecule magnet with a Kramers ground state. *Inorg. Chem.* **2008**, *47* (22), 10217–10219. <https://doi.org/10.1021/ic8014892>.

(21) Katoh, K.; Horii, Y.; Yasuda, N.; Wernsdorfer, W.; Toriumi, K.; Breedlove, B. K.; Yamashita, M. Multiple-decker phthalocyaninato dinuclear lanthanoid(III) single-molecule magnets with dual-magnetic relaxation processes. *Dalton Trans.* **2012**, *41* (44), 13582. <https://doi.org/10.1039/c2dt31400b>.

(22) Kan, J.; Wang, H.; Sun, W.; Cao, W.; Tao, J.; Jiang, J. Sandwich-type mixed tetrapyrrole rare-earth triple-decker compounds. effect of the coordination geometry on the single-molecule-magnet nature. *Inorg. Chem.* **2013**, *52* (15), 8505–8510. <https://doi.org/10.1021/ic400485y>.

(23) Wang, K.; Qi, D.; Wang, H.; Cao, W.; Li, W.; Liu, T.; Duan, C.; Jiang, J. Binuclear phthalocyanine-based sandwich-type rare earth complexes: unprecedented two  $\pi$ -bridged biradical-metal integrated SMMs. *Chem. - Eur. J.* **2013**, *19* (34), 11162–11166. <https://doi.org/10.1002/chem.201301101>.

(24) Cao, W.; Gao, C.; Zhang, Y.-Q.; Qi, D.; Liu, T.; Wang, K.; Duan, C.; Gao, S.; Jiang, J. Rational enhancement of the energy barrier of bis(tetrapyrrole) dysprosium SMMs via replacing atom of porphyrin core. *Chem. Sci.* **2015**, *6* (10), 5947–5954. <https://doi.org/10.1039/c5sc02314a>.

(25) Giménez-Agulló, N.; de Pipaón, C. S.; Adriaenssens, L.; Filibian, M.; Martínez-Belmonte, M.; Escudero-Adán, E. C.; Carretta, P.; Ballester, P.; Galán-Mascarós, J. R. Single-molecule-magnet behavior in the family of  $[\text{Ln}(\text{OETAP})_2]$  double-decker complexes ( $\text{Ln}=\text{lanthanide}$ , OETAP=octa(ethyl)tetraazaporphyrin). *Chem. - Eur. J.* **2014**, *20* (40), 12817–12825. <https://doi.org/10.1002/chem.201402869>.

(26) Clemente-Juan, J. M.; Coronado, E.; Gaita-Ariño, A. Magnetic polyoxometalates: From molecular magnetism to molecular spintronics and quantum computing. *Chem. Soc. Rev.* **2012**, *41* (22), 7464–7478. <https://doi.org/10.1039/C2CS35205B>.

(27) Biswas, S.; Bejoymohandas, K. S.; Das, S.; Kalita, P.; Reddy, M. L. P.; Oyarzabal, I.; Colacio, E.; Chandrasekhar, V. Mononuclear lanthanide complexes: Energy-barrier enhancement by ligand substitution in field-induced  $\text{Dy}^{\text{III}}$  SIMs. *Inorg. Chem.* **2017**, *56* (14), 7985–7997. <https://doi.org/10.1021/acs.inorgchem.7b00689>.

(28) Hamada, D.; Fujinami, T.; Yamauchi, S.; Matsumoto, N.; Mochida, N.; Ishida, T.; Sunatsuki, Y.;

Tsuchimoto, M.; Coletti, C.; Re, N. Luminescent Dy<sup>III</sup> single ion magnets with same N<sub>6</sub>O<sub>3</sub> donor atoms but different donor atom arrangements, 'fac'-[Dy<sup>III</sup>(HL<sup>DL-ala</sup>)<sub>3</sub>]<sup>·</sup>8H<sub>2</sub>O and 'mer'-[Dy<sup>III</sup>(HL<sup>DL-phe</sup>)<sub>3</sub>]<sup>·</sup>7H<sub>2</sub>O. *Polyhedron* **2016**, *109*, 120–128. <https://doi.org/10.1016/j.poly.2016.01.048>.

(29) Ren, M.; Xu, Z.-L.; Bao, S.-S.; Wang, T.-T.; Zheng, Z.-H.; Ferreira, R. A. S.; Zheng, L.-M.; Carlos, L. D. Lanthanide Salen-type complexes exhibiting single ion magnet and photoluminescent properties. *Dalton Trans.* **2016**, *45* (7), 2974–2982. <https://doi.org/10.1039/c5dt03897a>.

(30) Harriman, K. L. M.; Murugesu, M. An organolanthanide building block approach to single-molecule magnets. *Acc. Chem. Res.* **2016**, *49* (6), 1158–1167. <https://doi.org/10.1021/acs.accounts.6b00100>.

(31) Jiang, S.-D.; Wang, B.-W.; Sun, H.-L.; Wang, Z.-M.; Gao, S. An organometallic single-ion magnet. *J. Am. Chem. Soc.* **2011**, *133* (13), 4730–4733. <https://doi.org/10.1021/ja200198v>.

(32) Evans, P.; Reta, D.; Whitehead, G. F. S.; Chilton, N. F.; Mills, D. P. Bis-monophospholyl dysprosium cation showing magnetic hysteresis at 48 K. *J. Am. Chem. Soc.* **2019**, *141* (50), 19935–19940. <https://doi.org/10.1021/jacs.9b11515>.

(33) Le Roy, J. J.; Jeletic, M.; Gorelsky, S. I.; Korobkov, I.; Ungur, L.; Chibotaru, L. F.; Murugesu, M. An organometallic building block approach to produce a multidecker 4f single-molecule magnet. *J. Am. Chem. Soc.* **2013**, *135* (9), 3502–3510. <https://doi.org/10.1021/ja310642h>.

(34) Prytula-Kurkunova, A. Y.; Pichon, C.; Duhayon, C.; Amirkhanov, V. M.; Sutter, J.-P. Mononuclear lanthanide complexes containing [O-O]-chelating sulfonylamidophosphate type ligands. *Eur. J. Inorg. Chem.* **2019**, *2019* (42), 4592–4596. <https://doi.org/10.1002/ejic.201900976>.

(35) Demir, S.; Jeon, I.-R.; Long, J. R.; Harris, T. D. Radical ligand-containing single-molecule magnets. *Coord. Chem. Rev.* **2015**, *289*–*290*, 149–176. <https://doi.org/10.1016/j.ccr.2014.10.012>.

(36) Huang, G.; Daiguebonne, C.; Calvez, G.; Suffren, Y.; Guillou, O.; Guizouarn, T.; Le Guennic, B.; Cador, O.; Bernot, K. Strong magnetic coupling and single-molecule-magnet behavior in lanthanide-TEMPO radical chains. *Inorg. Chem.* **2018**, *57* (17), 11044–11057. <https://doi.org/10.1021/acs.inorgchem.8b01640>.

(37) Watanabe, A.; Yamashita, A.; Nakano, M.; Yamamura, T.; Kajiwara, T. Multi-path magnetic relaxation of mono-dysprosium(III) single-molecule magnet with extremely high barrier. *Chem. – Eur. J.* **2011**, *17* (27), 7428–7432. <https://doi.org/10.1002/chem.201003538>.

(38) Meihaus, K. R.; Corbey, J. F.; Fang, M.; Ziller, J. W.; Long, J. R.; Evans, W. J. Influence of an inner-sphere K<sup>+</sup> ion on the magnetic behavior of N<sub>2</sub><sup>3-</sup> radical-bridged dilanthanide complexes isolated using an external magnetic field. *Inorg. Chem.* **2014**, *53* (6), 3099–3107. <https://doi.org/10.1021/ic4030102>.

(39) Costes, J. P.; Titos-Padilla, S.; Oyarzabal, I.; Gupta, T.; Duhayon, C.; Rajaraman, G.; Colacio, E. Analysis of the role of peripheral ligands coordinated to Zn<sup>II</sup> in enhancing the energy barrier in luminescent linear trinuclear Zn-Dy-Zn single-molecule magnets. *Chem. – Eur. J.* **2015**, *21* (44), 15785–15796. <https://doi.org/10.1002/chem.201501500>.

(40) Hu, K.-Q.; Jiang, X.; Wu, S.-Q.; Liu, C.-M.; Cui, A.-L.; Kou, H.-Z. A trimetallic strategy towards Zn<sup>II</sup><sub>4</sub>Dy<sup>III</sup><sub>2</sub>Cr<sup>III</sup><sub>2</sub> and Zn<sup>II</sup><sub>4</sub>Dy<sup>III</sup><sub>2</sub>Co<sup>III</sup><sub>2</sub> single-ion magnets. *Dalton Trans.* **2015**, *44* (35), 15413–15416. <https://doi.org/10.1039/C5DT02175H>.

(41) Yamashita, A.; Watanabe, A.; Akine, S.; Nabeshima, T.; Nakano, M.; Yamamura, T.; Kajiwara, T. Wheel-shaped Er<sup>III</sup>Zn<sup>II</sup><sub>3</sub> single-molecule magnet: a macrocyclic approach to designing magnetic anisotropy. *Angew. Chem. Int. Ed.* **2011**, *50* (17), 4016–4019. <https://doi.org/10.1002/anie.201008180>.

(42) Feltham, H. L. C.; Lan, Y.; Klöwer, F.; Ungur, L.; Chibotaru, L. F.; Powell, A. K.; Brooker, S. A non-sandwiched macrocyclic monolanthanide single-molecule magnet: the key role of axiality. *Chem. – Eur. J.* **2011**, *17* (16), 4362–4365. <https://doi.org/10.1002/chem.201100438>.

(43) Cucinotta, G.; Perfetti, M.; Luzon, J.; Etienne, M.; Car, P.-E.; Caneschi, A.; Calvez, G.; Bernot, K.; Sessoli, R. Magnetic Anisotropy in a Dysprosium/DOTA Single-Molecule Magnet: Beyond Simple Magneto-Structural Correlations. *Angew. Chem. Int. Ed.* **2012**, *51* (7), 1606–1610. <https://doi.org/10.1002/anie.201107453>.

(44) Boulon, M.-E.; Cucinotta, G.; Luzon, J.; Degl'Innocenti, C.; Perfetti, M.; Bernot, K.; Calvez, G.; Caneschi, A.; Sessoli, R. Magnetic anisotropy and spin-parity effect along the series of lanthanide complexes with DOTA. *Angew. Chem. Int. Ed.* **2012**, *52* (1), 350–354. <https://doi.org/10.1002/anie.201205938>.

(45) Liu, J.-L.; Chen, Y.-C.; Zheng, Y.-Z.; Lin, W.-Q.; Ungur, L.; Wernsdorfer, W.; F. Chibotaru, L.; Tong, M.-L. Switching the anisotropy barrier of a single-ion magnet by symmetry change from quasi- $D_{5h}$  to quasi- $O_h$ . *Chem. Sci.* **2013**, *4* (8), 3310–3316. <https://doi.org/10.1039/C3SC50843A>.

(46) Palacios, M. A.; Titos-Padilla, S.; Ruiz, J.; Herrera, J. M.; Pope, S. J. A.; Brechin, E. K.; Colacio, E. Bifunctional  $Zn^{II}$  $Ln^{III}$  dinuclear complexes combining field induced SMM behavior and luminescence: enhanced NIR lanthanide emission by 9-anthracene carboxylate bridging ligands. *Inorg. Chem.* **2014**, *53* (3), 1465–1474. <https://doi.org/10.1021/ic402597s>.

(47) Jiang, Z.; Sun, L.; Yang, Q.; Yin, B.; Ke, H.; Han, J.; Wei, Q.; Xie, G.; Chen, S. Excess axial electrostatic repulsion as a criterion for pentagonal bipyramidal  $Dy^{III}$  single-ion magnets with high  $U_{eff}$  and  $T_B$ . *J. Mater. Chem. C* **2018**, *6* (15), 4273–4280. <https://doi.org/10.1039/c8tc00353j>.

(48) Liu, S.-S.; Xu, L.; Jiang, S.-D.; Zhang, Y.-Q.; Meng, Y.-S.; Wang, Z.; Wang, B.-W.; Zhang, W.-X.; Xi, Z.; Gao, S. Half-sandwich complexes of  $Dy^{III}$ : A Janus-Motif with facile tunability of magnetism. *Inorg. Chem.* **2015**, *54* (11), 5162–5168. <https://doi.org/10.1021/ic502734z>.

(49) Wu, J.; Jung, J.; Zhang, P.; Zhang, H.; Tang, J.; Guennic, B. L. *Cis-trans* isomerism modulates the magnetic relaxation of dysprosium single-molecule magnets. *Chem. Sci.* **2016**, *7* (6), 3632–3639. <https://doi.org/10.1039/C5SC04510J>.

(50) König, S. N.; Chilton, N. F.; Maichle-Mössmer, C.; Pineda, E. M.; Pugh, T.; Anwander, R.; Layfield, R. A. Fast magnetic relaxation in an octahedral dysprosium tetramethyl-aluminate complex. *Dalton Trans* **2014**, *43* (8), 3035–3038. <https://doi.org/10.1039/c3dt52337c>.

(51) Blagg, R. J.; Ungur, L.; Tuna, F.; Speak, J.; Comar, P.; Collison, D.; Wernsdorfer, W.; McInnes, E. J. L.; Chibotaru, L. F.; Winpenny, R. E. P. Magnetic relaxation pathways in lanthanide single-molecule magnets. *Nat. Chem.* **2013**, *5* (8), 673–678. <https://doi.org/10.1038/nchem.1707>.

(52) Zhang, P.; Zhang, L.; Wang, C.; Xue, S.; Lin, S.-Y.; Tang, J. Equatorially coordinated lanthanide single ion magnets. *J. Am. Chem. Soc.* **2014**, *136* (12), 4484–4487. <https://doi.org/10.1021/ja500793x>.

(53) Gifi, Albert. *Nonlinear Multivariate Analysis*; Wiley Series in Probability and Statistics; Wiley: New York, 1991.

(54) Mair, P.; Leeuw, J. D. *Homals: Gifi Methods for Optimal Scaling*; 2021.

(55) Dray, S.; Dufour, A.-B.; Thioulouse, and J.; Jombart, with contributions from T.; Pavoine, S.; Lobry, J. R.; Ollier, S.; Borcard, D.; Legendre, P.; Chessel, S. B. and A. S. B. on earlier work by D. *Ade4: Analysis of Ecological Data: Exploratory and Euclidean Methods in Environmental Sciences*; 2020.

(56) Husson, F.; Josse, J.; Le, S.; Mazet, J. *FactoMineR: Multivariate Exploratory Data Analysis and Data Mining*; 2020.

(57) Akaike, H. A New Look at the Statistical Model Identification. *IEEE Trans. Autom. Control* **1974**, *19* (6), 716–723. <https://doi.org/10.1109/TAC.1974.1100705>.

(58) R Core Team. *R: A Language and Environment for Statistical Computing*; R Foundation for Statistical Computing: Vienna, Austria, 2020.

(59) Ripley, B.; Venables, W. *nnet: Feed-Forward Neural Networks and Multinomial Log-Linear Models*; 2021.

(60) Kassambara, A.; Mundt, F. *factoextra: extract and visualize the results of multivariate data analyses*; 2020.